

FINAL REPORT

Next Generation Buried Object Scanning Sonar (BOSS) for
Detecting Buried UXO in Shallow Water

SERDP Project MR-2752

NOVEMBER 2018

Jason Sara
EdgeTech

Distribution Statement A

This document has been cleared for public release



This report was prepared under contract to the Department of Defense Strategic Environmental Research and Development Program (SERDP). The publication of this report does not indicate endorsement by the Department of Defense, nor should the contents be construed as reflecting the official policy or position of the Department of Defense. Reference herein to any specific commercial product, process, or service by trade name, trademark, manufacturer, or otherwise, does not necessarily constitute or imply its endorsement, recommendation, or favoring by the Department of Defense.

REPORT DOCUMENTATION PAGE					Form Approved OMB No. 0704-0188	
<p>The public reporting burden for this collection of information is estimated to average 1 hour per response, including the time for reviewing instructions, searching existing data sources, gathering and maintaining the data needed, and completing and reviewing the collection of information. Send comments regarding this burden estimate or any other aspect of this collection of information, including suggestions for reducing the burden, to Department of Defense, Washington Headquarters Services, Directorate for Information Operations and Reports (0704-0188), 1215 Jefferson Davis Highway, Suite 1204, Arlington, VA 22202-4302. Respondents should be aware that notwithstanding any other provision of law, no person shall be subject to any penalty for failing to comply with a collection of information if it does not display a currently valid OMB control number.</p> <p>PLEASE DO NOT RETURN YOUR FORM TO THE ABOVE ADDRESS.</p>						
1. REPORT DATE (DD-MM-YYYY) 26/11/2018		2. REPORT TYPE SERDP Final Report			3. DATES COVERED (From - To) 5/23/2017 - 9/23/2019	
4. TITLE AND SUBTITLE Next Generation Buried Object Scanning Sonar (BOSS) for Detecting Buried UXO in Shallow Water				5a. CONTRACT NUMBER 17-C-0031		
				5b. GRANT NUMBER		
				5c. PROGRAM ELEMENT NUMBER		
6. AUTHOR(S) Jason Sara				5d. PROJECT NUMBER MR-2752		
				5e. TASK NUMBER		
				5f. WORK UNIT NUMBER		
7. PERFORMING ORGANIZATION NAME(S) AND ADDRESS(ES) EdgeTech 1141 Holland Drive; Suite 1 Boca Raton, FL 33487					8. PERFORMING ORGANIZATION REPORT NUMBER MR-2752	
9. SPONSORING/MONITORING AGENCY NAME(S) AND ADDRESS(ES) Strategic Environmental Research and Development Program (SERDP) 4800 Mark Center Drive, Suite 16F16 Alexandria, VA 22350-3605					10. SPONSOR/MONITOR'S ACRONYM(S) SERDP	
					11. SPONSOR/MONITOR'S REPORT NUMBER(S) MR-2752	
12. DISTRIBUTION/AVAILABILITY STATEMENT DISTRIBUTION STATEMENT A. Approved for public release: distribution unlimited.						
13. SUPPLEMENTARY NOTES						
14. ABSTRACT This paper summarizes the findings of a limited scope study targeted at improving the output products of a class of acoustic subbottom imaging systems generically called BOSS. It makes recommendations on how to enhance and improve existing fielded BOSS systems for improved UXO detection.						
15. SUBJECT TERMS BOSS, eBOSS, Buried Object Imaging, Buried Object Scanning Sonar, Multi-Source Imaging, SAS, Subbottom Survey, Synthetic Aperture Sonar, UXO Detection, UXO Remediation						
16. SECURITY CLASSIFICATION OF:			17. LIMITATION OF ABSTRACT UNCLASS	18. NUMBER OF PAGES 94	19a. NAME OF RESPONSIBLE PERSON Jason Sara	
a. REPORT UNCLASS	b. ABSTRACT UNCLASS	c. THIS PAGE UNCLASS			19b. TELEPHONE NUMBER (Include area code) 561-288-9223	

Table of Contents

List of Tables	iv
List of Figures	iv
List of Acronyms	ix
Keywords	xi
Acknowledgements	xii
Abstract	1
Objective	3
Background	4
Materials and Methods	7
The Case for Multi-Source Imaging	7
Example with a simulated mortar shell	7
The Geometry of Look Angles	3
UXO Shapes	4
Unoptimized Multisource Architecture	3
Optimized Multisource Architecture	4
Separation Between Sources	4
Pulse Repetition Rate (PRR)	7
Determining the Number of Hydrophone Rows	7
Determining Multisource Image Range	9
Determining the Length of the Across-Track Subaperture	10
Generating Synthetic Target Data	11
Simulated Multisource Imaging with a 0.4 m Cylindrical Target	12
Simulated Multisource Imaging with a Rotated Cylindrical Target	15
Acoustic Color Map Creation	19
Resolution, Altitude, and Bandwidth Tradeoffs	20
Resolution Enhancements	22
Measuring Shape and Dimension of an Object	23
Trade Space Study	25
Beamforming with Sediment Sound Speed	27
Measuring Sediment Sound Speed	30

Shallow Water Artifacts.....	31
Next Generation Transmit Source Selection.....	33
Tonpilz	33
Single crystal.....	34
Textured ceramics	34
Shallow Water Baffle Design	35
Next Generation Hydrophone Design.....	36
Acoustic Positioning and Alternative System Concept	37
INS:	38
DVL:	38
LBL:	38
GNSS with satellite-based corrections:	39
USBL:	39
Re-nav:	39
Feature-based Navigation:	39
Hydrographic modeling:	39
Structural Acoustics Requirements.....	40
Relationship to Other UXO Research.....	40
Conclusions and Implications for Future Research/Implementation.....	42
Proposed Next Steps : Technology Risk Reduction	42
Proposed Next Steps : Concept Validation.....	43
Proposed Next Steps : System Build Out	44
Conclusions.....	44
Literature Cited	46
Appendix A: History of BOSS Systems	48
Appendix B: Baffle Design.....	52
Appendix B.1: MATLAB program for airgap baffle design:	55
Appendix C: PC SWAT Simulations.....	61
References:.....	64
Appendix D: MATLAB Script for Computing Trade Space Table.....	65
Appendix E: APL-UW MuST Multisource	69

List of Tables

Table 1. Measurements from horizontal image slices of a truncated prolate spheroid with a 22-cm diameter and 50-cm length. The row in bold indicates the estimated dimensions.	25
Table 2. Trade Space Table for single track-line coverage.....	26

List of Figures

Figure 1. Simulations for this effort used a 2-ms chirp pulse that spans 7.5 to 37.5 kHz. (Top) Time-series waveform of the transmitted pulse. (Middle) Spectrum of the transmitted pulse. (Bottom) Range resolution of system is illustrated by the envelope of the match filtered time-series of an ideal point-source reflector.....	4
Figure 2. Overview of eBOSS. Transmitter sends out a wide band chirp pulse. This sound wave propagates through the seabed. Backscattered energy is received on multiple hydrophones. Each hydrophone has a dedicated ADC converter that generates a time-series waveform per element. Each time series is match filtered to create a dechirped time series. A time delay beamformer reconstructs a 3D voxel image of the terrain using an along-track synthetic aperture and an across-track real aperture.....	5
Figure 3. Field data collected with a Bluefin BOSS-40 system of a buried cable with a 4-inch diameter. This illustrates a typical voxel image set from a contemporary BOSS system.	5
Figure 4. Track lines for paths A, B, C, and D. With respect to a common across track origin, A is at -2.2 meters, B is at -0.7 meters, C is at +0.7 meters, and D is at +2.2 meters. Transmitter is aft of the receive array by 0.2 meters. This is a common geometry that will be used in subsequent simulations. Beamformed results of the mortar example are show in Figure 5.	8
Figure 5. Beamformed results for tracks A through D with a mortar target buried 0.5 meters in medium sand. Each of these show different parts of the mortar being imaged due to the differences in across track positions of the transmit/receive apertures. This supports the need for multiple sources and multiple look-angles to image buried UXO.....	2
Figure 6. Azimuthal angle of a target with respect to the eBOSS platform's location. This figure shows the convention that will be used throughout the document. Since strong acoustic returns tend to be specular in nature, different angular locations can produce substantially different beamformed image results. Therefore, it is important to capture UXO images at all aspect angles to paint a more complete picture. .	3
Figure 7. Monostatic and bistatic geometries for sensing the same facet. In the bistatic case, the receive aperture is spatially separated from the transmitter. As will be shown, bistatic geometries can capture backscatter from facets without having a transmitter at the facet's normal, potentially reducing the number of sources for a multisource imaging solution.....	4
Figure 8. Far field target strength (dB) as a function of angle and frequency for a cylinder with a radius of 0.1 m and length of 0.4 m. Based on Urlick's formula for target strength of a cylinder. At 5 degrees off normal incidence, target strength is reduced by a factor of more than 10. For the eBOSS system, this shows that the sensing aperture needs to intersect a normal plane to the cylinder's body to within 5 degrees. The 3-D plot is approximate and intended to emphasize that the symmetry in this shape allows for detection at many elevation angles.....	5
Figure 9. Far field target strength as a function of angle and frequency for a 0.2 m square plate. 3-D plot when off axis is approximate and not based on actual formula but meant to show the dependence on	

both angular degrees of freedom. This example illustrates that eBOSS's ability to image a facet can depend on both elevation and azimuthal angles. 2

Figure 10. Unoptimized multisource array architecture for an all-aspect view-angle beamforming system. Because there are transmit sources at all across-track positions within the coverage swath, the normal vectors for all observable facets will eventually intersect a monostatic beamforming aperture as the platform translates forward. For a monostatic aperture, specular returns are captured at normal incidence. 3

Figure 11. Proposed sonar geometry for multisource imaging. Figure shows the relationship between source spacing, altitude, and imaging ring angular limits. The position of the peripheral sources determines the across track range of the multisource image. R is the image range given source positions, which are set based on sonar operating altitude. Δy is the spacing between transmitters given the sonar's desired operating altitude. 4

Figure 12. Proposed transmit source spacing for multisource beamforming. For each transmit source, R_{min} and R_{max} define the recommended region for beamforming. Sources are spaced at the R_{min} interval to provide full coverage. Voxels that fall within the R_{min} radius are excluded to avoid the strong specular scattering artifacts from the seabed. Beamforming voxels beyond R_{max} radius get progressively weaker and are therefore also excluded. The illustrated target lies almost entirely within the imaging bands for the D transmit source. 6

Figure 13. Plan view beamformed image from PC SWAT simulation of 6 ideal point source reflectors at various positions in the across track axis buried 0.5 m in medium sand. The target return strength decreases due to refraction loss as the critical angle is approached. The R_{max} criterion proposed for beamforming is also crosschecked. Note that the point source reflector at the across-track coordinate of +3 meters is not visible. The platform is centered at an across-track offset of -2.2 m in this single source simulation. 6

Figure 14. Ray paths for target at outer edge of imaging annulus used to calculate the minimum PRI required to prevent ping to ping interference. 8

Figure 15. Maximum sonar velocity for a given number of sources, rows of hydrophones, and platform altitude. 9

Figure 16. Multisource image range as a function of sonar operating altitude for 4, 6, and 8 sources. 10

Figure 17. Multisource imaging of a target midway between adjacent sources determines the lengths of the hydrophone segments. The receive aperture for a given transmit source extends to the adjacent sources. A 0-degree target-facet midway between sources will be seen as a specular return at the hydrophones at the end of the segment similar to the bistatic imaging case. 11

Figure 18. Comparison of 4-source images of free field truncated prolate spheroid for a hydrophone segment length. (Left) Hydrophone segment length is equal to the sonar altitude above target. (Right) The length is equal to $\sqrt{2}$ times the sonar altitude above the target. The longer hydrophone segment captures the specular reflections off the target and provides data for complete image reconstruction when the target falls midway between two adjacent sources. 11

Figure 19. Truncated prolate spheroid target shape used in simulations. (Left) Image provided by NSWC-PCD. (Right) Center positions of finite elements modeling surface of rigid truncated prolate spheroid. 12

Figure 20. Sequential physical/SAS apertures for the simulated four-source platform with the optimized architecture. The beamforming subaperture for the A source is shown. Subapertures for other sources are

similar. The across-track aperture is physical only, whereas the along-track aperture has 4 physical rows and is supplemented by a synthetic aperture.	12
Figure 21. Cylinder target with hemispherical end caps used in some PC SWAT simulations. Most UXO tend to have a cylindrical-type body.	13
Figure 22. Beamformed results of a simulated cylinder show that the strongest returns are from the body of the cylinder. Free field simulation with target 2.5 m below platform. The cylinder body, described in Figure 21, is lying parallel to the wing and is located 2.5 meters below the platform. This orientation will be referred to as the non-rotated (0-degree rotation angle) cylinder. The first 4 subfigures show the individual beamforming results from four transmit sources using a 2.8 meter across track aperture. The A and D sources show returns from the hemispherical endcaps which are very weak compared to the cylinder body. The B and C sources show returns from the cylinder body. The additional subfigures for B-Bistatic and C-Bistatic show results for bistatic apertures where the receive aperture is shifted over by 1 m for the B and C sources respectively. See discussion.	13
Figure 23. Composite results for the four sources shown in Figure 22. Since the cylinder has a finite width, the mosaic shows returns from both sides of the cylinder body. At CPA, the location being ensonified on the surface of the cylinder changes more rapidly resulting in a somewhat less coherent and therefore weaker beamformed signal result.	14
Figure 24. Beamforming results of a PC SWAT simulation of 6 ideal point source reflectors located 2.5 meters below the sensing platform. The transmit source is located at the A position (-2.2 meters on the port side). Top image shows the monostatic case where the receive aperture is centered at the A transmit source location. Middle image shows a bistatic case where the receive aperture is offset by 2.2 meters, finally the bottom image shows a bistatic case where the receive aperture is offset by 4.4 meters. These offsets can be used to create voxel image sets that image facets at azimuthal angles that cannot be achieved by the monostatic configuration. Too high an offset will compromise the image resolution. For the 4.4 m offset case the width of the point source reflector at 0 is approximately twice as wide as the monostatic case.	16
Figure 25. Beamformed results of a simulated 45-degree rotated cylinder. Free field simulation with target 2.5 m below sensing platform. The A and D transmit source images have significantly higher signal level than the B and C sources since they are at the appropriate position to pick up the cylinder facet normal. To form each of these 6 images, beamformed results for all pings are overlaid using a maximum intensity projection. The first 4 images (labeled as A through D) are for all pings for each respective source overlaid. The final 2 images are intended to show the directionality of the facet returns from the A and D apertures. A-Aft shows the overlay of the first half of pings from the A transmit source – before the BOSS platform reaches CPA, and the D-Fore similarly shows the overlay of the last half of the pings from the D transmit source – after the BOSS platform passes CPA. In these final 2 images, only the hemispherical endcap is seen as the BOSS platform is not at the proper location to sense the cylinder’s body facet return.	17
Figure 26. Mosaic of beamformed results from all 4 sources for the 45-degree rotated cylinder.	17
Figure 27. Beamformed results of a simulation of the 22-degree rotated cylinder. Free field simulation with target 2.5 m below sensing platform. The B and C transmit source images have significantly higher signal level than the A and D sources since they are at the appropriate position to pick up the cylinder facet normal.	18
Figure 28. Mosaic of beamformed results from all 4 sources for the 22-degree rotated cylinder.	18

Figure 29. Acoustic color map created from the D source simulation of the 45-degree rotated cylinder. The span of azimuthal angles is limited to what can be measured from the D source. The A, B, and C sources could be used to complete the 360-degree map. The angle axis in the plot is approximate because this is a near field technique and each ping represents a range of angles due to the size of the receive aperture.....	20
Figure 30. Mosaic of beamforming results for 45-degree cylinder 5.5 meters below eBOSS platform. This is a free field simulation. The resolution is degraded due to the high altitude. The BOSS platform's 2 m x 2 m aperture was designed for a 2-m altitude. These low altitudes may be operationally challenging to achieve. It is common to operate a conventional BOSS system with 2-meter wingspan at about 5 meters altitude. The purpose of this figure is to emphasize that this type of higher altitude operation will compromise image quality.	21
Figure 31. Mosaic of beamforming results for 45-degree cylinder 2.5 meters below BOSS platform but using only the low half of the transmitted band. This is a free field simulation. This band, from 7.5 to 22.5 kHz, is similar to the bandwidth of a conventional BOSS system. Restricting to this lower band will result in a system that is easier to implement due to reduced hydrophone segment channel counts (1/2 wavelength spacing criteria). The lower band can also show more elastic properties beneficial for structural acoustics. Resolution is inferior to the full bandwidth transmission results.	21
Figure 32. Mosaic of beamforming results for 45-degree cylinder 2.5 meters below eBOSS platform but using only the high half band of the transmission pulse. This is a free field simulation. This band from 22.5 to 37.5 kHz is close to what can be achieved with a commercially available transmit source. Resolution is comparable to that of the full band beamformed results. Note that the beamforming aperture remains unchanged at 2 x 2 meters. While structural acoustics may benefit from lower frequency band operation, the high half band is acceptable for measuring object size and shape metrics.	22
Figure 33. Significant focal planes used in procedure for measuring target length and diameter. Focal plane A generates the horizontal plane image with the highest pixel amplitude. Focal plane B passing through target axis, is used to measure target diameter and length. Note that 45 degrees is the midpoint angle in the Rmin/Rmax imaging bands and represents the approximate viewing angle for target focal points.....	24
Figure 34. Focal planes can be used to estimate the size and shape of an object. The images show simulated horizontal slices of a rigid truncated prolate spheroid (bullet shape) with a 22-cm diameter and a 50-cm length. The focal planes shown are A) z=1.38 m B) z=1.44 m C) z=1.48 m D) z=1.52 m.....	25
Figure 35. Geometry for refraction at the seabed due to higher sediment sound speed. In beamforming simulations, a look-up table was precomputed to account for time delay differences due to sediment sound speed. The table indices were the horizontal range to focal point, burial depth, and altitude. Once the seabed intercept point is known, the total time delay can be computed by summing the water propagation time and the sediment propagation time. Compensating for refraction can significantly improve the resolution of beamforming buried objects.	28
Figure 36. A simulated mosaic of beamforming results with refraction compensation for a 45-degree rotated cylinder buried at 0.5 meters in medium sand. See Figure 37 for imagery of the same target without refraction compensation.	29
Figure 37. Mosaic of beamforming results for 45-degree rotated cylinder buried 0.5 meters in medium sand, refraction compensation was not enabled. The imagery is inferior without refraction compensation. See Figure 36 for the same target imaged with refraction compensation.	29

Figure 38. Reflection coefficient of a sandy seafloor and its slope as a function of incidence angle. The peak in the slope of $dR/d\theta$ can be used to estimate the critical angle.	31
Figure 39. The number of sources in the sonar array determines the minimum measurable sediment sound velocity. With an increased number of sources, the range of measurable sediment sound velocities increases.	31
Figure 40. Beamformed results from the Bluefin 40 BOSS system of a 4" cable. Swath was extended to 20 meters to show the effect of surface reflection artifacts on the beamforming. Image shows that surface reflection artifacts are strong compared to the cable return. Surface artifacts were not a problem for this data set because the BOSS platform was at about a 12-meter depth below the sea surface. These surface artifacts would be a problem for shallow water operation.	32
Figure 41. Possible concept geometry for surface artifact suppression. An air baffle above the hydrophone panels suppresses surface reflections. In addition, a directional transmit source can provide a beam pattern with a high source-level below the platform (and into the seabed) but a weak source-level above the platform so that less acoustic energy is transmitted towards the surface. About a 120-degree beam width is desired to ensonify the seabed.	33
Figure 42. Baffle options for shallow water operation needed to suppress surface reflections. The air gap baffle is preferred due to reduced weight and more consistent properties over time. Corprene absorbs water and changes properties with gradual water absorption and over time. For deeper water operation, the baffle can either be removed or, in the case of an air baffle, the sealing plugs can be removed to flood the baffle.	35
Figure 43. Partially populated eBOSS panel prior to being potted. Two of the 16 PVDF hydrophone segments are populated. The panel also includes dedicated ADCs for each segment. A digital interface is used to configure the system and to upload data to a centralized data collection unit.	36
Figure 44. High channel count eBOSS modular panel strategy. Multiple rows of hydrophones are desired to maintain $\frac{1}{2}$ wavelength separation in the along-track axis for a combined SAS and physical along-track aperture. Multiple columns of hydrophones are desired to maintain $\frac{1}{2}$ wavelength separation in the across-track axis for the across-track pure physical aperture. PVDF is an etchable material so multiple hydrophones can be created in a 2-dimensional grid on a single PVDF sheet. Digitizing electronics would be housed on a separate printed circuit that is bonded to the PVDF etched sheet.	37
Figure 45. BlueFin 12 AUV with 40 channel BOSS hydrophone wing. Each wing has 20 hydrophones embedded in it with a 2" pitch. Other payloads also shown.	49
Figure 46. Razor AUV with eBOSS. Four 16-channel wing tiles are mounted below the across track wing. A Corprene signal conditioning plate / baffle (not shown) suppresses surface reflections.	49
Figure 47. Atlas Sea Horse with eBOSS Payload. Hydrophone wing consists of 4 panels, 64 channels total, with 2" spacing between segments. The wing rotates into the across-track position after deployment.	50
Figure 48. Ceros BOSS. This demonstrator had 32 hydrophone staves arranged in a 4 x 8 grid and a steerable 6 Tonpilz transmit array.	50
Figure 49. SERDP BOSS-160 demonstrator being deployed in Panama City, FL. Each carbon fiber wing is embedded with 4 rows by 20 hydrophone staves with a 2" pitch. The optionally floodable air gap baffle is seen at the wing tops.	51
Figure 50. Multisource geometry for MuST Focus Platform. An omni-directional transmit source is placed at each end of the receive aperture. Four hydrophone panels of 16 channels each are also shown.	69

List of Acronyms

2D – Two dimensional

3D – Three dimensional

ADC – Analog to Digital Converter.

APL-UW – Applied Physics Lab / University of Washington.

AUV – Autonomous Underwater Vehicle.

Bellhop3D – Gaussian beam program developed by Michael Porter.

BOSS – Buried Object Scanning Sonar. Term is used to refer to a series of imaging sub-bottom profilers developed by FAU professor Dr. Steven Schock.

CPA – Closest Point of Approach.

DVL – Doppler Velocity Log, an acoustic method used to measure velocity based on Doppler shift of returned signal.

eBOSS – A newer generation of BOSS systems built by EdgeTech, as opposed to the original BOSS systems built by FAU.

ESTCP – Environmental Security Technology Certification Program.

FAU – Florida Atlantic University.

FFT – Fast Fourier Transform.

FM – Frequency Modulation.

FPGA – Field Programmable Gate Array.

GTD – Geometric Theory of Diffraction.

GNSS – Global Navigation Satellite System.

GRAB – Gaussian Ray Bundle.

INS – Inertial Navigation System.

ITAR - International Traffic in Arms Regulations.

kHz – KiloHertz (1000 Hertz).

LBL – Long Base Line – technique used for acoustic positioning.

LFM – Linear Frequency Modulation.

MATLAB - MATrix LABoratory is a multi-paradigm numerical computing environment and proprietary programming language developed by MathWorks.

MuST – Multi Sensor Towbody platform – an APL-UW SERDP ongoing demonstrator project.

NSWC-PCD – Naval Surface Warfare Center, Panama City Division

PMN-PT – Lead Magnesium Niobate – Lead Titanate, a ceramic material with acoustic to voltage properties used to transmit sound pressure waves.

PC SWAT – Personal Computer Shallow Water Acoustic Toolset.

PVDF – Polyvinylidene fluoride. A pressure wave sensing material used for hydrophones in underwater acoustics.

PZT – Lead Zirconate Titanate. This is a ceramic material with acoustic to voltage properties used to transmit or receive sound pressure waves.

SAS – Synthetic Aperture Sonar.

SLAM – Simultaneous localization and mapping.

SNR – Signal to Noise Ratio.

UW – Under Water.

USBL – Ultra Short Baseline. A technique used for acoustic positioning.

UXO – Unexploded Ordnance.

Keywords

BOSS

eBOSS

Buried Object Imaging

Buried Object Scanning Sonar

Multi-Source Imaging

SAS

Subbottom Survey

Synthetic Aperture Sonar

UXO Detection

UXO Remediation

Acknowledgements

Work performed under SERDP project MR-2752 included efforts from several organizations and individuals. I would like to thank those who contributed. First this is a follow-on to the work of FAU Professor Steven Schock on a series of related systems, some of which were funded by SERDP. While he is not writing this report, he is the architect of this design, and even with his present disabilities has been able express his ideas for a future concept of this enhanced system. We are also grateful to NSWC-PCD Panama City staff for their expert guidance in acoustics and system simulations necessary to validate and tune this design – in particular Raymond Lim, Gary Sammelmann, José Fernandez, Rodolfo Arrieta, and Daniel Sternlicht. We have also received guidance from Kevin Williams of University of Washington.

Abstract

Detection and identification of underwater Unexploded Ordnance (UXO) is a significant problem in remediation efforts to reclaim formerly used defense sites. Presently there is no system available that can accurately survey and map the location of UXO at underwater sites and reliably discriminate UXO from debris. The UXO survey problem is complicated by a wide range of targets as well as clutter both natural and man-made.

The Buried Object Scanning Sonar (BOSS) systems are a family of low frequency penetrating imaging sonars that employ a wing that is populated with an array of hydrophone sensors, which uses synthetic aperture sonar beamform processing to create a 3D image of buried objects. The EdgeTech BOSS (eBOSS) is the successor to the original BOSS systems and is free from the ITAR restrictions that limited the application of the original BOSS systems. The eBOSS consists of newly developed hardware and software created using internal funding.

Low frequency sonars such as eBOSS and BOSS cannot produce target imagery suitable for recognizing/differentiating UXO from other buried clutter because those single source systems generate incomplete target imagery, a result of the limited target views. At certain target aspects, the sonars will measure echoes off only a target end providing no target shape or dimensional information. Low-frequency sonars can provide the raw inputs to produce acoustic color maps or other structural acoustics for target classifiers.

This effort defines a strategy to improve the imaging performance of a future eBOSS-type system, which is targeted for UXO remediation. The key improvement over existing systems is the utilization of multiple sources to illuminate all sides of each target and to allow generation of imagery for measuring size and shape metrics as well as acoustic color maps. Multi-source ensonification of a target field will create full 360-degree viewing angles of buried objects, which is valuable because most targets have specular returns related to their shape and orientation.

Additional improvements over previous versions of the BOSS have also been identified. Image resolution will be improved via higher bandwidth sources and basic enhancements to beamforming algorithms. We show that refraction corrections and real-time measurements of sediment sound velocity are necessary for producing usable images of buried UXO. We also present a method for measuring the critical angle which yields the sediment sound velocity. Shallow water operation will be improved by suppressing surface reflections and multipath interference by employing baffling and directional sources.

To overstate the obvious, an all aspect angle ensonification strategy requires that transmit sources be placed on all sides of targets in a coverage swath. This means that a future system will require a longer wing aperture with multiple transmit sources spaced across this aperture.

The across-track wing aperture of this future system will be populated with multiple rows of hydrophones. The multiple rows are desirable to supplement the along-track SAS aperture with a physical aperture to maintain $\frac{1}{2}$ wavelength sample spacing along track. As the minimum velocity increases and/or the number of transmit sources (which are operated round robin) increases, the number of hydrophone rows required must also increase to maintain $\frac{1}{2}$ wavelength spacing along track because there is a maximum ping rate. The maximum ping rate is constrained by the required slant range recorded per each ping.

The future eBOSS system will have higher data collection rates and related higher channel count hydrophone arrays. A straight forward strategy will be proposed to achieve this higher channel count system using segmented/modular panels and etched PVDF. The manufacturing process for such an array will need to be validated and stress tested for reliability.

As a next step system, we propose to enhance the SERDP funded APL-UW Focus vehicle, which already contains an eBOSS system, with next generation imaging features so that the concepts described here can be tested with real-world field data.

This study is guided by the belief that superior classification can be achieved by a system that guarantees the sensing of all specular scattering from UXO. It proposes a hardware architecture that can meet this objective. What is the combination of hardware, signal processing data products (e.g., images and acoustic color), and operational strategies needed to meet the metrics defined by the stake holders associated with SERDP/ESTCP? The final answer to this question will undoubtedly require an iterative process relying on in-the-field lessons learned as the current generation of eBOSS systems is tested. We believe this report details methods that will remain valuable throughout this process.

Objective

The objective of this work is to improve the ability to remediate underwater sites by developing a system for the detection and classification of proud, partially buried, and buried ordnance in shallow (< 5 m) and moderate depth (< 100 m) water. The focus of this research is to develop algorithms and design an acoustic array that will image buried UXO (Unexploded Ordnance) with sufficient detail to measure their length, diameter, and shape. These metrics can be used as features for a standalone UXO classifier or as an input constraining the solution of a classifier using acoustic color map features. This improved Buried Object Scanning Sonar (BOSS) technology, which is the EdgeTech BOSS (eBOSS), will increase the probability of detecting and classifying objects that have settled or have been buried in shallow water sites.

The BOSS will be redesigned to generate UXO imagery that will measure length, diameter, and shape of buried objects. BOSS was originally designed to detect and to generate images of mines buried 1 meter in the seabed. This operational requirement and the constraints of installing BOSS on a 12-inch diameter UUV drove the design of BOSS about 12 years ago. SERDP sponsored experiments demonstrating that BOSS could: a) detect UXO and b) generate low resolution imagery and burial depth estimates of UXO over a limited range of target orientations. However, the BOSS imagery lacked the detail needed for accurate measurement of UXO dimensions and for UXO classification.

This study investigates an eBOSS design for imaging and classifying UXO. The technical approach is to generate synthetic datasets consisting of scattering from buried UXO-shaped rigid bodies. Multiple acoustic sources are used to ensonify all aspects of the UXO targets. The synthetic data, acquired by parallel discrete arrays of hydrophones, are processed by revised eBOSS algorithms designed to produce imagery suitable for measuring UXO length, diameter, and shape. Once the eBOSS is completed and used to acquire data, the multisource datasets produced will be available to other research programs that are developing classification algorithms. An example acoustic color map from the proposed system will be presented.

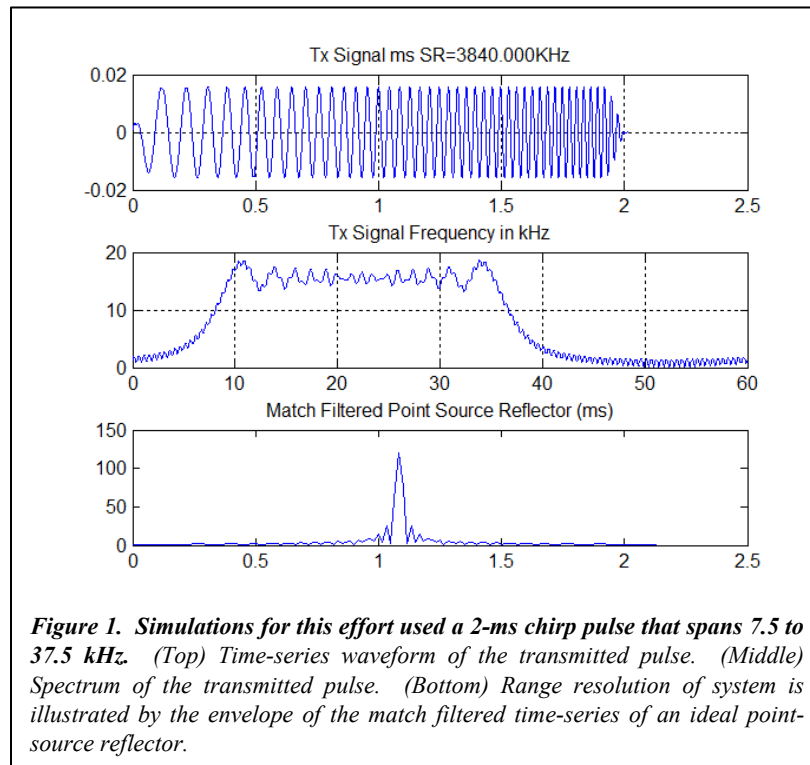
The system will be developed for SERDP by a small business capable of taking sonar systems through all stages of commercialization including research, design, manufacture, sales, and distribution. The intent is to deliver a system free of any International Traffic in Arms Regulations (ITAR) restrictions.

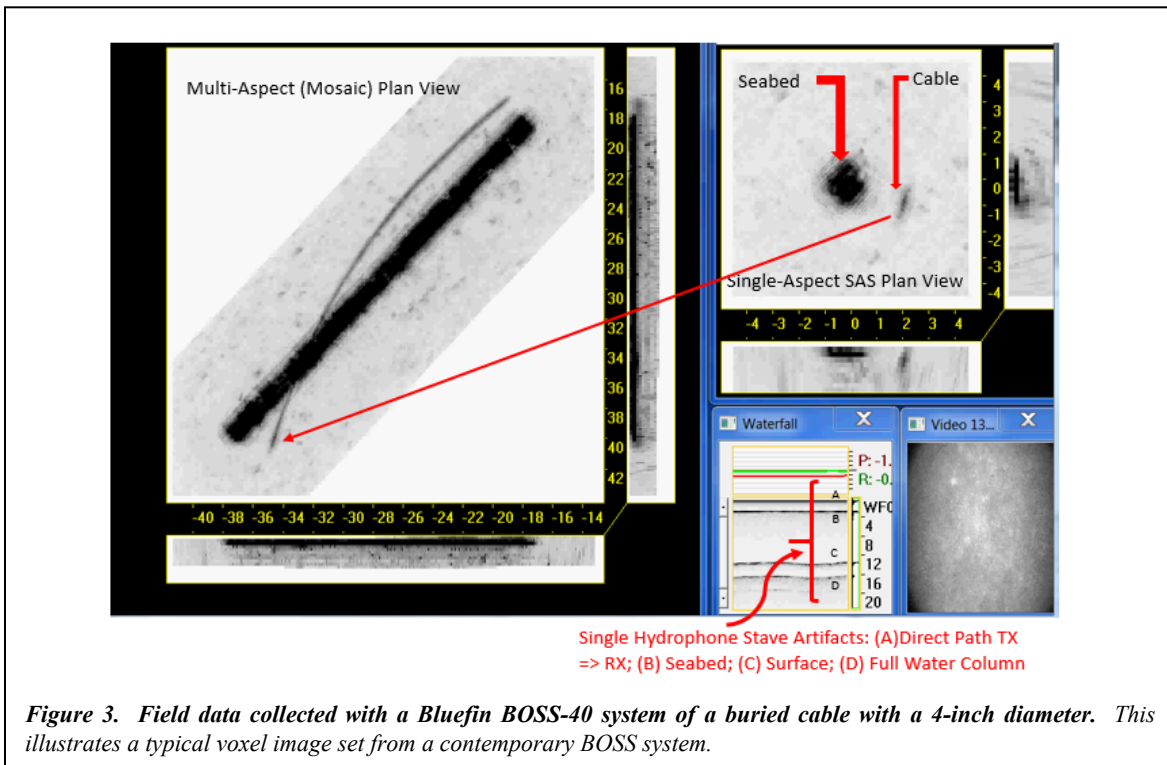
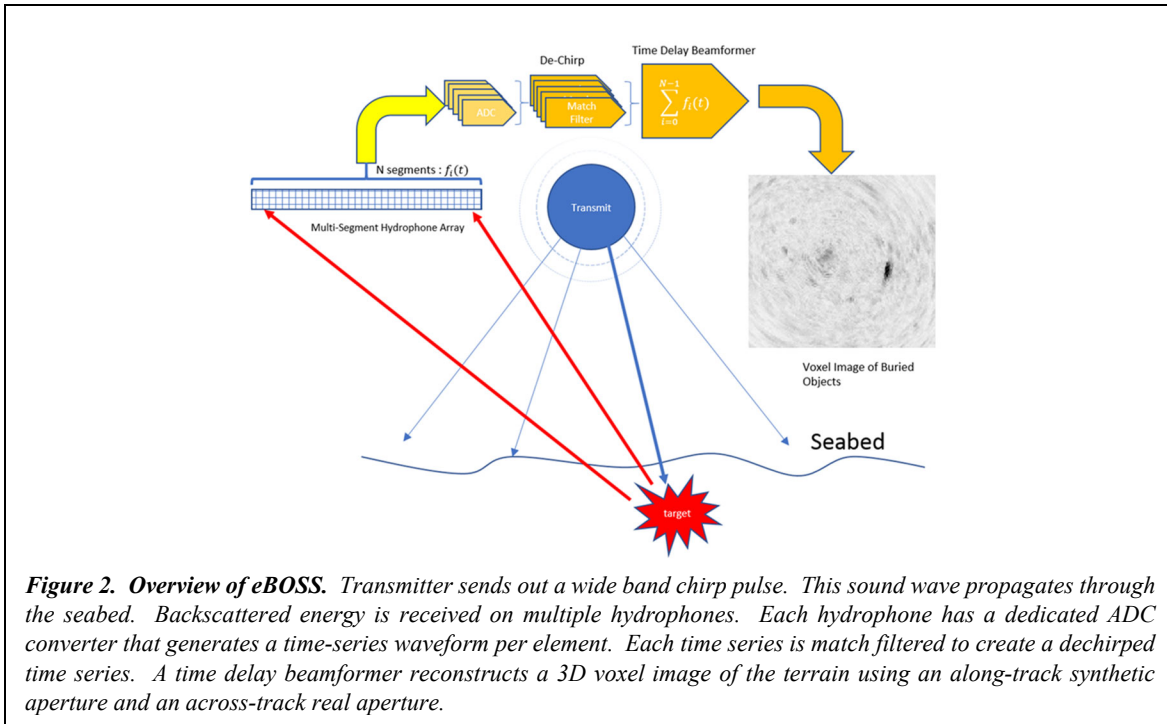
Background

Over the past 20 years, there has been a progression of multiple generations of BOSS systems. Appendix A describes some of the more significant BOSS platforms.

As a brief introduction, eBOSS systems are designed to image buried objects. They necessarily operate at sub-bottom frequencies below 50 kHz because propagation losses in sediment increase with frequency. A transmitter is used to ensonify the seabed with a wide-bandwidth FM chirp pulse, see Figure 1. Multiple hydrophone staves measure scattered sound from buried targets. Hydrophone data is digitized with high sample rate ADCs (Analog to Digital Converters). Each digitized time series is match filtered to dechirp the time series data. The dechirped data is a high resolution analytic (complex) time series. A time-delay beamformer coherently combines stave data to derive a 3D voxel image of buried objects. See Figure 2.

Extensive field data was collected from the Bluefin 40 system described in Appendix A. Figure 3 illustrates one line of field data from this BOSS system flying over a 4-inch diameter buried steel cable.





At the left of Figure 3 is the multi-aspect image which shows a plan view (looking down) and 2 side views (vs. depth) of the image of the cable. The multi-aspect image is an overlay (mosaic) of multiple signal-aspect images. At the top right is one such single-aspect image, which shows a single (SAS processed) ping of cable data. This cable is like a very long cylinder and will produce

a strong specular return at the normal to the cable face. The return can be seen in the single aspect image – only a short segment is seen at any time as the sensing platform intersects the cable’s facet normal. To paint the whole cable, these single aspect images must be overlaid on top of each other (in the multi-aspect image mosaic).

Below the single aspect image is a time series waterfall display of 1 of the 40 hydrophone staves used to create the beamformed single aspect image. The single channel image in Figure 3 shows several acoustic returns that are approximately horizontal lines:

- (A) Direct path signal from transmitter to hydrophone. This is approximately constant from ping to ping and will arrive before any other reflector in the field. It does not normally interfere with beamforming.
- (B) Seabed return. This is the approximate altitude of the platform. It is particularly strong and almost always obscures the beamformed results near nadir, as can be seen in both the single and multi-aspect images.
- (C) Surface return. This is approximately at the depth of the platform. It can be a problem in shallow water as it is strong enough to create artifacts in beamformed imagery.
- (D) Full water column returns, and other multiples. These are also strong enough to produce artifacts in shallow water beamformed results.

The field data illustrated in Figure 3 shows the current state of BOSS imagery that this effort seeks to improve. In addition to the items noted above, higher resolution is desired to create size and shape metrics for UXO’s. Note that in the figure the width of the cable appears to be much wider than 4 inches. The width also appears to get narrower as the sensor platform gets closer to the cable. This suggests that proximity does matter for spatial resolution, and therefore, the ability to operate at lower altitudes (i.e. closer to an object) can improve image quality.

Suppression of multiples and surface reflections, such as those illustrated in Figure 3, will be discussed later in the section on Transmit Source Design and Baffling.

The proposed improvements to be discussed are:

- Suppression of seabed returns which obscure the nadir region below the sensing platform.
- Resolution improvement using lower altitude operation and higher system bandwidth.
- Multisource imaging to capture all target facets.

Materials and Methods

This is a paper study inspired and backed by a 20+ year history of field data from test fields of planted UXO, mines, clutter, and pipelines. These data sets were collected from contemporary and previous BOSS systems.

Dr. Steven Schock performed the initial MATLAB simulations based on a multi-faceted model of some candidate UXO targets. Most of his MATLAB scripts have not been preserved but some of the results are presented in the monthly reports.

In simultaneous work performed by NSWC-PCD, PC SWAT (see Appendix C) was used to generate many simulation data sets of targets based on Dr. Schock's initial modeling recommendations. The more accurate PC SWAT simulations demonstrated some weaknesses in the architecture based on Dr. Schock's initial MATLAB simulations, which were subsequently corrected. The conclusions from this process, as well as some of the rationale for the conclusions, are presented here. Many simulations were performed but, for brevity, only a fraction of the simulations are included here. MATLAB was the primary tool used to process the simulated data.

There are cost/complexity tradeoffs in building an enhanced BOSS system. We evaluated these tradeoffs by consulting experts in the field to build an opinion of what is reasonably possible and to define a strategy of risk reduction for future development.

The Case for Multi-Source Imaging

The field data presented in Figure 3 show that only a small portion of a long cable is captured in each ping, and that a mosaic of these pings must be combined in the multi-aspect image to paint the whole cable. The whole cable is painted over time as the platform advances.

This is not the case for smaller targets such as UXO. For these types of targets:

- It is usually the case that only part of a UXO target will be imaged by current generation BOSS platforms.
- Targets at many views may be acoustically weak and not seen at all.

Example with a simulated mortar shell

A PC SWAT simulation of a mortar shell will be used to illustrate the effects and importance of multi-source imaging. The mortar shell is modeled as 1-meter long, 0.16-meter diameter, and buried 1/2 meter in medium sand.

To image the mortar, a BOSS platform transmitting a waveform spanning from 7.5 kHz to 37.5 kHz will be used. This pulse is shown in Figure 1 and will be used for all simulations performed in this study.

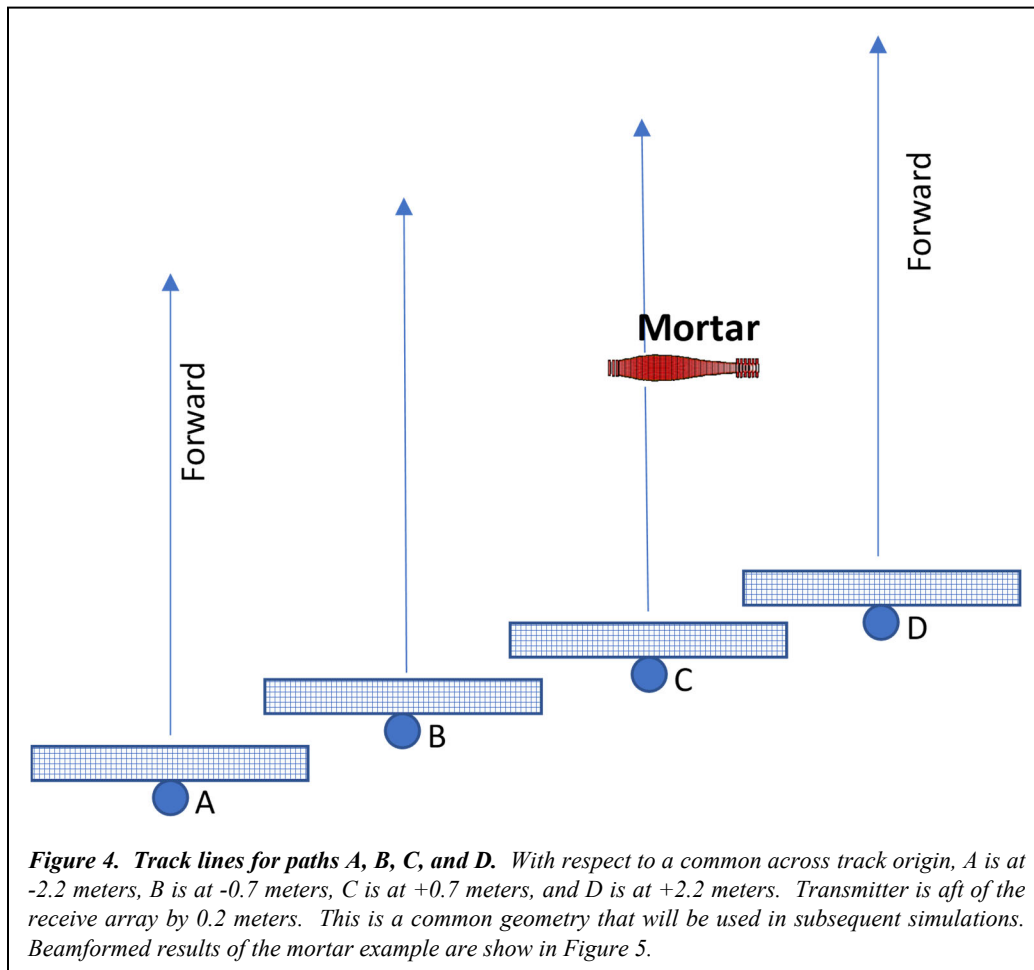
The altitude of the sensing platform is set to a constant 2 meters above the seabed. The wing will be 2-m wide in the across-track axis, have 100 hydrophones at 2-cm spacing (1/2 wavelength at

the maximum 37.5 kHz frequency), and have a 2-m wide synthetic (SAS) aperture on the along-track axis. In the along-track direction with the origin at 0, the mortar is simulated at a location +1 meter (towards the starboard side of that origin). The orientation and relative location of the target is shown in Figure 4.

Four track line offsets for the transmit/receive aperture of the sensing platform will be used, namely

- | | |
|-----------------------------|---------------------------------|
| A. -2.2 meters (port side), | C. 0.7 meters (starboard side), |
| B. -0.7 meters (port side), | D. 2.2 meters (starboard side). |

In the interest of representing a practical configuration, the transmit source is placed aft of the hydrophone array by 0.2 meters but centered in the across track direction with respect to the hydrophone aperture. In subsequent simulations of a multisource system, these A, B, C, and D track line offsets will become the locations of transmit sources for a multi-source system.

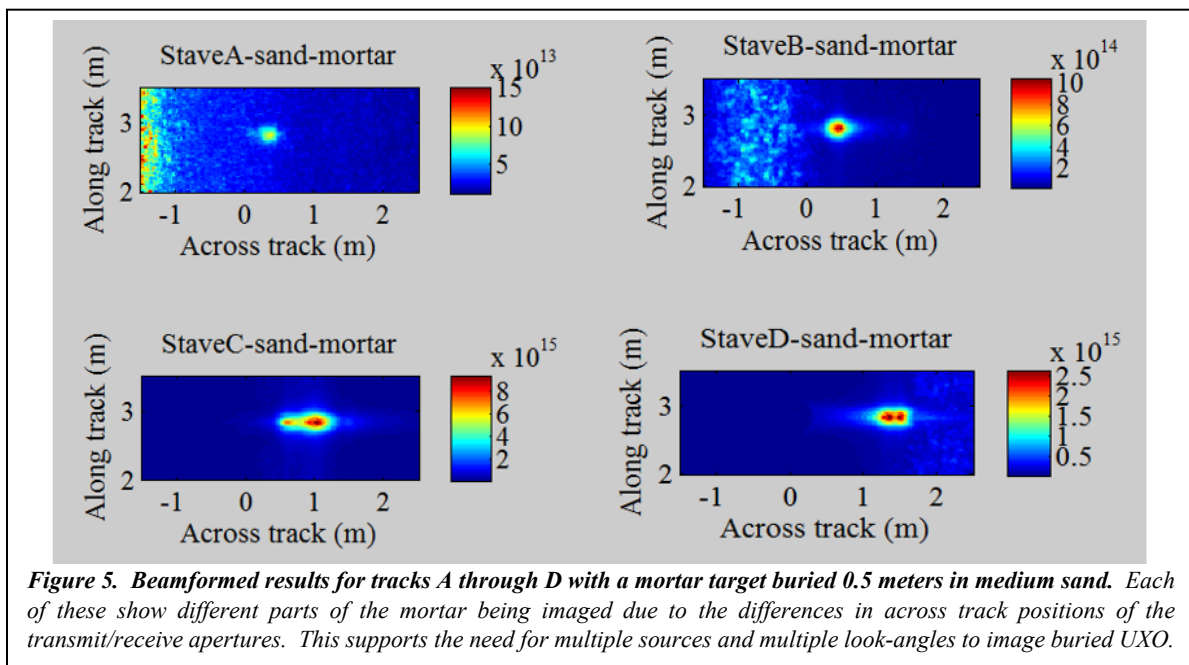


The plan view beamformed results from each of the A through D transmit positions vs. time is shown in Figure 5. While the beamformed results do show the seabed scattering noise, many other noise sources have not been enabled in PC SWAT and the actual noise level is lower in the simulation than reality. A color bar in each sub-image shows the approximate signal level of each position. The individual track lines for each source are discussed next.

For the A source, which has a 3.2-m horizontal range from the target's center at closest point of approach (CPA), the signal level is 80 times lower than the C source. The target would not be seen in actual field data recorded using source A and is substantially below a real-world noise level. It would only appear as a small glint in the field – there would be no chance of locating this relatively large UXO with data from track A alone. Since most surveys using the BOSS often employ swaths on the order of ± 10 meters, the following conclusions can be drawn:

- A UXO of comparable size and orientation would remain unseen with a contemporary generation BOSS system.
- Accurate platform positioning control is essential to provide 100% coverage of any UXO field – it is not uncommon for track lines of a survey to have position errors on the order of multiple meters.

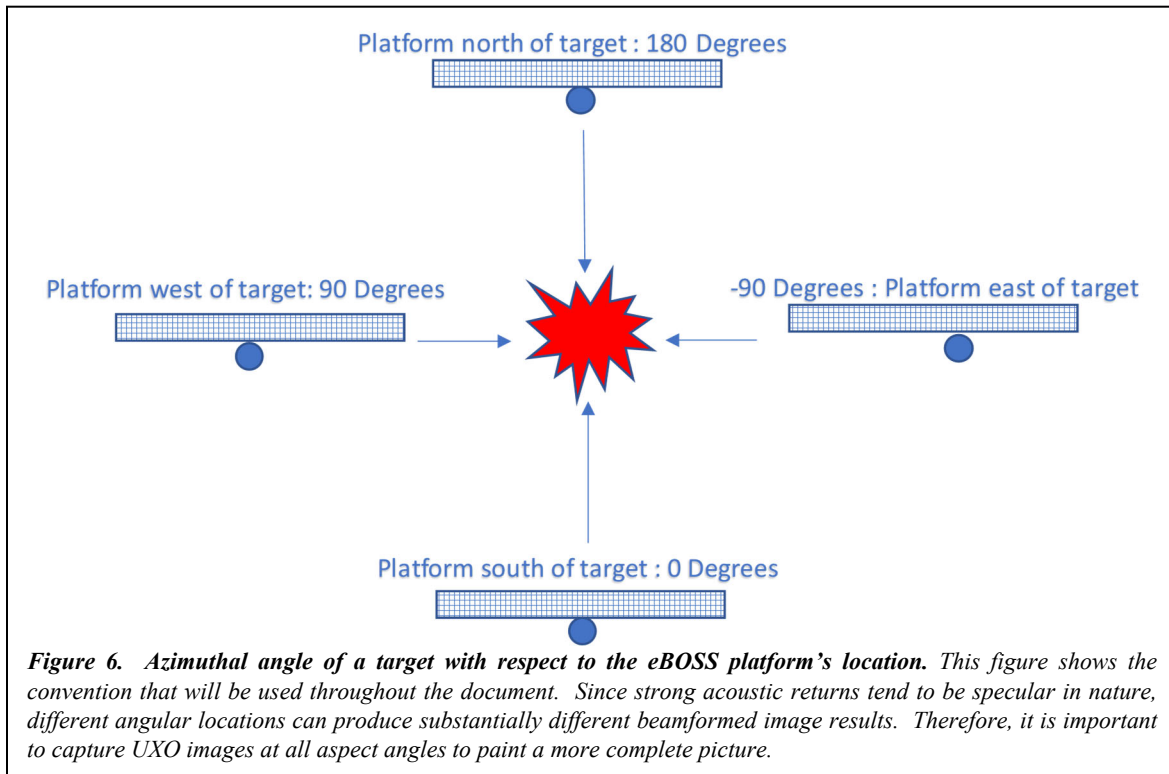
For the B source, the signal is low, 10 times lower than the C source, and might be incorrectly classified as a small rock or other clutter. Clearly, the size or shape of the target cannot be estimated from this image. Note that the B source has a 1.7-m horizontal range to the center of the mortar at CPA and is less than 1-meter horizontal range from the nose of the target at CPA. From the signal levels of the four images, the C source is in the best position to image the mortar and the D source picks up glints from the mortar's tail.



The key message of this section is that sensor platform positioning is critical for detecting UXO. As discussed later, being less than 3 meters away in horizontal range at CPA is not required to successfully image UXO. The main reason that the A source could not image this target is that this target, like most objects, is primarily visible via its strong specular returns. The aperture associated with the A source is not in a location to receive any such returns. The track-line spacing of 1.4 m in this example is much denser than can be reliably achieved in a typical survey, and shows the value of a multiple transmit source sensing platform for capturing UXO imagery.

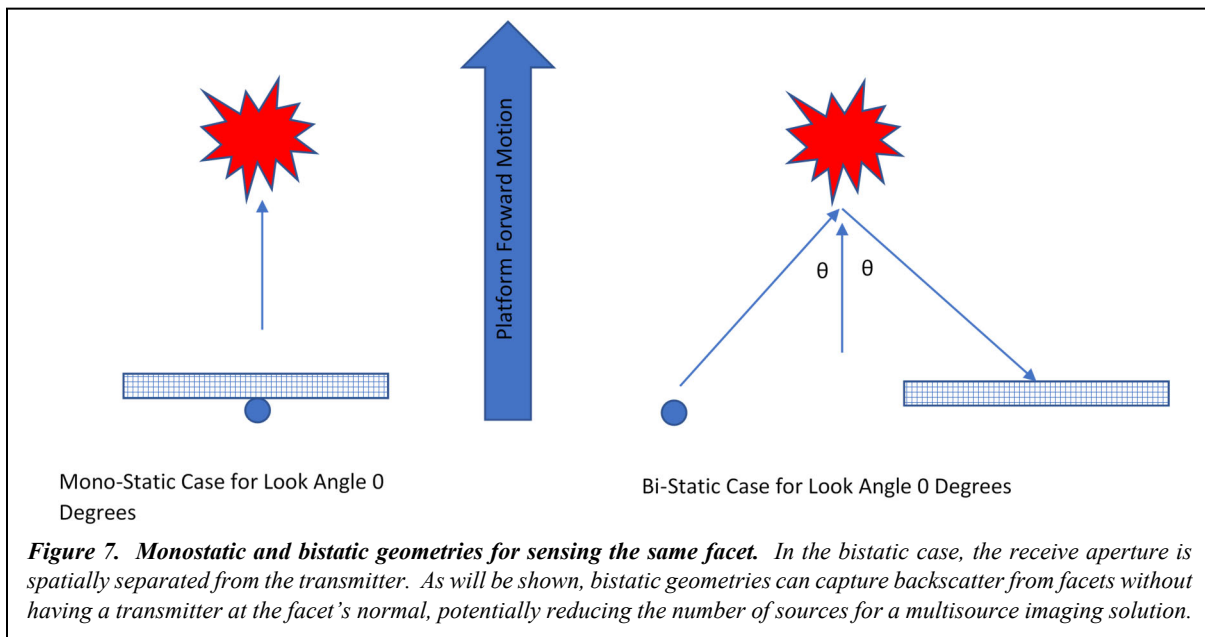
The Geometry of Look Angles

This study is primarily focused on the importance of exploiting multiple look angles on acoustic targets, and how to capture the specular returns from buried targets. These look angles are defined by a focal point on the target and the location of the sensing platform. Figure 6 defines viewing angles in the monostatic imaging case by showing a plan view (looking down) on a platform and a target. Here the platform consists of a hydrophone line array and single transmit source. Since the transmit source is approximately centered on the hydrophone array this is called the monostatic case - the transmitter and receiver(s) are approximately at the same location. As a northbound platform approaches a target, the look-angle will be 0 degrees if the platform is due south of the target. After the platform passes the target and is north of the target, the look-angle will be 180 degrees. The actual look direction has 2 degrees of freedom, the second of which might be called an elevation angle, which would be zero if the target were in the same horizontal plane as the sensing platform. Negative elevation angles indicate that the focal point is below the platform.



To capture strong specular returns present in most targets, the eBOSS sensing platform needs to be located at a wide range of look angles. For monostatic imaging, a target facet will be seen when the vector normal to that facet approximately intersects the sensing platform. If a UXO is not imaged from all look angles only part of the target's facet structure may be captured. This can make it difficult to measure size and shape information or create a complete acoustic color map.

It is also possible to bi-statically image target facets. In the bistatic case, the transmit source and receive aperture are separated. Figure 7 illustrates an approximately equivalent bistatic geometry for the 0-degree azimuthal look angle case. It is called equivalent because a facet seen at 0 degrees in the monostatic geometry is seen in this bistatic geometry when the facet normal bisects the angle formed between the transmit source and the receive aperture.



UXO Shapes

This section presents several common UXO shapes. While formulas are included, the exact formulas are not important. The shapes presented are:

- A cylinder, which has axial symmetry – a common shape for the body of a UXO.
- A small square plate – perhaps representative of a tail fin. This facet shape has a more directional return.
- A sphere – a common shape for an end of a UXO such as a bullet tip. This shape is omnidirectional (non-specular return).

The first UXO shape to be discussed is the cylinder. Based on Urlick [13] Table 9.1, the target strength (TS) for a cylinder can be calculated from

$$t = \frac{aL^2}{2\lambda} \left(\frac{\sin\beta}{\beta} \right)^2 \cos(\theta)$$

where

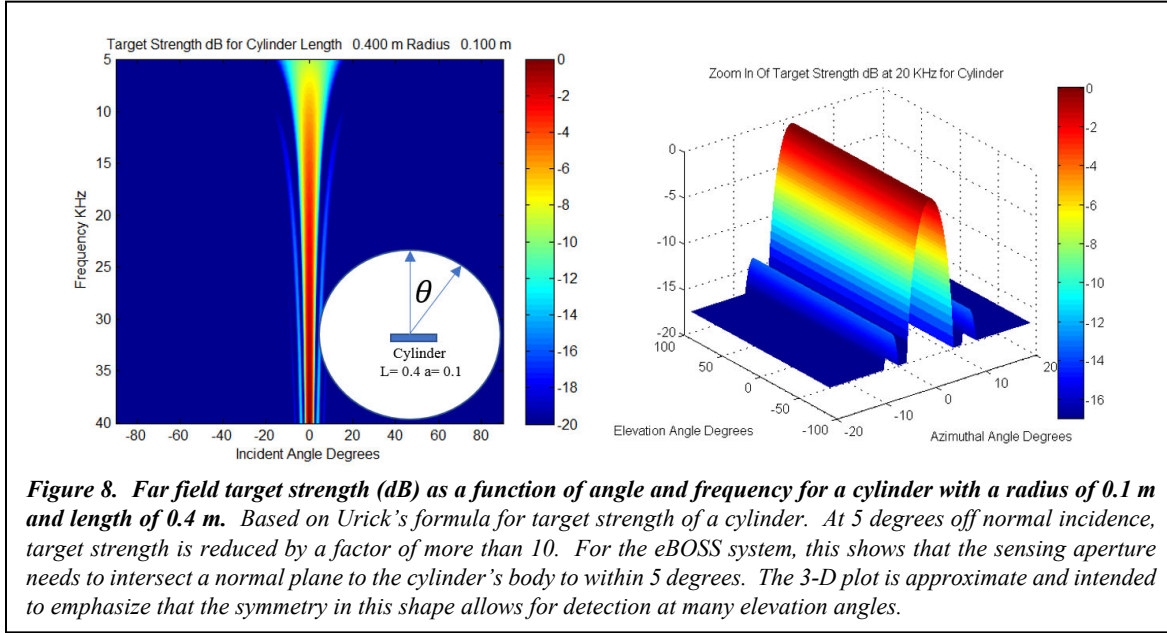
$$TS = 10 \log(t)$$

and

$$\beta = \left(\frac{2\pi}{\lambda} \right) L \sin(\theta),$$

λ = wavelength,
 a = cylinder radius,
 L = cylinder length,
 θ = incident angle.

Figure 8 shows the far-field target strength of a typical UXO cylinder with a 0.4-m length and 0.1-m radius for frequencies between 5 kHz and 40 kHz.



For the frequencies of interest, this cylinder shape produces a strong specular reflection normal to the cylinder body that rapidly drops off by more than a factor of 10 at angles of incidence greater than 5 degrees. Also note that for higher frequencies, the drop off is more rapid and the specular return is more directional. If lying horizontal on the seabed most cylinders can be detected by a conventional (non-multisource) BOSS system that mows the field because the plane defined by the cylinder normal will ultimately intercept the BOSS's trajectory. Many UXO's have a cylinder-like shape and therefore can be imaged by a conventional BOSS, provided that their normal (if buried) falls within the critical angle.

Another example shape is a rectangular plate. Also based on Urick [13] Table 9.1, the target strength can be calculated from

$$t = \left[\frac{ab}{\lambda} \frac{\sin(\beta)}{\beta} \cos(\theta) \right]^2$$

where

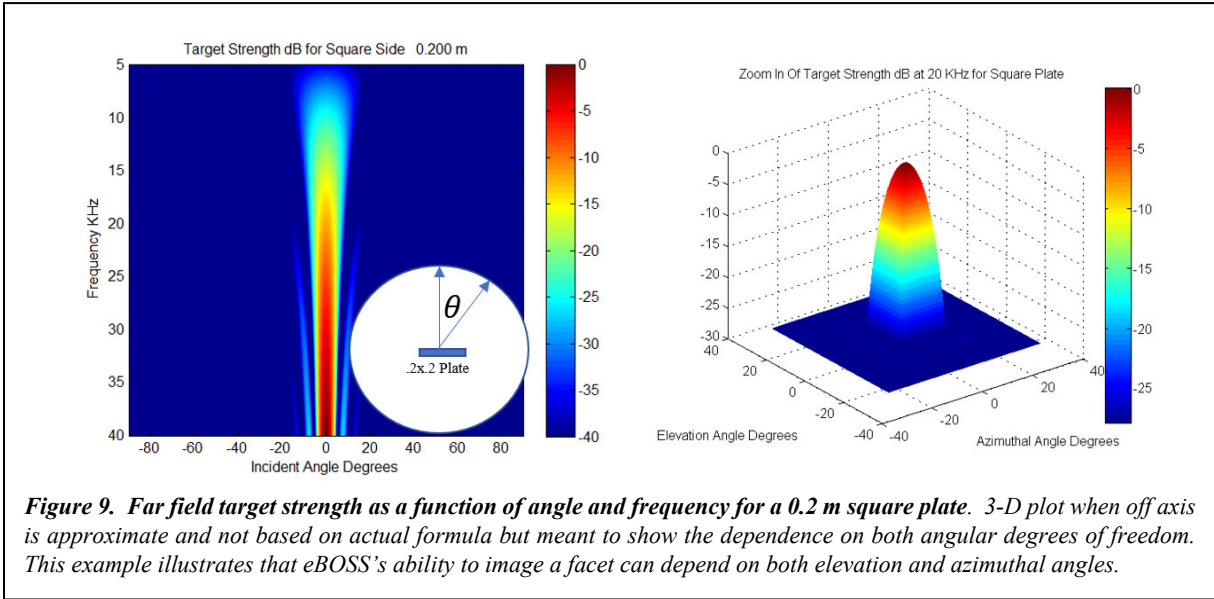
a and b are the side dimensions of the rectangle,

$$\beta = \frac{2\pi}{\lambda} a \sin(\theta),$$

and

λ is the wavelength.

The far field target strength for a small 0.2-m square plate for frequencies between 5 kHz and 40 kHz is shown in Figure 9. This shape is highly directional in both angular degrees-of-freedom and is therefore important to have the platform intersect this facet's normal. A conventional single-source BOSS system is less likely to capture this facet and make a detection.



Another common type of UXO shape is an approximately spherical body, such as the end of a mortar or bullet. The sphere produces a close to omni-directional / non-specular target strength, similar to a point-source reflector. Aspect angle is not important for imaging a spherical body. For a large sphere with respect to wavelength, Urlick table 9.1 lists an approximate formula as:

$$t = a^2/4$$

where

a is the radius.

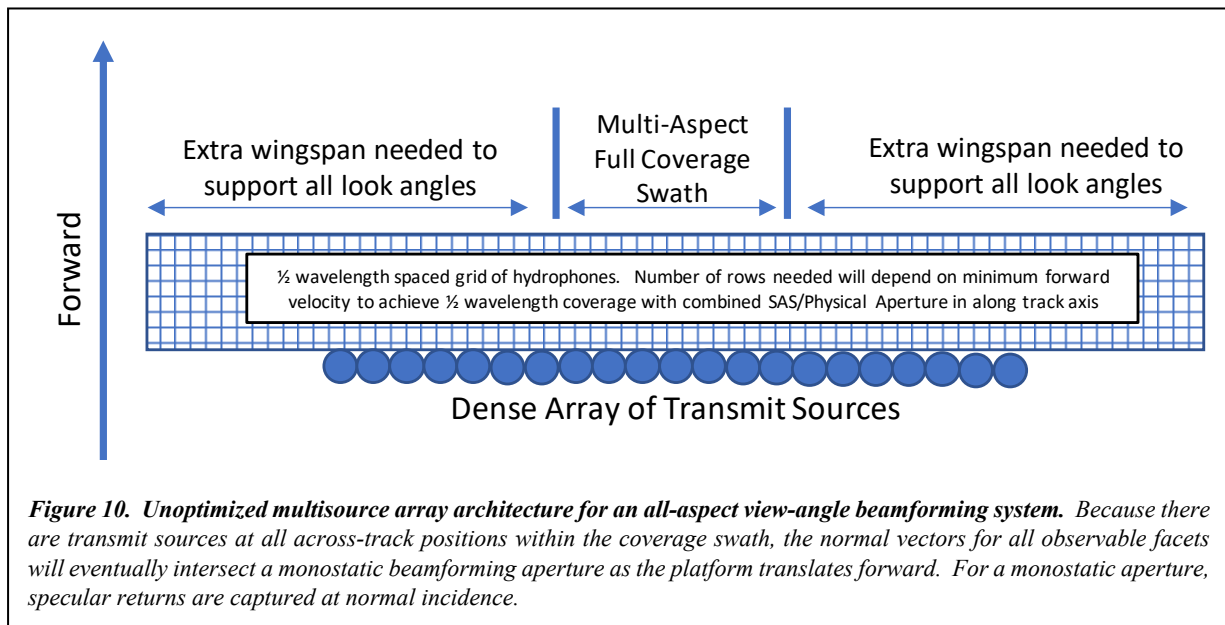
The target strength of an example sphere and cylinder will now be compared. One object simulated in subsequent sections is a 0.4 m wide cylinder with a hemispherical (spherical) endcap and with a 0.1-meter cylinder radius. Using the above formula, the (far field) target strength of a 0.1 m radius sphere is -26 dB. The target strength of the cylinder at its (specular) normal ranges between

-13 dB (for 7.5 kHz) to -7 dB (for 37.5 kHz). In this case, the target strength of the cylinder body normal is 13 dB to 19 dB higher than the endcap, so it would be reasonable to expect the specular return from the cylinder body facet to dominate the beamformed image results for this object.

Unoptimized Multisource Architecture

This section presents an impractical design for a UXO hunting platform to illustrate a concept. To image a target facet, the platform transmit/receive aperture must intersect the normal to the target's facet, which is where the specular returns can be captured in the monostatic imaging case.

Let a remediation site be surveyed at a constant (and low) altitude so that, over time, the platform's aperture passes through all points at this altitude. Suppose that this idealized platform contains transmit sources that are densely populated along the across-track axis of the sensor platform's wing. The across-track length of this wing aperture is determined by the desired coverage swath per line. Multiple hydrophones are positioned across this wing aperture to provide across track resolution and directivity. A synthetic (SAS) aperture is created in the along-track direction as the platform advances through the environment. This architecture is illustrated in Figure 10.



At the risk of being redundant, please note the obvious limitations of this system. Not all target facets are observable. Any facet normal that does not point out of the sea bed within the critical angle of the sediment is not observable (because the sensing platform cannot be positioned to intersect that normal). This means that the zero-elevation case, which is commonly used to create a 1 degree-of-freedom acoustic color map, is not available to any non-invasive acoustic system. Any flush buried facets with a normal that is near 90 degrees in elevation angle (pointing close to straight up) will have a similar repose to the strong seabed return and will be difficult to image.

Optimized Multisource Architecture

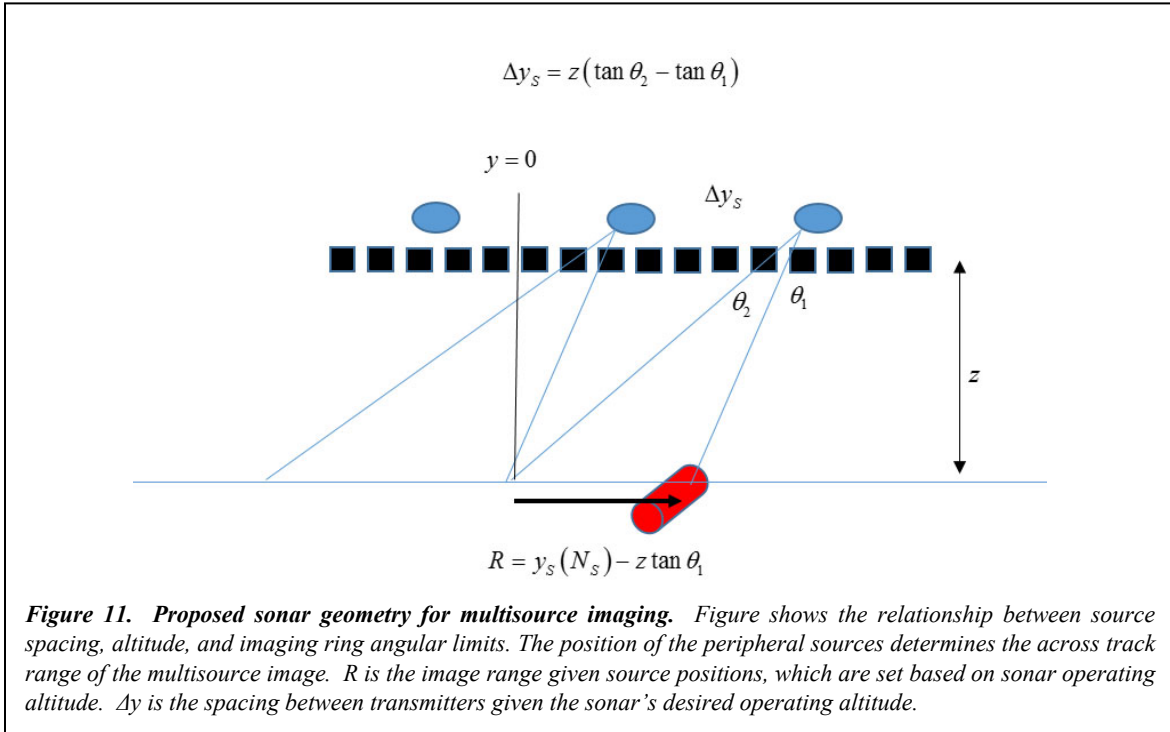
Next, an optimized multisource architecture is proposed that can be derived from an operating altitude. Equations will be provided to calculate

- Separation between sources,
- Pulse repetition rate (PRR) and pulse rate interval (PRI),
- Number of hydrophone rows in the along-track axis,
- Maximum forward velocity of the platform,
- Subaperture width, *i.e.* the across-track subapertures centered on each source,
- Total width of the receive aperture and wing

Separation Between Sources

The across-track geometry of the optimized multisource array design is shown in Figure 11. The graphic illustrates an optimized source spacing for a given operating altitude. Multisource imaging requires that sources pass along opposite sides of a target to ensonify all its observable facets. The hydrophone data is processed using nearfield focusing within a fixed range of angles of seabed incidence, $\theta_1 \leq \theta \leq \theta_2$, forming an imaging annulus as shown in Figure 12.

For the analyses in this paper, we set $\theta_1 = 35^\circ$, which is the minimum angle of incidence to be evaluated. This will prevent the strong specular reflections from the seafloor and of sand ripples from degrading target imagery. We also set $\theta_2 = 55^\circ$ to avoid the high sediment-water interface transmission loss near the critical angle for sand. Figure 12 shows the coverage of the imaging annulus, $35^\circ \leq \theta_i \leq 55^\circ$, on the seabed and the source spacing.



To simplify the algorithm, these angular constraints are referenced to the horizontal range at the seabed, that is, only the subbottom *beneath* the annulus on the seafloor is evaluated. Future work will evaluate the angular cone.

Using minimum and maximum incident angles of 35 and 55 degrees respectively, the imaging bands are defined by the following R_{\min} and R_{\max} limits:

$$R_{\min} = \textit{Altitude} * \tan(35)$$

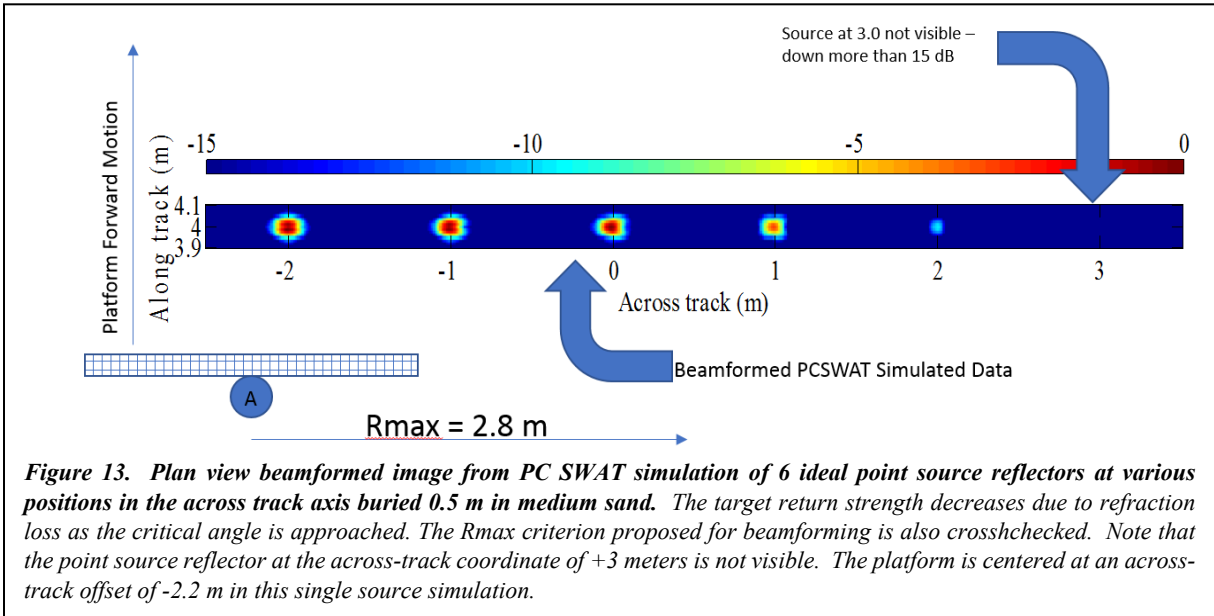
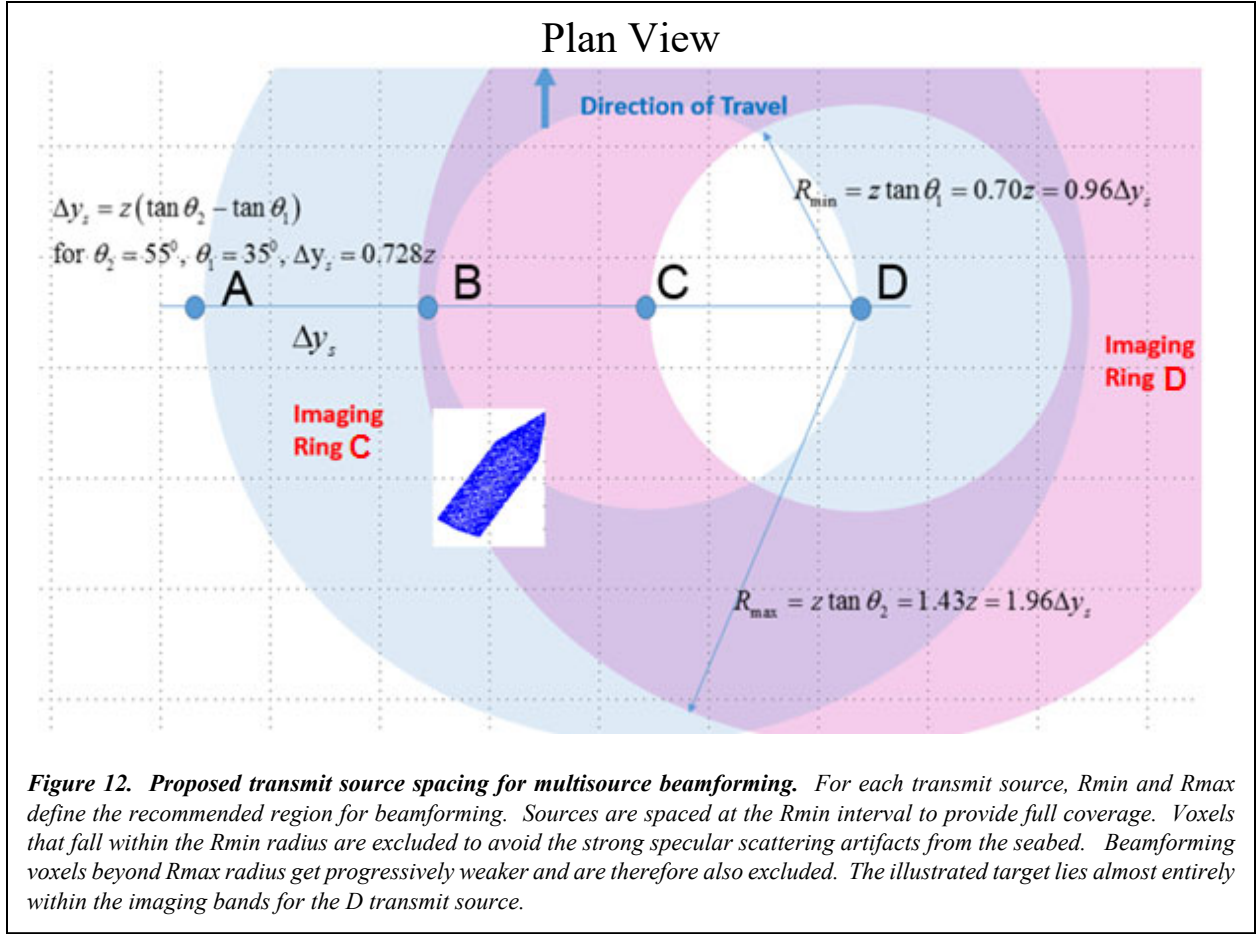
$$R_{\max} = \textit{Altitude} * \tan(55)$$

For a 2-meter altitude, these angles evaluate to

$$R_{\min} = 1.4 \text{ m}$$

$$R_{\max} = 2.86 \text{ m.}$$

Figure 13 shows the beamformed results of a PC SWAT simulation designed to cross check the R_{\max} criteria. The simulation uses 6 point-source reflectors that are buried 0.5 meters in medium sand, which has a known sound velocity of 1767 m/s. Let a single-source BOSS platform have an altitude of 2 meters with a horizontal offset of -2.2 m of the origin (port side). Then, let the six point-source reflectors be evenly spaced at offsets of -2 m through 3 m in the across-track axis. Figure 13 illustrates the beamformed signal as it gets progressively weaker beyond the R_{\max} limit. The point-source reflector at offset +1.0 (3.2 meters from the platform origin) seems strong, but this figure is a multi-aspect composite image. The stronger value at CPA masks the weaker results (not shown) as the platform gets farther from CPA either fore or aft of the targets. The target at 3.0 m is more than 15 dB weaker than the target at -2.0 m, which is not visible in this log-space image. While the choice of 55 degrees for R_{\max} is approximate, simulation results show that this value is reasonable.



Pulse Repetition Rate (PRR)

The pulse repetition rate for a given transmitter is set to ensure that the rows of hydrophones spatially sample the environment at half wavelength in the along-track axis without redundant sampling. When the source ping rate is set properly, space is sampled at a constant half-wavelength interval. The pulse repetition rate of a given source, PRR_s , depends on the half wavelength hydrophone element spacing Δx , the number of hydrophone rows N_r , and sonar velocity V , and is given by

$$PRR_s = \frac{V}{N_r \Delta x}.$$

When multiple sources are employed, the rate of sequential source transmission depends on the number of sources N_s and is given by

$$PRR_{ss} = N_s PRR_s.$$

Determining the Number of Hydrophone Rows

The data from the farthest point in the imaging ring must be acquired before the next source pings. The allowable number of hydrophone rows is based on the longest two-way travel time for a target buried 1 m at the outer edge of the imaging annulus as shown in Figure 14.

A conservative two-way travel time approximation is given by

$$T_{2way} = \frac{\left(\frac{z+1}{\cos \theta_2} + \sqrt{\left(\tan \theta_2 (1+z) + \frac{\sqrt{2}z}{2} \right)^2 + (z+1)^2} \right)}{c}.$$

Refer to Figure 11 for a description of the geometry, where z is the platform altitude and the maximum burial depth of interest is 1 meter. This formula assumes that the sediment and seawater sound velocities are identical. Since the sound speed in sediment is higher than water, the time calculated by this formula is slightly larger than the actual two-way travel time. Therefore, it is a valid approximation to use when calculating the minimum PRR.

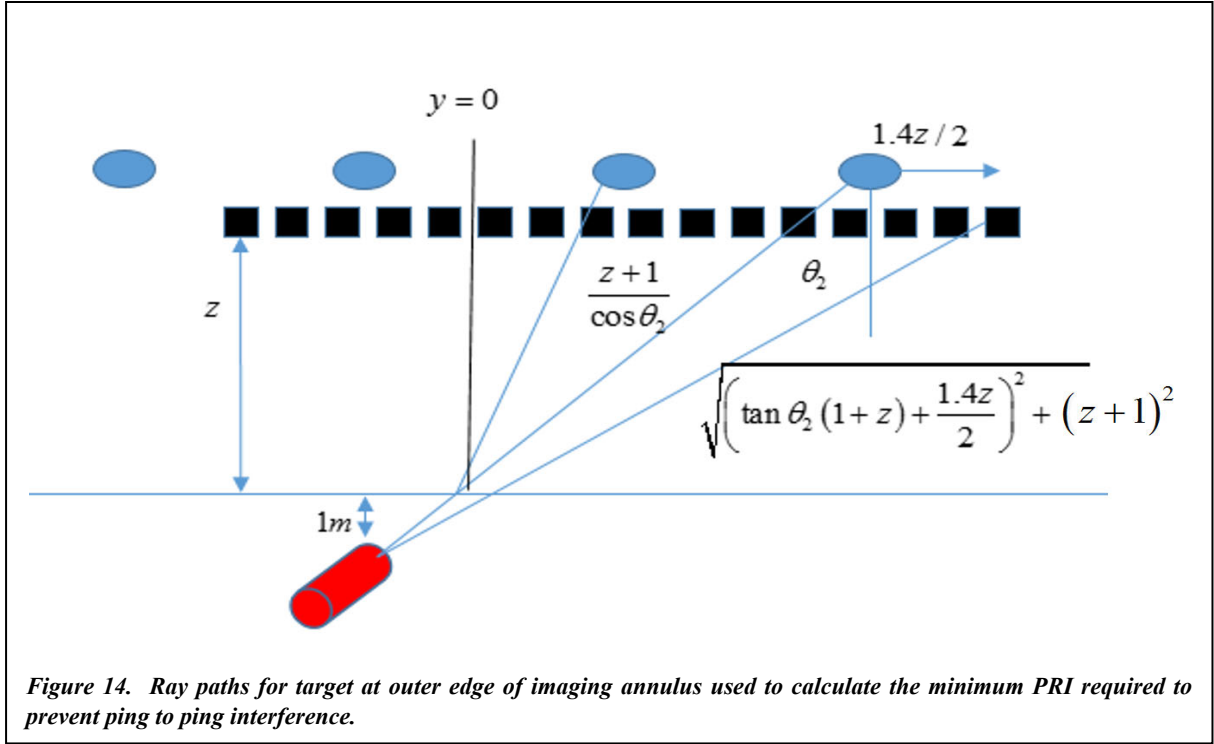
The minimum pulse repetition interval for adjacent transmitters is

$$PRI_{min} = T_{2way} + T_{pulse}$$

where T_{pulse} is pulse length.

Therefore, the minimum PRI for a single source in a round robin transmission mode is

$$PRI_{min,1} = PRI_{min} N_s.$$



The minimum number of hydrophone rows in the along-track axis that are needed to satisfy the spatial sampling criterion of the SAS aperture for a given PRI and forward velocity is

$$N_r = \left\lceil \frac{PRI_{min} N_s V}{\Delta x} \right\rceil$$

where:

$\lceil \rceil$ indicates rounding towards positive infinity,

V is the forward velocity of the platform,

Δx is the hydrophone spacing.

Given the numbers of hydrophone rows and sources, and consistent with the PRR discussed in the previous section, the PRI for adjacent sources is

$$PRI = \frac{\Delta x N_r}{V N_s}$$

and the PRI for a given source, i , is

$$PRI_i = \frac{\Delta x N_r}{v}.$$

The distance traveled between transmissions of adjacent sources is

$$V \times PRI = \frac{\Delta x N_r}{N_s}.$$

The distance traveled between transmissions of the same source is

$$V \times PRI_i = \Delta x N_r.$$

The maximum allowable sonar velocity for N_r rows of hydrophones is

$$V = \frac{\Delta x N_r}{PRI_{min} N_s}.$$

Figure 15 plots the maximum sonar velocity for platforms with 1, 2, 3, and 4 rows of hydrophones. The velocities are calculated for sonar altitudes between 1 and 3 m above the target with a 2 cm hydrophone spacing. For velocities <0.5 m/s and altitudes <2 m, a 4-source array using only one row of hydrophones can be used.

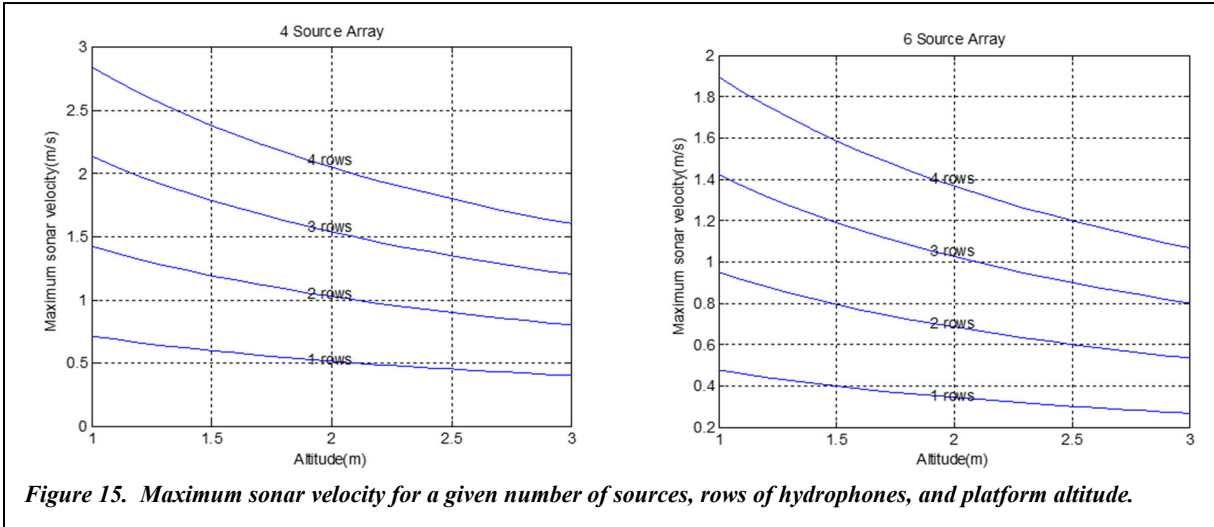


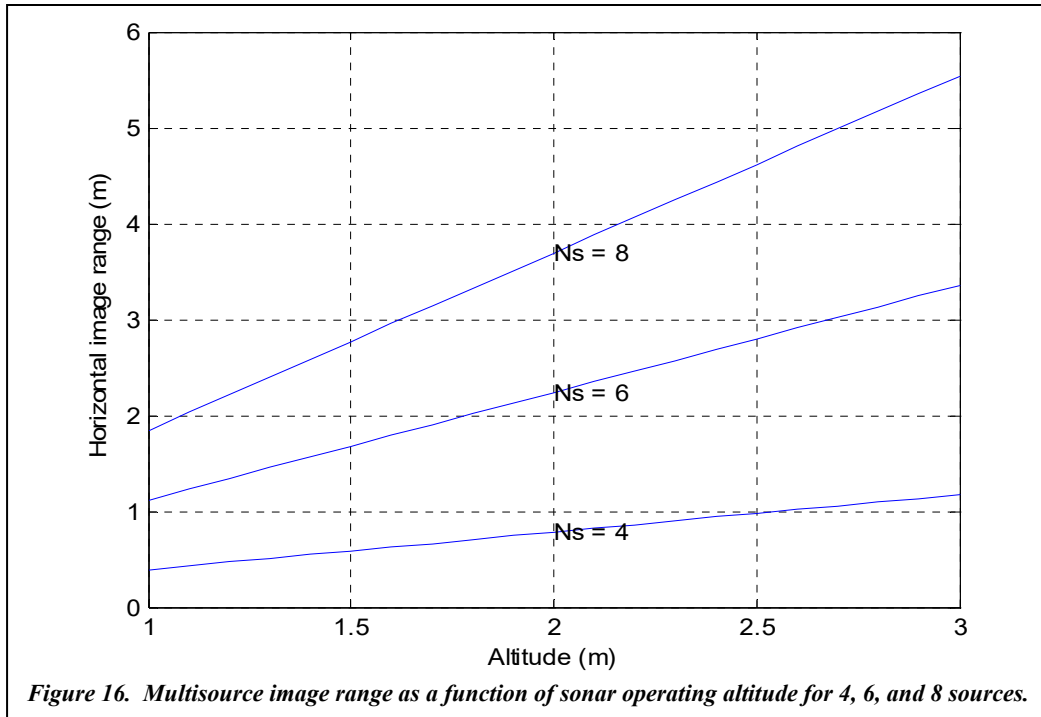
Figure 15. Maximum sonar velocity for a given number of sources, rows of hydrophones, and platform altitude.

The maximum velocity while employing a single row of hydrophones is

$$V_{N_r=1} = \frac{\Delta x}{PRI_{Smin}}.$$

Determining Multisource Image Range

The range at which a multisource system can image an object is much less than the range at which the sonar can detect buried objects. The equation in Figure 11 provides the expression for calculating image range and source separation, which are based on sonar operating altitude. Figure 16 is used to lookup image range (half of image swath) given the sonar's operating altitude and number of sources. Using the guideline for source spacing, a 6-source system at a 2-meter altitude will have a multisource image range of 2.2 meters (a 4.4-meter swath).

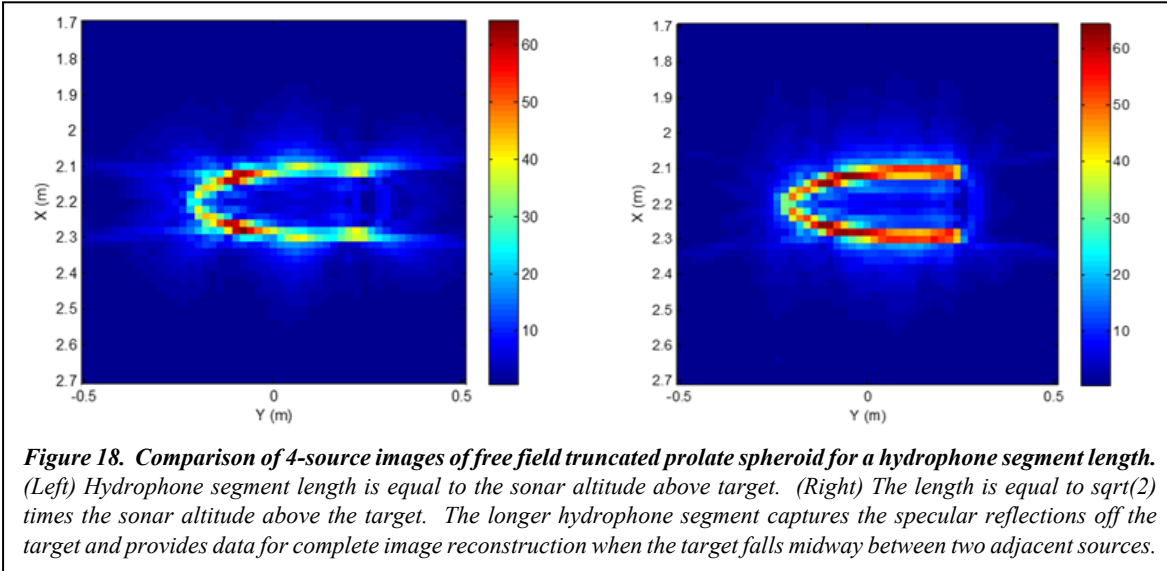
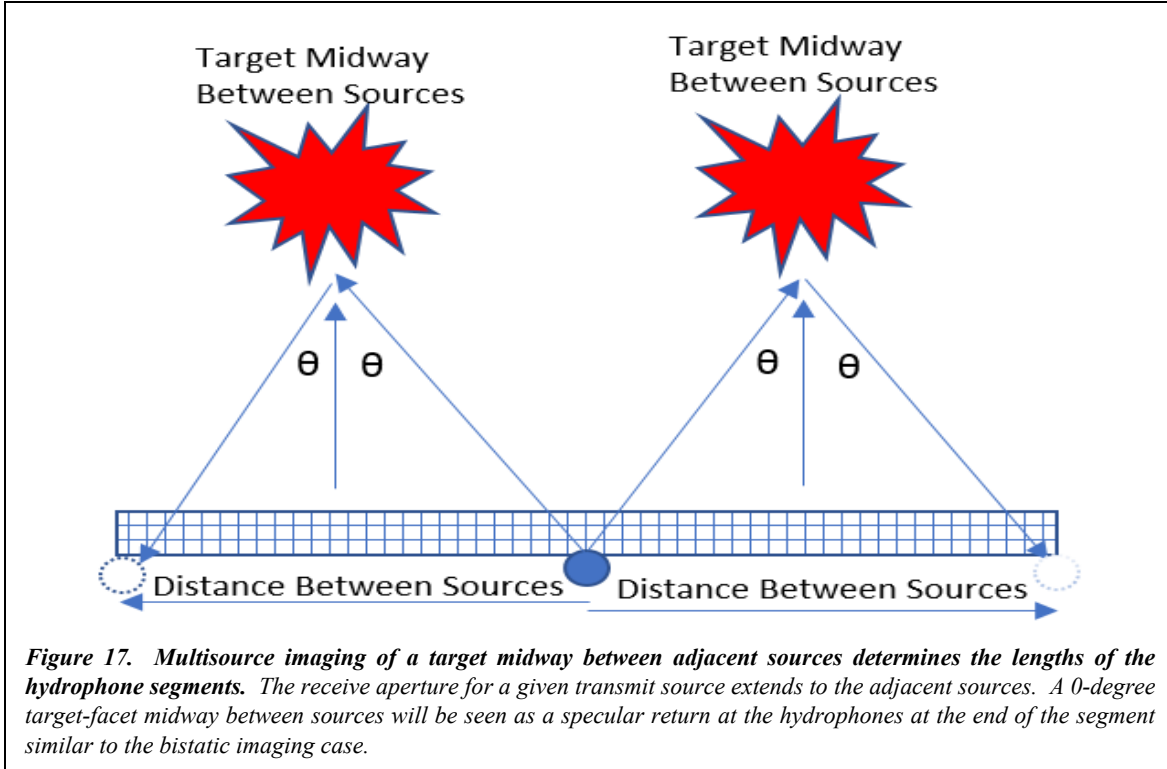


Determining the Length of the Across-Track Subaperture

Since the objective is to image buried targets, there is little value in using hydrophones that are near or beyond the critical angle. The loss in return signal strength has already been illustrated in Figure 13. This is a practical limitation. The critical angle limits the maximum effective aperture per transmit source.

There is also a minimum aperture length. For sparsely spaced sources, the subaperture of hydrophones centered on each source should be sufficiently long to capture specular reflections off all sides of a target that is located midway between adjacent sources. See Figure 17.

Figure 18 shows that if the hydrophone aperture is sufficiently long, specular reflections off each part of this target will be acquired, thereby allowing a more complete image. When the hydrophone segment length is approximately 1.4 altitudes, it is equal to twice the recommended source spacing and multisource imaging is complete.



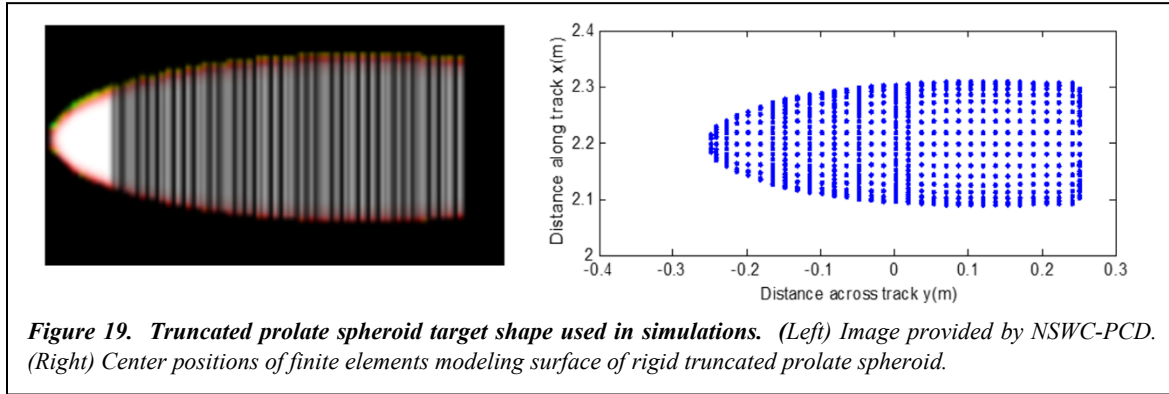
Generating Synthetic Target Data

In addition to PC SWAT, preliminary synthetic data for a UXO target in water (free field) was generated using (George and Bahl, 1995) [16]

$$p = \sum_{m=1}^{N_f} \frac{1}{R_{th}R_{ts}} \sum_{n=0}^{N_{fft}} X(\omega) e^{-j\omega \frac{R_{th}+R_{ts}}{c}} \frac{A \sin(k\sqrt{A} \sin \theta)}{2\pi\sqrt{A} \sin \theta} \cos \theta,$$

which is the pressure measured at a hydrophone caused by an acoustic pulse with amplitude spectrum $X(\omega)$ scattering off N_f facets with area A . The angle θ is between the facet normal and the source-to-facet vector. R_{th} and R_{ts} are facet-to-hydrophone and facet-to-source distances.

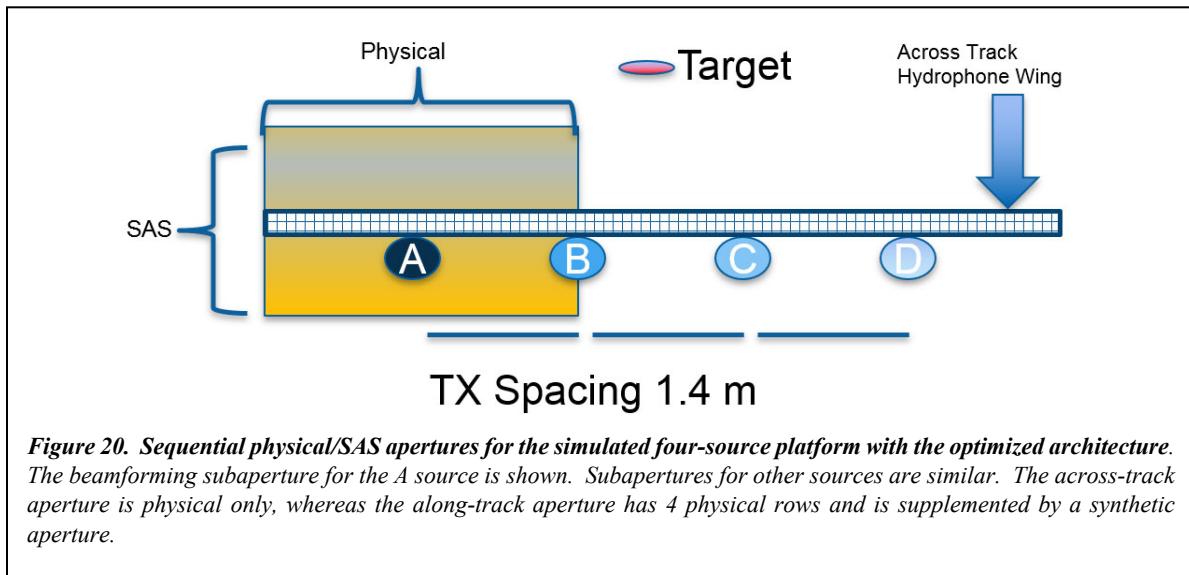
One target shape selected for this study is a truncated prolate spheroid, which is shown in Figure 19. NSWC-PCD performed several PC SWAT simulations with this shape.

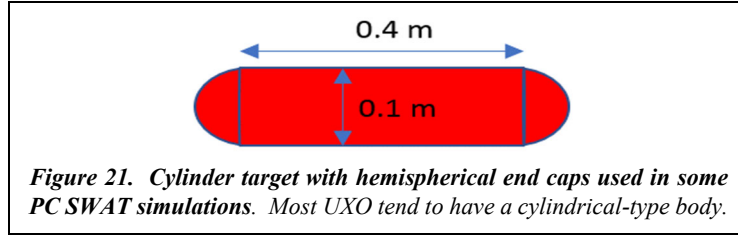


Simulated Multisource Imaging with a 0.4 m Cylindrical Target

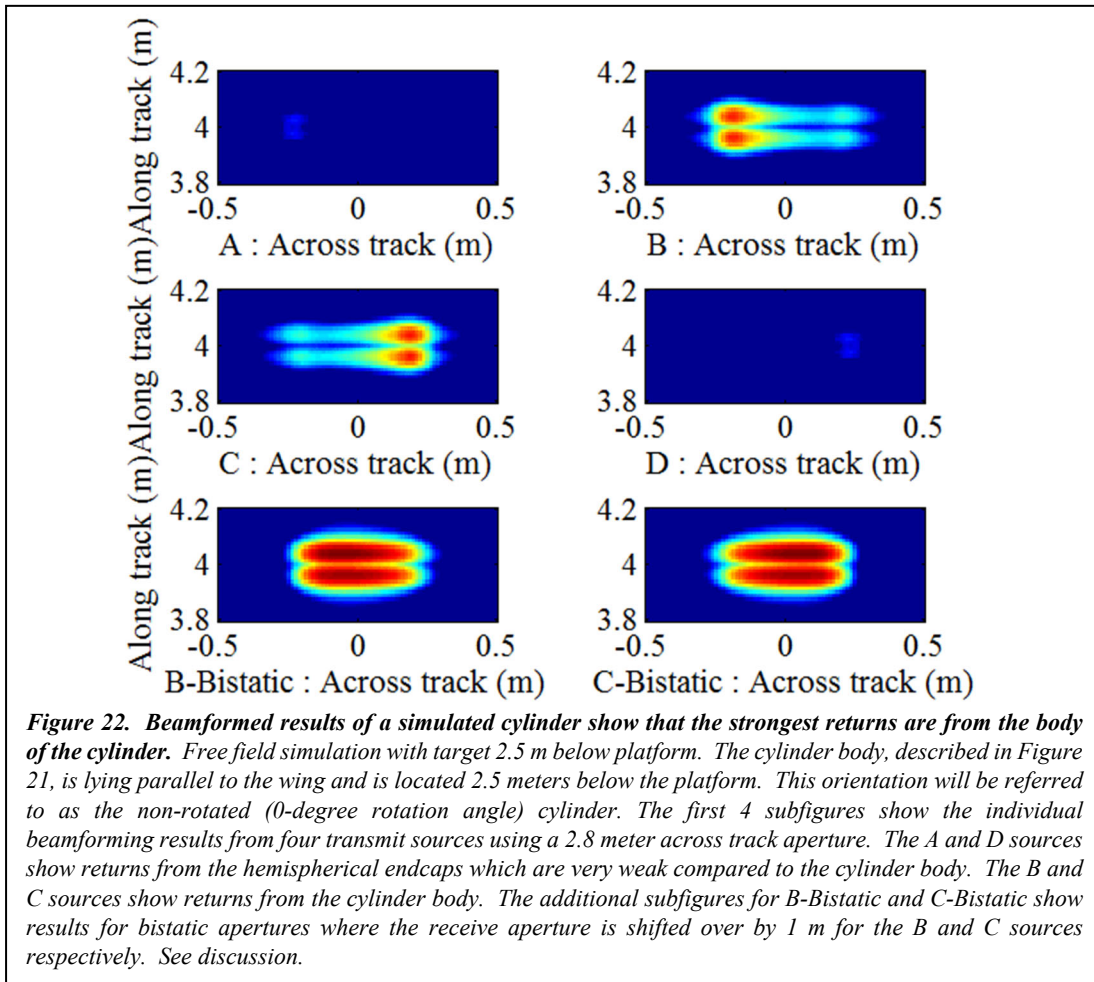
PC SWAT simulations for this architecture will now be presented using a 4-sourced platform that is designed to survey at a 2-meter altitude. Using the guidelines for an optimized architecture, the across-track width is 7.0 m including all the hydrophones. The along-track aperture has 4 physical rows and is supplemented with a synthetic aperture that is 2 meters long in the along-track axis.

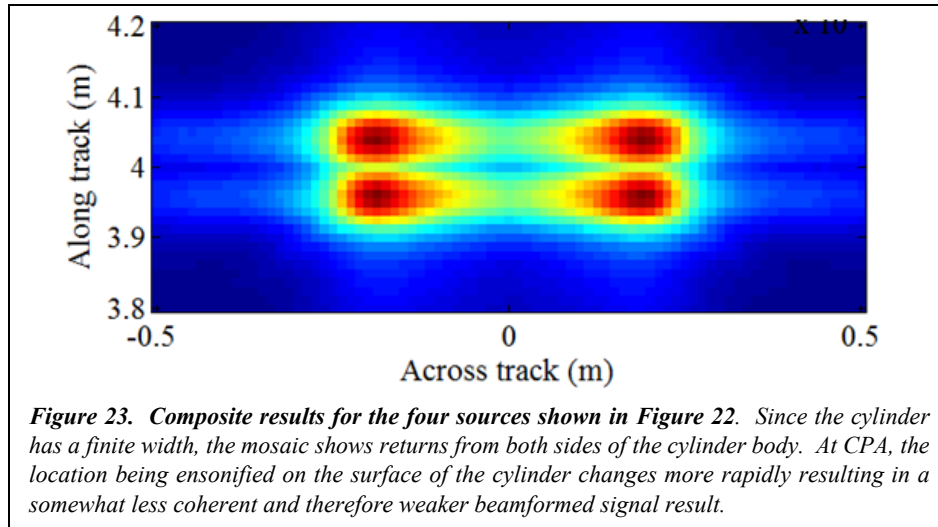
The target is placed ahead of the platform and 2.5 m below. As shown in Figure 20, this is at the center of the across-track aperture, which is midway between the B and C sources. Figure 21 shows the target is cylindrical, 0.4 m long, 0.1 m wide, and has hemispherical endcaps.





In the first simulation, the cylinder is positioned with its length parallel to the eBOSS wing, referred to as the 0-degree rotation of the cylinder. The simulation is free field (2.5 m of water between the sonar and the target). Using a 1.25 cm voxel resolution, Figure 22 shows the plan-view multi-aspect images from the four sources. The combination of all four sources is shown as a mosaic in Figure 23. The hemispherical endcap is substantially weaker than the cylinder body, which can be seen in the individual source images but does not contribute much to the composite image. This result will be common with all the simulations in this paper – the specular/directional returns from the cylinder body contribute nearly all the image content in these rigid body simulations.





Also note that the figures appear to show two, spatially separated targets rather than a single cylinder. In this scenario, the proposed source-target-receiver geometry cannot capture the top/middle of the cylinder. When the platform is directly above the target, the beamforming is less coherent because the view aspect is changing more rapidly in the forward direction. This results in a relatively lower level of processing/array gain. Additionally, the RMin restriction prevents the sonar from imaging the cylinder at higher elevation angles. Again, the RMin restriction is needed to mitigate the effects of the strong direct-path backscatter from the water-sediment interface.

In addition to the four monostatic source images in Figure 22, two bistatic images are also shown. The B-Bistatic image was created by shifting the receive aperture by +1 meter (to the starboard side - towards the target focal area). Similarly, the C-Bistatic image was created by shifting the receive aperture over by -1 meter (to the port side – also towards the target focal area). Both bistatic images provide similar results. Note that the bistatic processing of the data produces better images of the cylinder body than the monostatic cases.

Note that the high intensity regions in Figure 23 are not the endcap return. They are part of the cylinder facet return. This simulation was chosen as a stress case of the multi-source architecture. Since the receive aperture in these simulations ends at the adjacent transmit sources, this 0-degree target facet positioned midway between sources will have a backscattering beampattern with a peak that is directed at exactly the endpoint of the receive aperture. This means that the receive aperture can only capture $\frac{1}{2}$ of the signal energy from the facet. The other half of the energy is directed away from the receiver aperture. Shifting the aperture over to create a bistatic imager allows more of the energy to be captured.

The amount of additional aperture length depends on the beampattern, which varies with acoustic frequency, as well as target size and shape. Extending a monostatic aperture to capture all the energy for this special case may compromise beamforming signal-to-noise ratio. (Because

hydrophones that do not capture backscattered signal energy will still contribute noise.) For the B source, the target in this example is on the starboard side. Symmetrically extending the aperture will add hydrophone elements far away on the port side, which pick up progressively weaker signal for buried targets due to the effects of grazing angle and critical angles.

A more complex dynamic aperture might be a useful alternative to symmetrically extending the aperture. Dynamic aperture processing is achieved by shifting the receive aperture in the across track direction toward each focal point so that the targets on the port side of a transmit source have an aperture center biased toward the port side and vice versa. Future work is needed to test dynamic aperture processing and to determine if the imaging performance justifies the complexity of the algorithm.

To further probe the parameters for a dynamic aperture, Figure 24 shows a PC SWAT simulation of 6 point-sources buried 0.5 meters in medium sand. The receive aperture is set to 2-meters across track, but shifted toward these targets by either 0 m, 2.2 m, or 4.4 m. The images suggest that a shift on the order of 2.2 m (a little more than the source spacing) is justified. The higher shift of 4.4 m results in reduced across-track resolution.

Since the remaining simulations in this section are not concerned with this outlier 0-degree rotation target facet that is midway between two sources, the across track receive aperture will be set to 2 meters. Simulating a smaller across-track aperture reduced simulation time and had no material effect on the results.

Simulated Multisource Imaging with a Rotated Cylindrical Target

Next, the simulated cylinder is rotated by 45 degrees. The across-track receive aperture is set to 2 m (rather than 2.8 m) centered at the respective transmit source. The following simulations were performed with a smaller across-track aperture because the wider aperture was not needed for the known target rotation. A smaller aperture was used to reduce simulation time and will be used for the remainder of the report.

The single-source multi-aspect images in Figure 25 show that only the A and D sources, which are the farthest away, contribute to the composite image. The voxel data is very directional; source A only contributes information after the platform has passed the target, and source D only contributes information before the platform passes over the target. This is shown by the A-Aft and D-Fore partial mosaic which each respectively include only $\frac{1}{2}$ the pings of their sources. Figure 26 shows the mosaic generated from the composite of the four sources.

The directional nature of the individual source voxel sets suggests that an acoustic color map can be created by combining sources and by using the look angles for each ping/source combination.

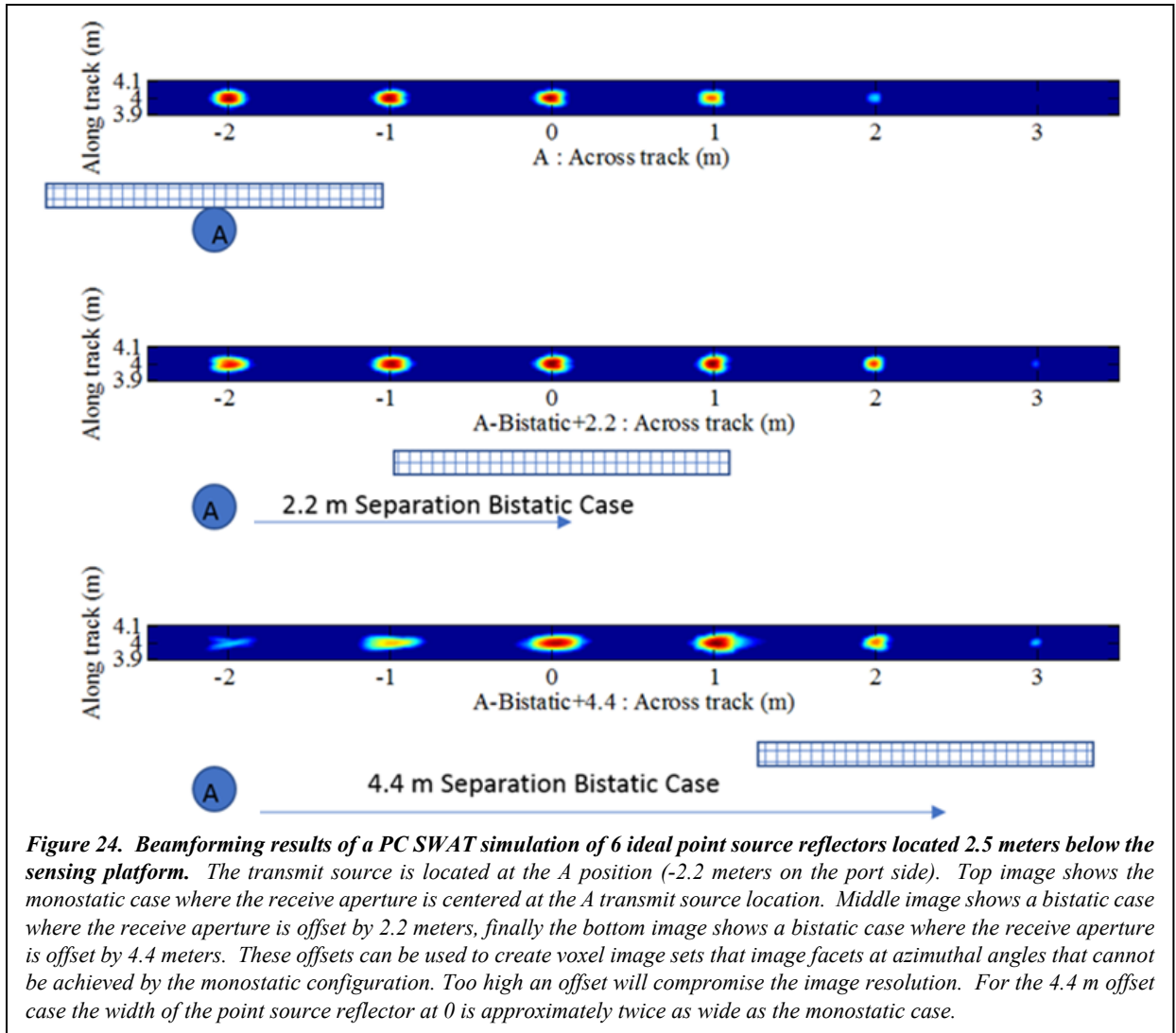
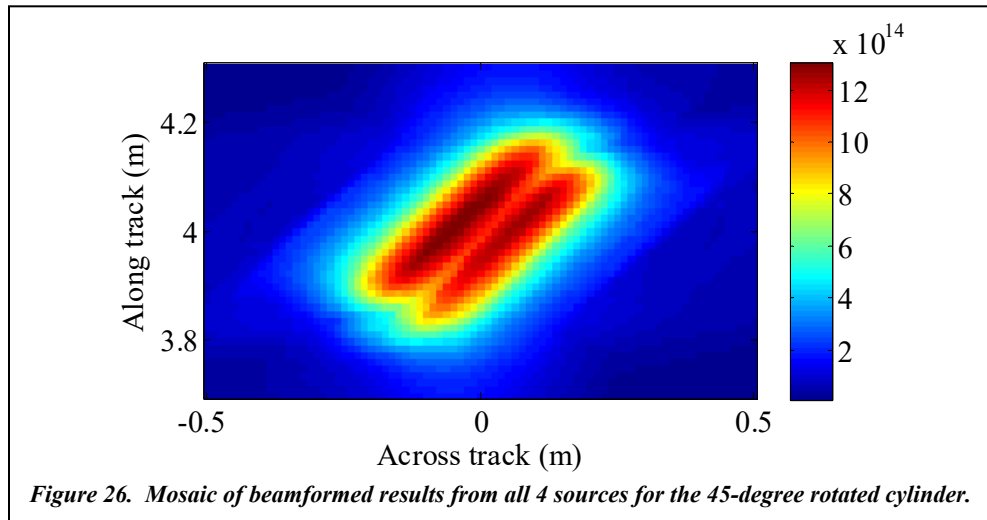
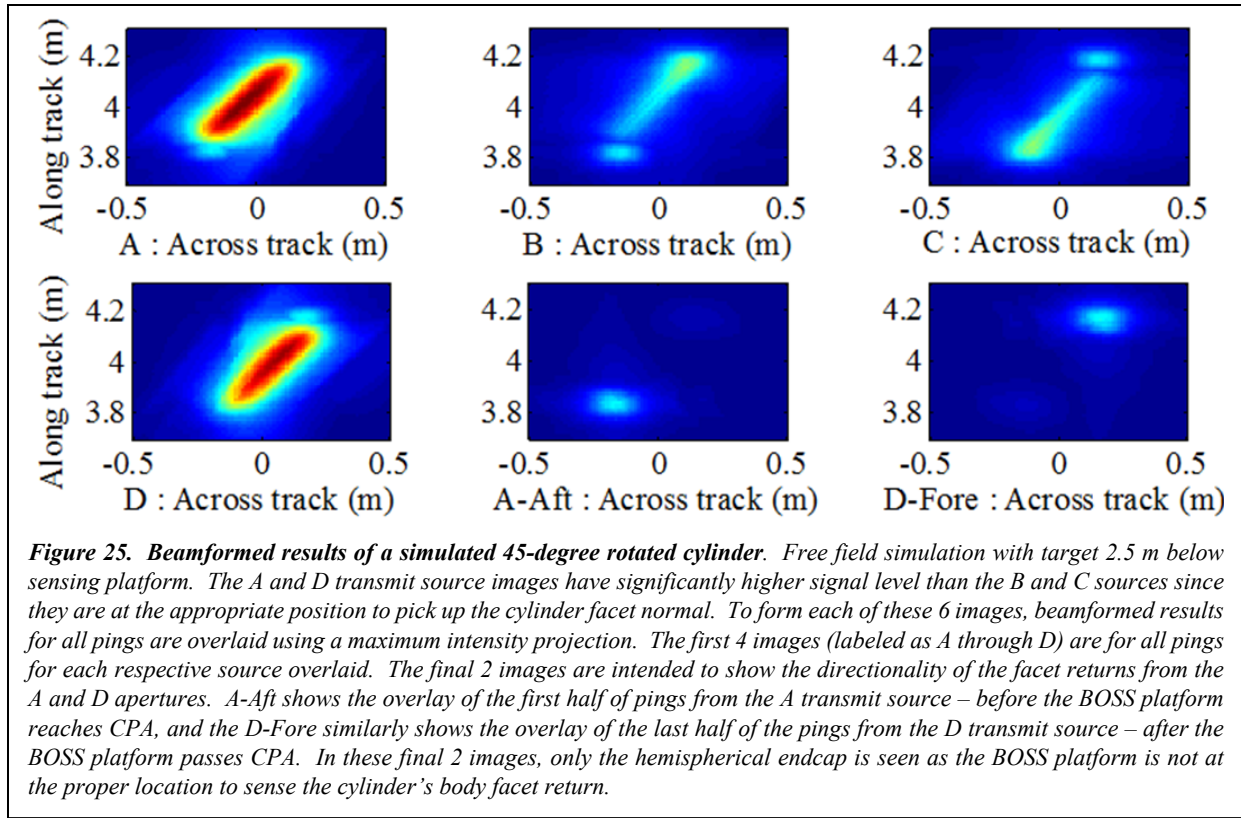
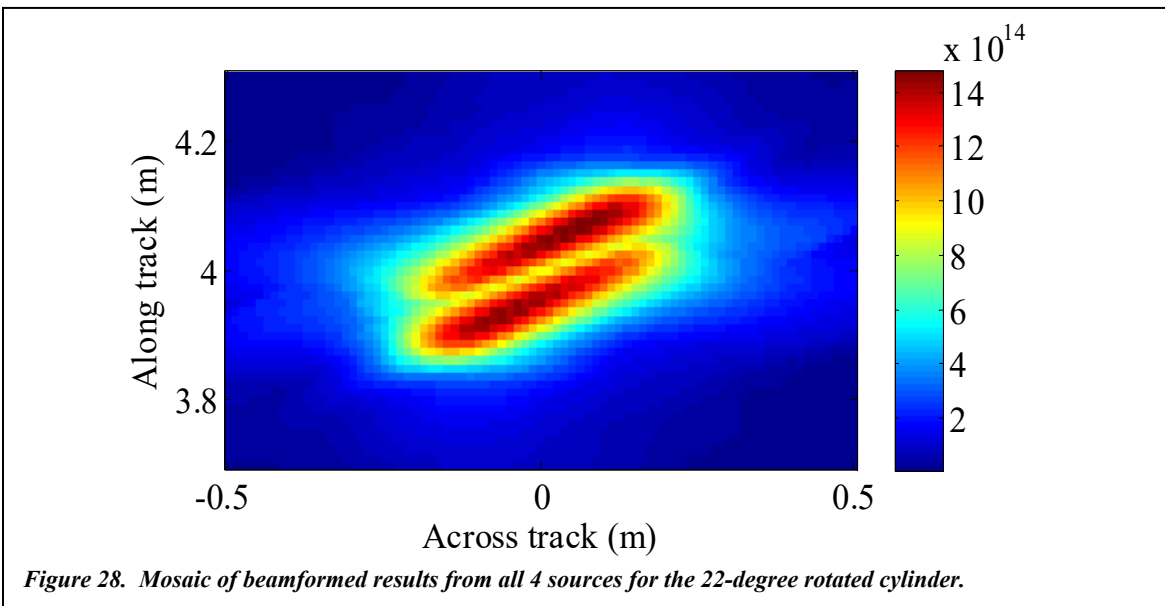
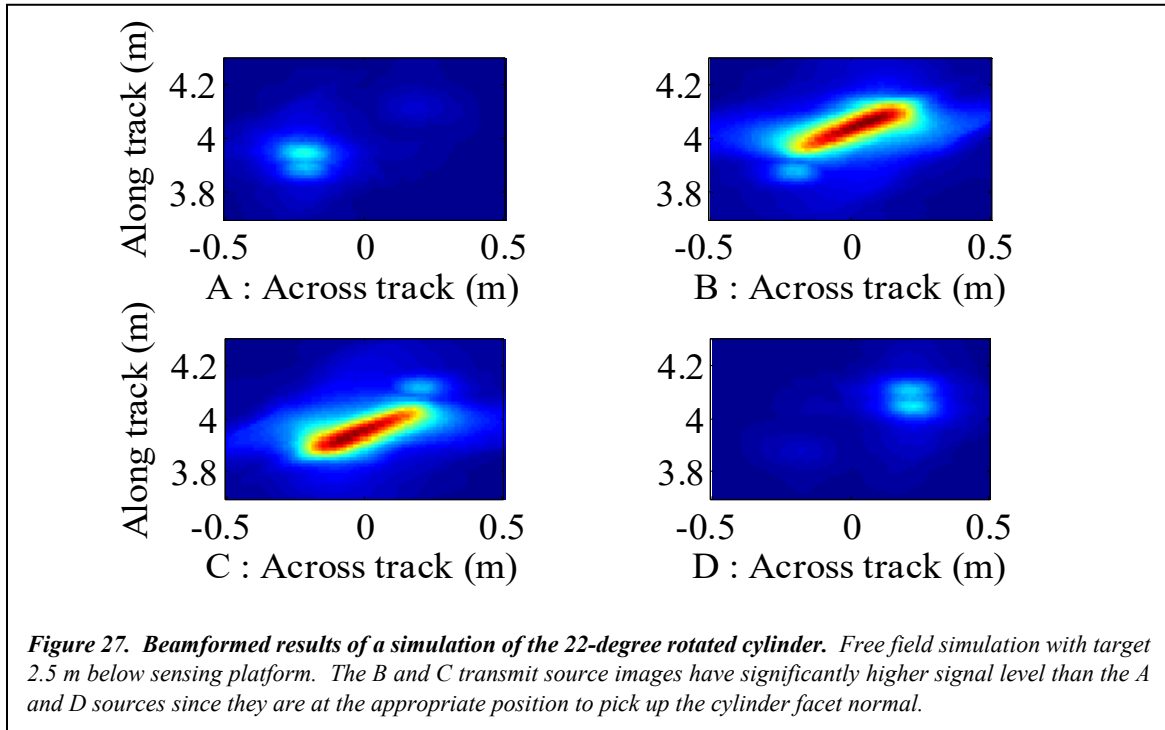


Figure 24. Beamforming results of a PC SWAT simulation of 6 ideal point source reflectors located 2.5 meters below the sensing platform. The transmit source is located at the A position (-2.2 meters on the port side). Top image shows the monostatic case where the receive aperture is centered at the A transmit source location. Middle image shows a bistatic case where the receive aperture is offset by 2.2 meters, finally the bottom image shows a bistatic case where the receive aperture is offset by 4.4 meters. These offsets can be used to create voxel image sets that image facets at azimuthal angles that cannot be achieved by the monostatic configuration. Too high an offset will compromise the image resolution. For the 4.4 m offset case the width of the point source reflector at 0 is approximately twice as wide as the monostatic case.



Finally, applying a rotation of 22 degrees to the cylinder (chosen because it is an angle midway between 0 and 45) results in Figure 27 and Figure 28. For the 22-degree rotation case, the closer B and C sources are the sole contributors to the mosaic.



Acoustic Color Map Creation

An acoustic color map is normally made in the far field of the sonar. A method for the near field has been used to create a color map from eBOSS data and it is as follows (assumes the focal point on the target has been determined):

For each ping:

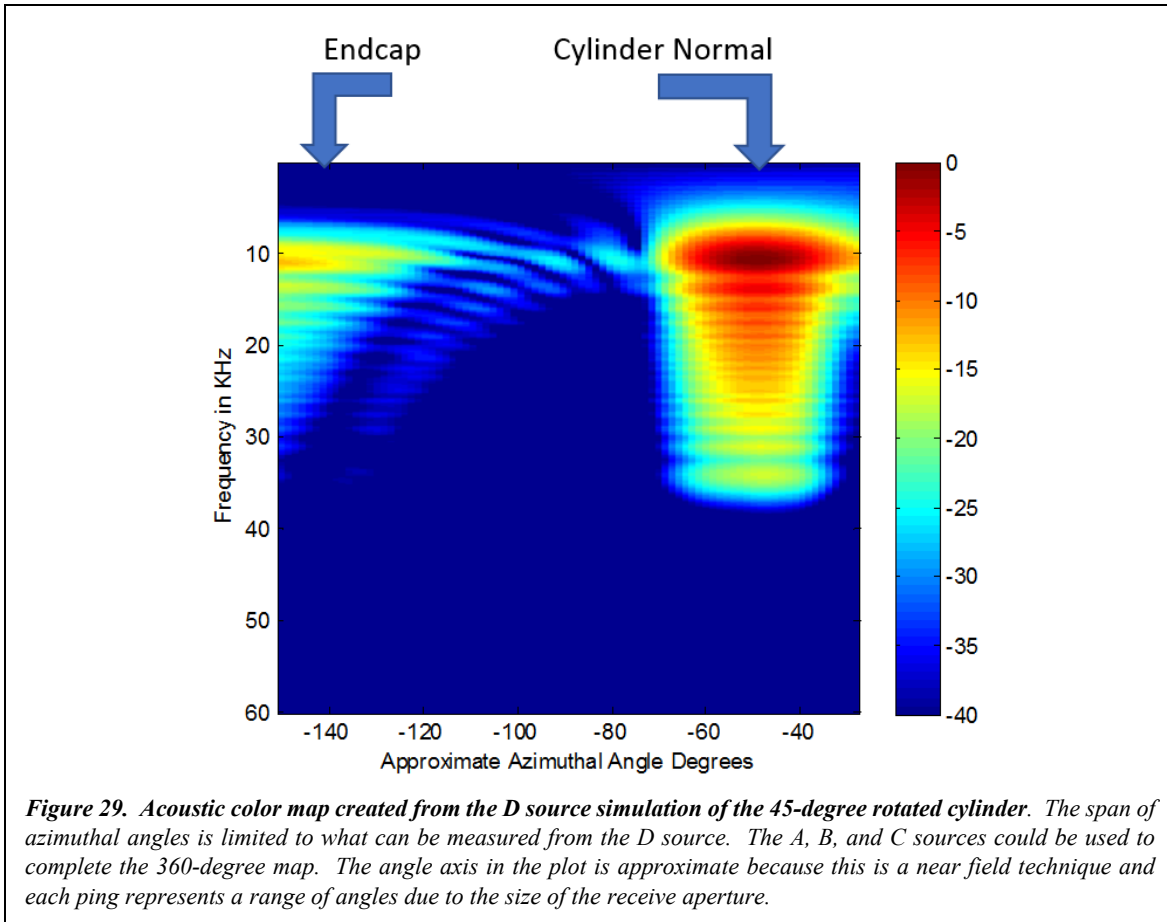
- Compute the look angle from the measurement platform to the target's focal point.
- Capture the time series centered on the target's focal point for all channels.
- Coherently sum the time series data from all channels to suppress scatter noise with processing gain.
- If the along-track aperture is synthetic, coherently sum the time series data from all channels and over all pings in the SAS aperture.
- Optionally, window the coherently summed time-series to taper the ends to zero. In this example we use a raised cosine taper at each end.
- Create the frequency map for that look angle using an FFT of the time series.

Using the 45-degree rotated cylinder and the data from transmit source D, Figure 29 shows this partial acoustic color map. The other sources can be used to complete the full 360-degree color map. Note that the color map can only display content for frequencies within the transmit source band, which is 7.5 kHz to 37.5 kHz in this report.

To create this map over all azimuthal angles, the R_{\min} and R_{\max} limits were disabled. Note that the elevation angle varies throughout this colormap and is not a constant 0 degrees. To get a more constant elevation angle, either more transmit sources are needed or in some cases bistatic beamforming should be used.

Previous studies suggest that using acoustic color as a classification system for UXO is a viable method for identification [18]. We (the authors of this study) have limited expertise in acoustic color. We do not know if the technique described here would be successful in creating a practical acoustic color map that could effectively classify UXO targets.

While our objective is to define a system that provides extensive look angle coverage, it is unclear how many view angles are needed to meet the performance requirements of ESTCP for site remediation. Including a more complete coverage of look angles will provide more flexibility to optimize algorithms and to react to changes in metrics.



Resolution, Altitude, and Bandwidth Tradeoffs

For multiple reasons, including the risk of collision with the seabed, platform operators prefer to operate winged eBOSS-type systems at higher than the ideal altitude of subbottom imaging. Figure 30 shows a plan view of beamformed results when the altitude of the example configuration is changed from 2.5 m above the target to 5.5 m. In this example, the target is again positioned with a 45-degree rotation.

Due to the relationship between angular resolution and slant range, the image resolution is degraded at the higher altitude compared to the results shown in Figure 26. In order to achieve quality eBOSS UXO imagery, platforms should operate at low altitudes or equivalently with very long wing apertures.

The previous sets of simulations have been run with approximately double the bandwidth (7.5 kHz – 37.5 kHz) of fielded BOSS systems. For example, the Bluefin-40 BOSS had a band from about 7.5 kHz – 19 kHz. For the 45-degree rotated cylinder which is 2.5 meters below the platform, Figure 31 and Figure 32 illustrate the effect of cutting the bandwidth in half and either using the lower half of the bandwidth (7.5 – 22.5 kHz) or upper half (22.5 – 37.5 kHz bands).

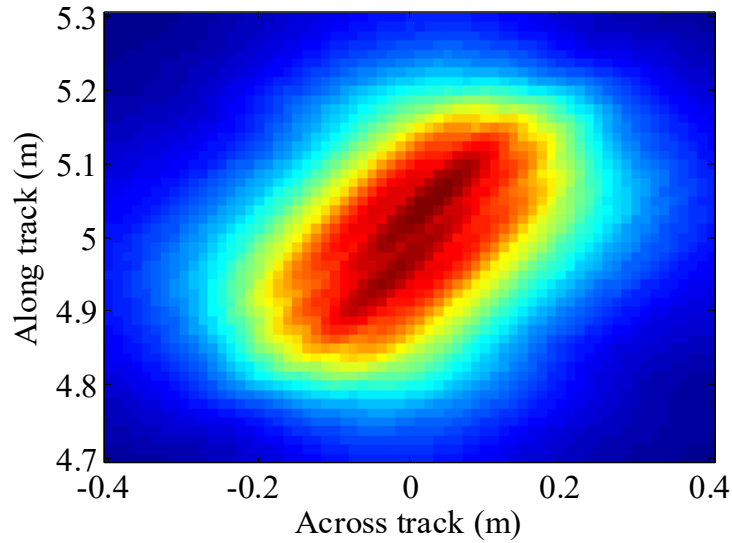


Figure 30. Mosaic of beamforming results for 45-degree cylinder 5.5 meters below eBOSS platform. This is a free field simulation. The resolution is degraded due to the high altitude. The BOSS platform's 2 m x 2 m aperture was designed for a 2-m altitude. These low altitudes may be operationally challenging to achieve. It is common to operate a conventional BOSS system with 2-meter wingspan at about 5 meters altitude. The purpose of this figure is to emphasize that this type of higher altitude operation will compromise image quality.

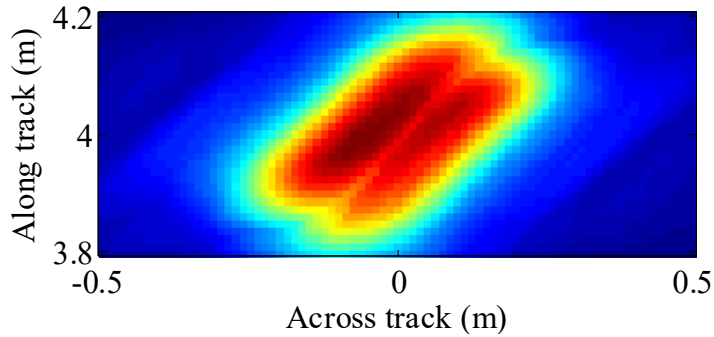
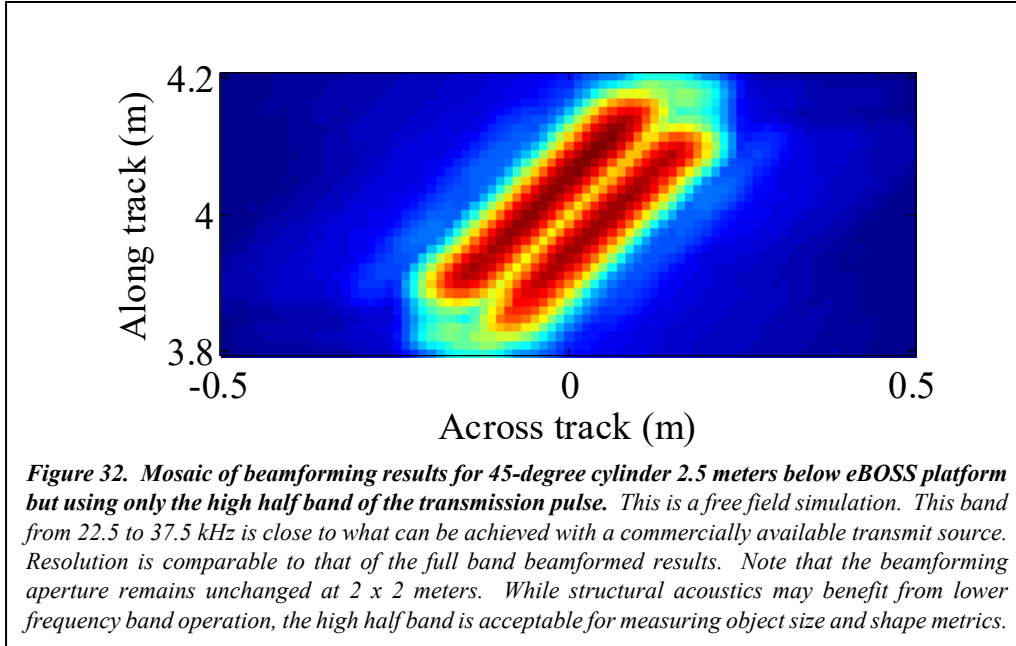


Figure 31. Mosaic of beamforming results for 45-degree cylinder 2.5 meters below BOSS platform but using only the low half of the transmitted band. This is a free field simulation. This band, from 7.5 to 22.5 kHz, is similar to the bandwidth of a conventional BOSS system. Restricting to this lower band will result in a system that is easier to implement due to reduced hydrophone segment channel counts (1/2 wavelength spacing criteria). The lower band can also show more elastic properties beneficial for structural acoustics. Resolution is inferior to the full bandwidth transmission results.

The bandwidths are the same for both the high-band and low-band results. Therefore the range resolution should be the same for each (ignoring frequency dependent attenuation), since the aperture size was held constant at 2 x 2 m. However, the plan-view spatial resolution of the beamformed results shows otherwise. The low-band result (which has a lower center frequency) is noticeably degraded whereas the high-band result (which has a higher center frequency) has a higher resolution than the full band result.



Both transmit sources are likely to be commercially available. However, a source that can achieve the full band of 7.5 kHz to 37.5 kHz is not available and may be difficult to produce. Next, we describe some frequency-related cost/benefit tradeoffs to be considered when designing a future system.

To measure the size and shape of an object, the high-band source might be a good compromise for a SERDP eBOSS system, not only due to its availability but because a higher frequency source is smaller in size. Therefore easier to design a multi-source system with a set of these sources.

For structural acoustics, elastic properties which may be useful for classification are dominant in the lower half of the band. In addition to the benefits of acoustic color, a system based on the lower band would be easier to build because it would require about $\frac{1}{4}$ of the hydrophone density. Note that the number of hydrophone staves would be reduced for a given aperture size because the wavelengths are longer. This reduction can be significant when considering that a higher frequency source may require multiple hydrophone rows, in the along-track axis, to supplement the SAS aperture. For a longer wavelength the along-track ping rate can also be reduced allowing for lower ping rate operation or fewer rows of hydrophones.

Resolution Enhancements

The resolution can also be enhanced within the beamforming process. One common technique is to measure a coherence factor, which ranges from 0 (incoherent) to 1 (fully coherent), for each voxel, and scale the voxel by its coherence factor. This is performed for each voxel using a near-field time-delay beamformer that coherently sums the complex (analytic) values that are associated with that voxel from each of the stave's time-series record. The work in [14] presents a similar technique for phase-coherent imaging. Let $Stave\ Value_j$ represent the time-series data record of stave j and let t_{ij} be the discrete time associated with stave j for the voxel of interest, i .

$$Voxel\ Value(i) = \sum_j Stave\ Value_j(t_{ij})$$

$$Voxel\ Incoherent\ Sum(i) = \sum_j abs[Stave\ Value(t_{ij})]$$

$$Coherence\ Factor(i) = \frac{abs[Voxel\ Value(i)]}{Voxel\ Incoherent\ Sum(i)}$$

$$Resolution\ Enhanced\ Voxel(i) = Voxel\ Value(i) \times Coherence\ Factor(i)$$

These techniques were implemented using simulation data sets and were shown to provide noticeable resolution enhancement when the signal to noise level was high.

This section discussed two possible post processing techniques that may be worth testing in a future eBOSS system for enhancing resolution. A bandpass filter which raises the center frequency of the input to the beamformer was shown to improve resolution in Figure 32. The second technique uses the coherency metric.

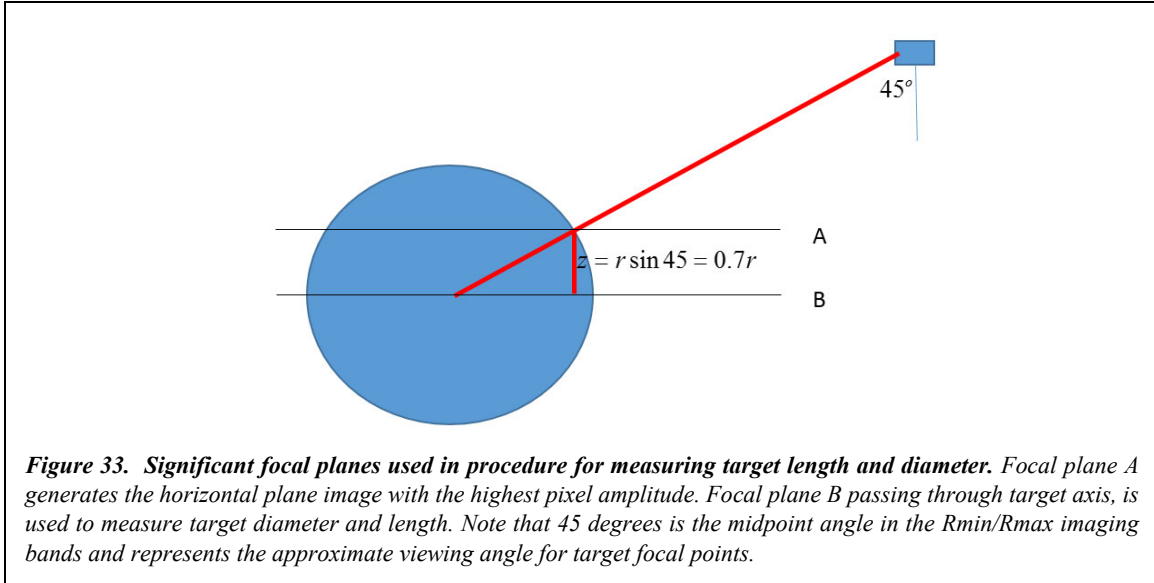
Measuring Shape and Dimension of an Object

It is convenient to present a plan view of a beamformed 3-D voxel field using a maximum projection metric to collapse multiple depth planes into a downward looking 2-D projection. This will tend to make targets appear larger than reality due to the system's resolution limits. For a simple target like a cylinder lying horizontally, a more accurate measure of target size is to select the single depth plane where the target seems longest, and which likely slices through the central axis of the target. This is a common method that has been used with conventional BOSS imagery in the past. Based on past field data experience, the voxel field usually contains clutter as well as significant sediment scattering noise. To that end the method is subjective and subject to interpretation. This section is an attempt to provide some quantitative metrics and rationale for this technique.

The method for measuring target dimensions is based on imaging horizontal slices of the target at various focal depths. To measure a target's length and width, begin by evaluating the previously evaluated voxel values at depth intervals equal to the spatial resolution of the system. The horizontal image slice with the maximum voxel value corresponds to the direct path return from the target and is represented in Figure 33 by plane A. The voxel layers are then iteratively evaluated with progressively lower focal planes until the target's length stops increasing. The horizontal image slice at this focal depth is represented as plane B in the Figure 33. When the length is at its maximum, the image plane is on the center axis of the target, which is where the image should be used to measure the target's dimensions. In practice, the algorithm will need to account for the orientation of both the target and of the system. An example is provided next.

A truncated prolate spheroid (bullet shape) with a 22-cm maximum diameter and a 50-cm length was simulated to demonstrate the measurement method. A subset of horizontal image slices for four focal depths are shown in Figure 34. The maximum value above each corresponding

horizontal slice is an average of the 10 highest pixel values. Table 1 summarizes the result of the measurement procedure applied to each focal plane between images A and D. The measured length of the 50-cm long target is 50 cm and the measured diameter of the 22-cm diameter target is 24 cm.



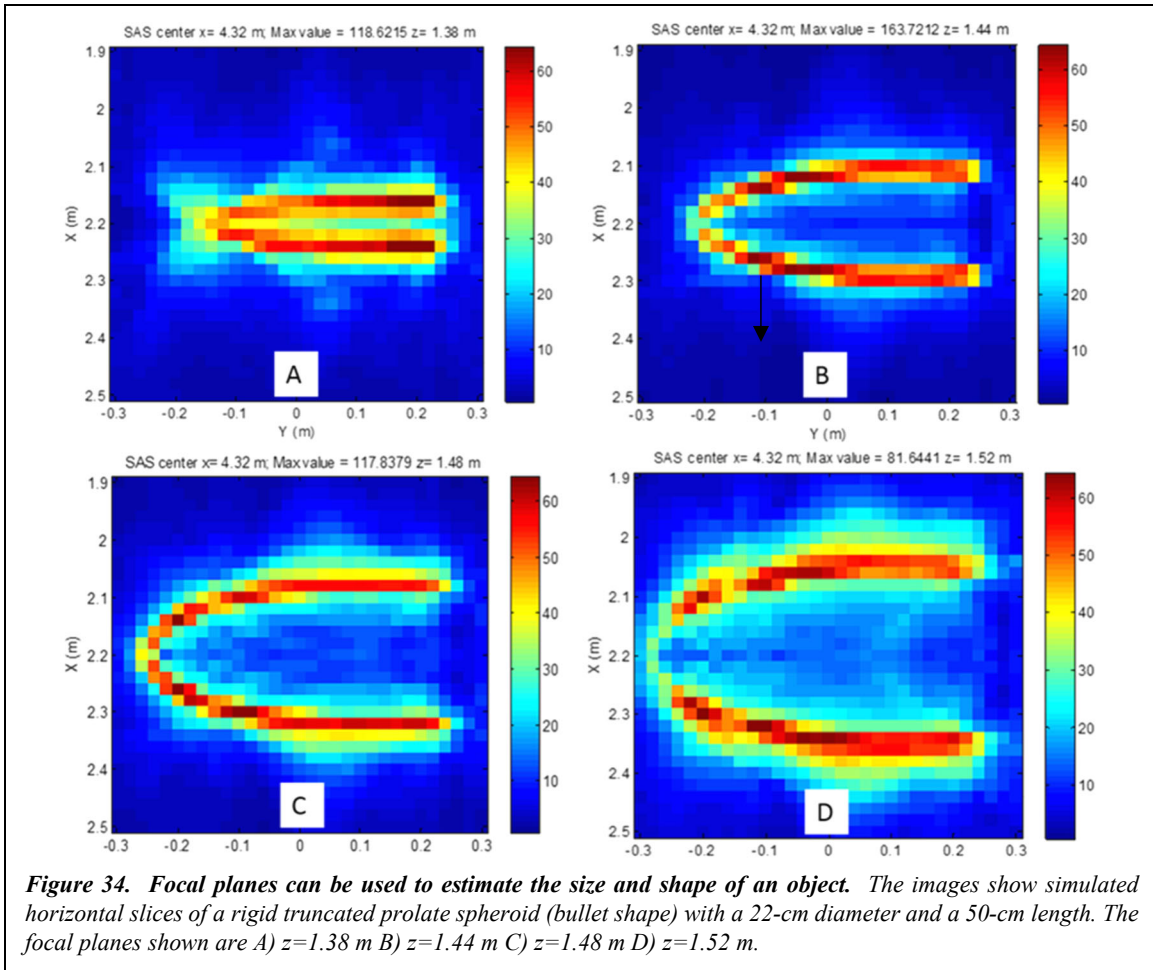


Table 1. Measurements from horizontal image slices of a truncated prolate spheroid with a 22-cm diameter and 50-cm length. The row in bold indicates the estimated dimensions.

Focal Depth (m)	Average Maximum	Width (cm)	Length (cm)
1.38	119	8	36
1.4	151	12	38
1.42	168	16	44
1.44	164	20	44
1.46	139	20	46
1.48	118	24	50
1.5	97	28	50
1.52	82	30	50

Trade Space Study

An objective of this effort is to perform a trade-space study over possible parameters for a next generation eBOSS system. Some parameters to be evaluated are:

Operating altitude: Lower altitudes produce higher spatial-resolution results for a given aperture size and provide a better ratio of along-track aperture to useable swath.

Transmit frequency band (F_{Min} , F_{Max}): Wider bandwidth improves range resolution. Higher center frequency improves beamforming resolution. Lower frequencies may benefit structural acoustics.

Platform forward velocity: Platform velocity affects system complexity. Slow forward velocities can reduce complexity because multi-source systems require a high ping rate to achieve coverage free of grating lobes. However, platforms have a minimum operating velocity due to stability and control. Faster forward velocities may need additional rows of hydrophones to maintain $\frac{1}{2}$ wavelength spacing in the along-track SAS aperture.

A system can be designed based on the above system parameters. A MATLAB script in Appendix D provides the scripts to calculate the parameters. One negative of a multi-source system is the large across track wing aperture. To limit the aperture size, this table assumes that the peripheral sources are mounted on the extreme ends of the across track wing, and therefore their receive across-track apertures are not symmetric. For example, the most extreme port side transmit source uses only the hydrophones available starboard of that source.

The key values computed are:

- Number of transmit sources (to populate the wing aperture with R_{min} spacing)
- Number of hydrophones per row ($\frac{1}{2}$ wavelength spacing criteria)
- Number of hydrophone rows
- Resolutions: range, along-track, and across track

The table below shows some sample configurations.

Table 2. Trade Space Table for single track-line coverage

Trade Space Table	Example 1	Example 2	Example 3	Example 4
$F_{Min} - F_{Max}$ (kHz)	7.5 – 37.5			
Velocity (m/s)	1.5			
Altitude (m)	2	1.5	1.0	1.0
Wingspan (m)	4.2	3.2	2.1	4.9
Hydrophone Spacing (cm)	2			
Hydrophones \times Rows	211×4	158×3	106×3	246×5
TX Sources	4	4	4	8
All aspect angle swath (m)	1.4	1.05	0.7	3.5
Width of Subapertures (m) (Subset of hydrophones processed for each TX source. Approx. $1.4 \times$ altitude)	2.8	2.1	1.4	1.4
Range Resolution (cm)	2.5			
Across-Track Resolution (cm)	6.6			
Along-Track Resolution (cm)	3.3			

In the 2-meter altitude case, the wingspan required is quite large for the width of coverage provided. This is due to the system requirement of low elevation angles when capturing target facets – where transmitters are needed on both sides of the coverage swath to achieve lower

elevation angles. Essentially there is a large amount of “wing span” overhead to obtain a minimal all-angle coverage, but the swath increases on a 1:1 basis as additional transmit sources are added. The swath is defined as the “full coverage” swath – the region which can image nearly all look angles. A tradeoff could be made that uses a wider swath for the configurations at the expense of having fewer look angles for portions of that swath.

If it were possible to perfectly position the platform when mowing a field with track lines, then the wingspan to coverage ratio would approach 1:1. Consider the extreme case where there is only a single transmitter centered in the wing aperture, such as a traditional BOSS system. If a survey were conducted with multiple perfectly spaced track lines, then an all look angle mosaic could be created even though the individual track lines do not provide full coverage on their own. Platform positioning is discussed in the section on Acoustic Positioning and Alternative System Concept.

Beamforming with Sediment Sound Speed

Fielded generations of the BOSS software only support a single sound speed – the speed in water, which is measured with a sound velocity probe. Including a second sediment sound speed becomes more important as the burial depth of UXO increases. PC SWAT simulations were used to measure the effect of sediment sound speed on image quality using algorithms that compensate for the index of refraction at the sediment-water interface. Based on Snell’s law, assuming the seabed medium has a higher sound speed than water, sound waves propagating into the seabed will bend away from 0 degrees (normal incidence).

Refraction compensation is necessary to account for the difference in path length (and time difference) caused by the refraction of the acoustic waves in the seafloor. See Figure 35. For a given geometry of a transmitter and a focal point in the subbottom, we determine the point on the seafloor that a signal enters the subbottom to arrive at a focal point. Once this point is identified, the total time of flight between the transmitter and focal point can be calculated by 1) dividing the individual distances (in water and subbottom) by their respective sound speeds and then 2) summing the time of flights in water and in the subbottom. Locating this point on the seafloor requires solving a 4th order polynomial.

For refraction compensation simulations to run in reasonable amount of time, a precomputed refraction compensation table was generated as a function of *a*) horizontal range to focal point and *b*) burial depth at focal point. There is an implied 3rd table index – the altitude above the seafloor, which is the same for all transmit and hydrophone elements and therefore ignored as an index. The table entries contain the time delay factoring in both sound speeds and refraction. A unique look-up table must be generated for each combination of operating altitude, water sound speed, and sediment sound speed.

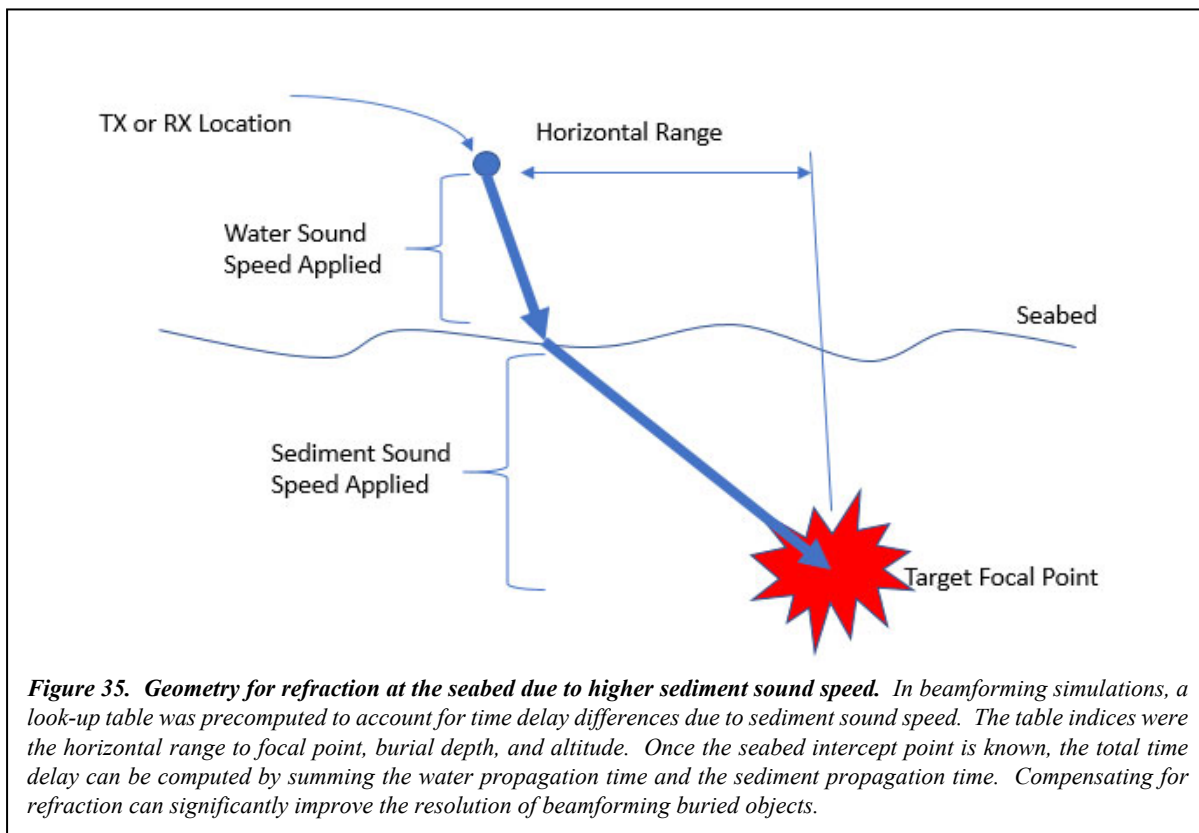
eBOSS beamforming is presently based on a near-field time-delay technique. The time delay for each transmitter-target-hydrophone triplet is the sum of 2 values, *i.e.* time delay between: 1)

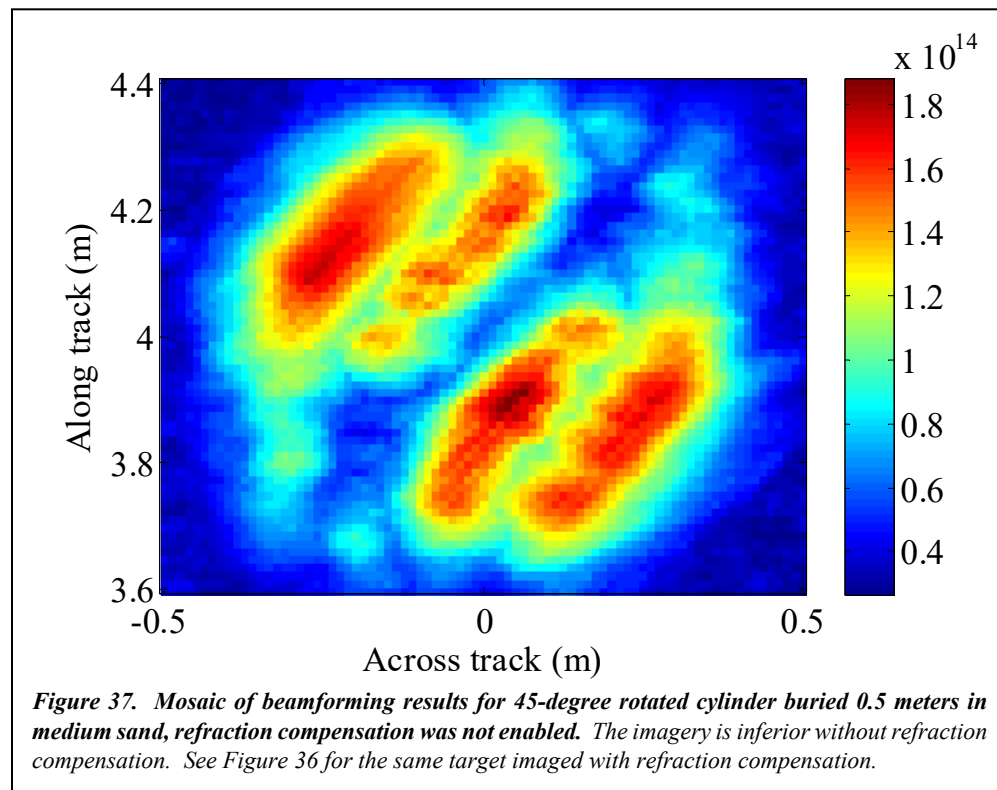
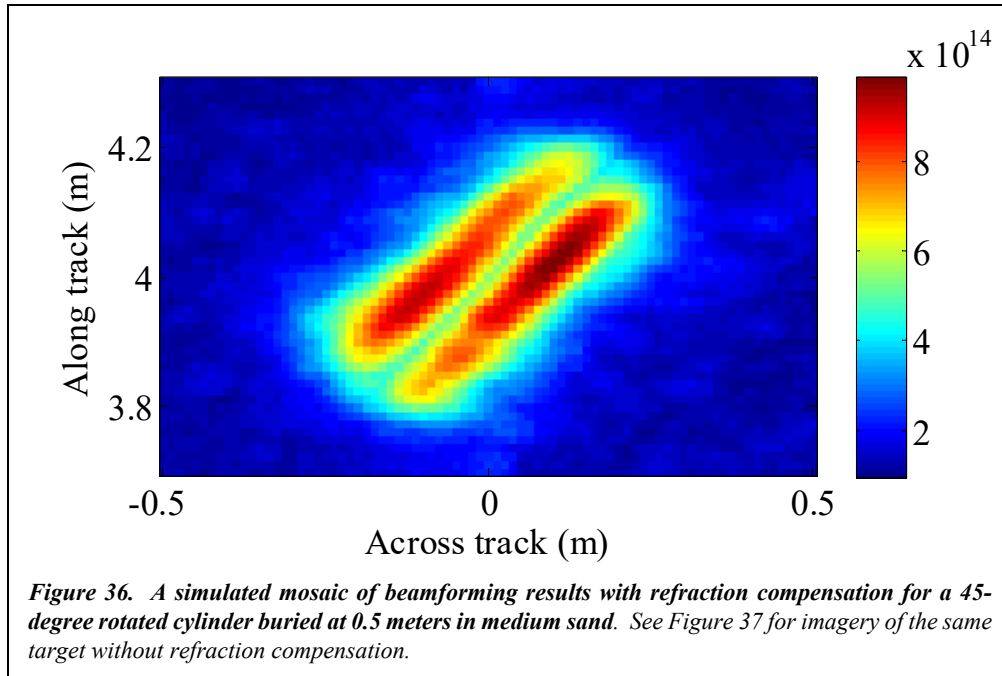
transmit source and focal point and 2) focal point and receive hydrophone. When refraction compensation is implemented two table lookups per triplet are performed.

Figure 36 shows the results of a PC SWAT simulation for a cylinder buried in medium sand at a burial depth of 0.5 m. An equivalent free field result for the 0.5 m burial depth case has already been shown in Figure 25. In this simulation, the seafloor consists of a medium sand with a sound velocity of 1767 m/s. The sound speed of water was set to be 1500 m/s.

The simulations in sand include sediment surface and volume scattering noise based on APL/UW recommendations [15], and are listed in Table 3 of Appendix C. Reverberation in a real environment would likely be higher due to other clutter objects in the field, and the noise seems low based on experience with historical Bluefin 40 field data.

The beamformed results show significant resolution improvement when refraction compensation is applied for the 0.5 m burial depth case. With refraction compensation, the resolution is close to the free-field case previously shown. Without compensation, image quality is severely degraded. See Figure 37. In addition to improved resolution, applying proper compensation provides some processing gain to overcome buried scattering noise.





Measuring Sediment Sound Speed

In the previous simulations the sediment sound velocity was known. However, when compensating for refraction, a fielded system's performance will depend upon the degree to which the sediment sound speed is mismatched to the actual sediment sound speed. With the large proposed hydrophone aperture of a future eBOSS, it might be possible to estimate sediment sound speed. This is worth exploring in follow-on work.

One of the significant advantages of the long across-track sonar aperture is the capability of measuring the critical angle at the seafloor, which can be used to derive sediment sound speed. In principal it is possible to estimate the sound speed if the seafloor is relatively flat. To understand the methodology for measuring sediment sound velocity consider equation (1) below, the expression for calculating the reflection coefficient of a fluid-fluid interface as a function of incidence angle, θ_i .

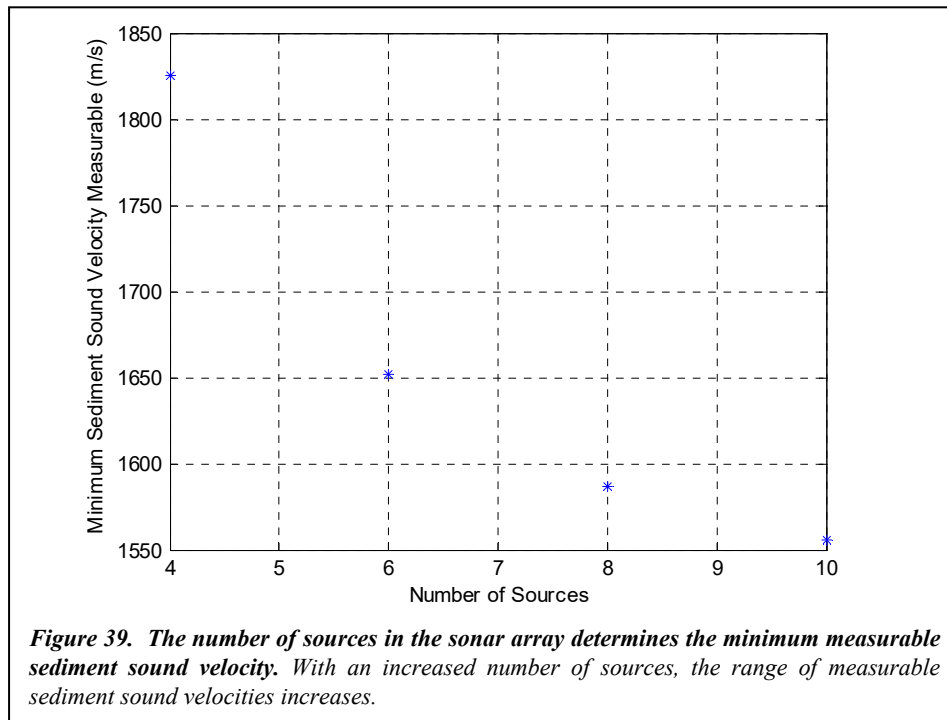
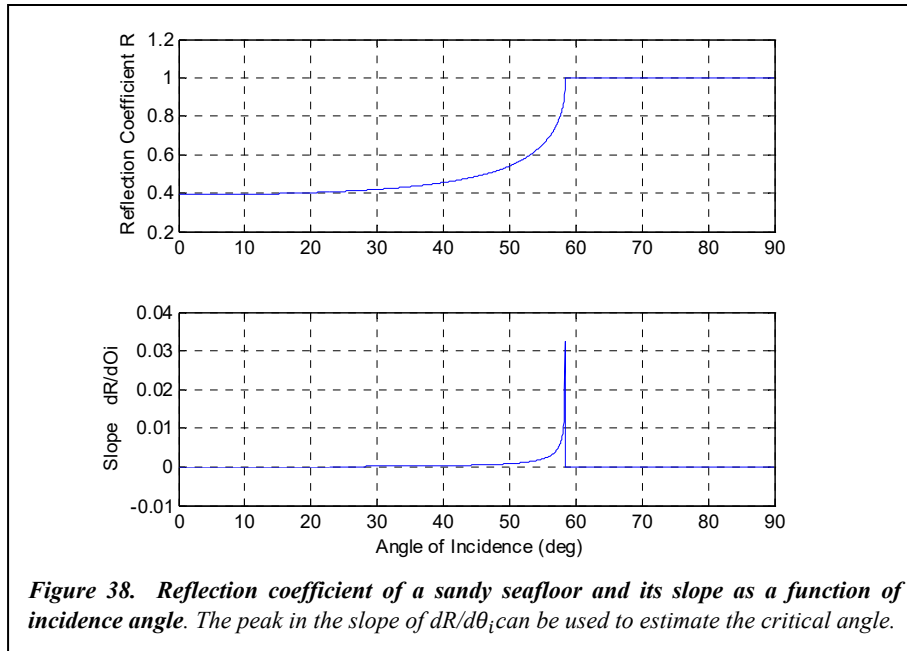
$$R = \frac{\frac{z_2}{z_1} \frac{\cos \theta_t}{\cos \theta_i}}{\frac{z_2}{z_1} + \frac{\cos \theta_t}{\cos \theta_i}} \quad (1)$$

where z_1 and z_2 are the acoustic impedances of seawater and sediments, respectively. The transmission angle in sediment, θ_t , is determined using Snell's Law given by

$$\frac{\sin(\theta_t)}{c_2} = \frac{\sin(\theta_i)}{c_1}.$$

Figure 38 illustrates the reflection coefficient vs incident angle and the derivative. As shown in the graphic, the slope $\frac{dR}{d\theta_i}$ is maximum at the critical angle θ_c , which is the angle of incidence beyond which all energy is reflected and $|R| = 1$. The reflection coefficient as a function of incidence angle can be calculated using each hydrophone by measuring the specular reflection from the outermost source off the seabed.

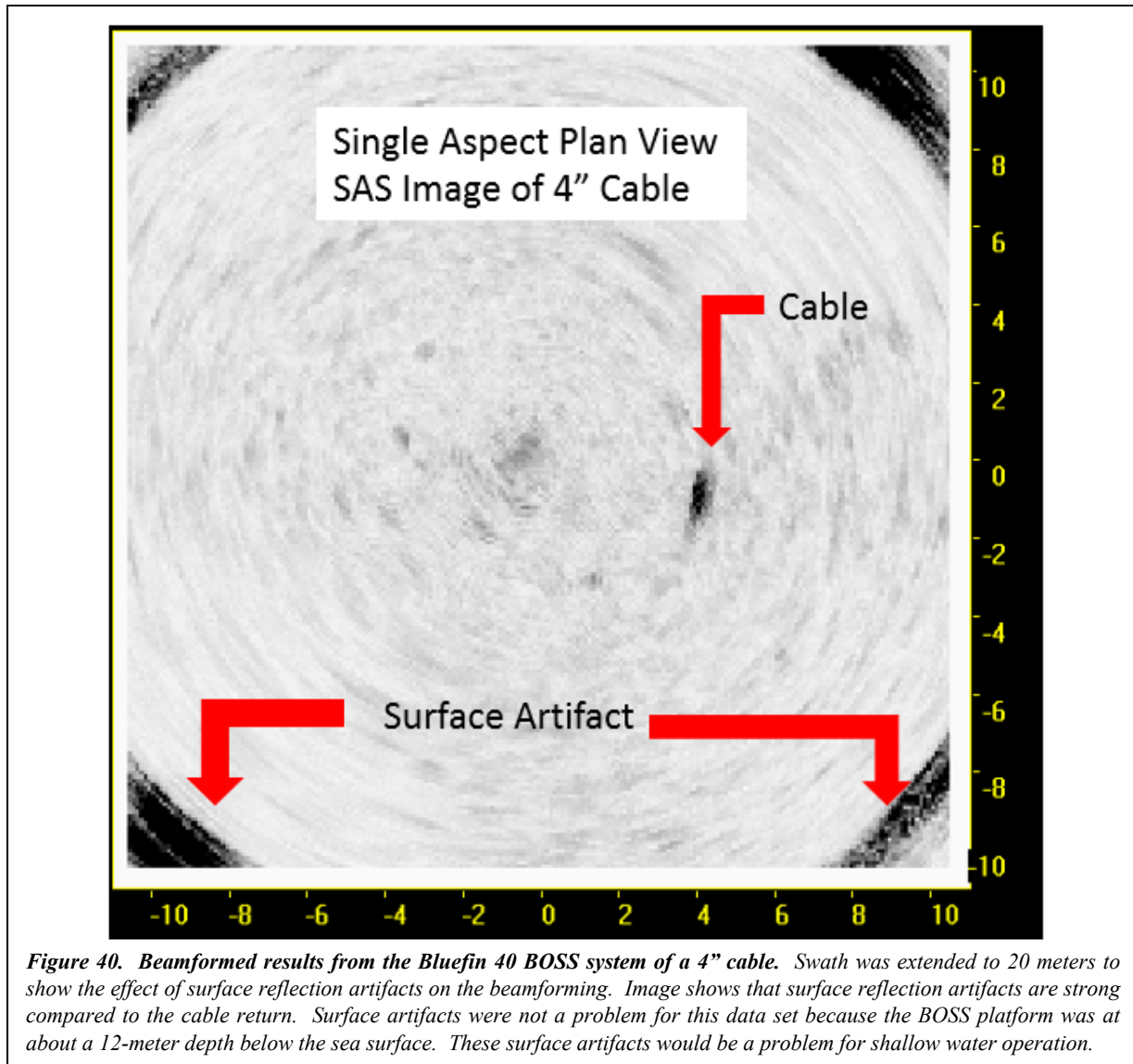
Increasing the width of the sonar array in the across-track direction provides a greater range of incidence angles to be measured. As the maximum distance between source and hydrophone increases, the range of observable sediment sound velocities increases due to the increased critical angle. The minimum measurable sound velocity is shown in Figure 39. As shown in the figure, for 6 sources the minimum measurable sediment sound velocities is 1650 m/s. Sediments with sound velocities above 1650 m/s include sands and some silts.

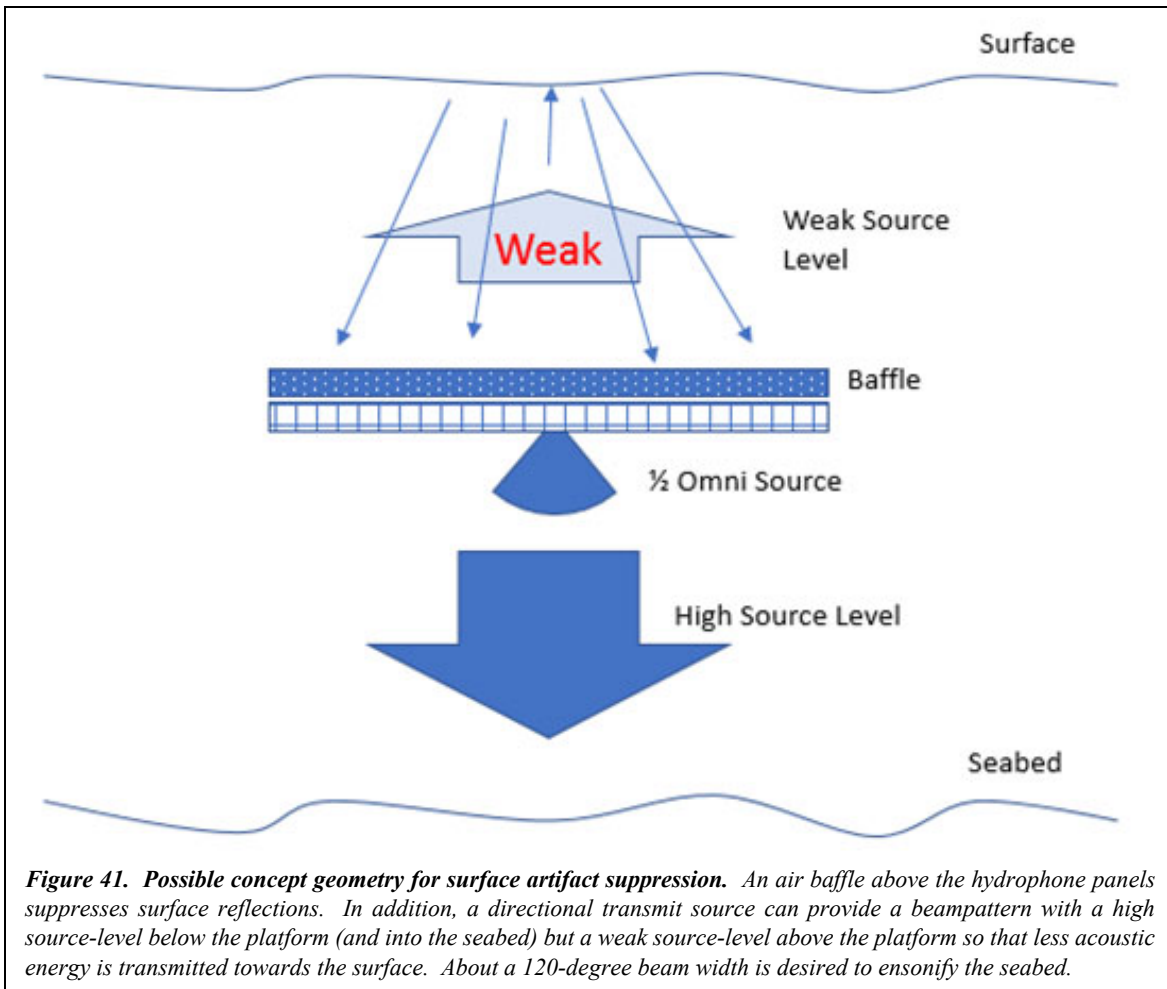


Shallow Water Artifacts

Targets buried in shallow water present special challenges for acoustic imaging systems. Figure 40 shows a single SAS ping from data acquired on an actual 4" cable discussed in Figure 3, but with the swath extended to 20 meters. In this case the platform was at a depth of approximately 13 meters, which can be inferred from the artifact that appears in the image. The surface reflection is strong and can interfere with imaging a buried object in shallow water. As noted previously, other multiples such as the full water column return (altitude plus depth) can also generate artifacts.

Surface reflections can be the strongest artifacts. Two techniques are proposed here to suppress this artifact, namely (a) a directional source – ideally one that is close to omnidirectional below the platform but weak above the platform and (b) a sound baffle positioned above the hydrophone arrays to absorb the acoustic energy reflected from the surface. See Figure 41.





Next Generation Transmit Source Selection

Current generation BOSS systems have used standard products such as the broadband (8 kHz to 19 kHz) Neptune D/11/BB, which is a spherical omni-directional crystal. There are several deficiencies with this type of transmit source.

- Provides inadequate image resolution with its suboptimal bandwidth. Structural acoustics will benefit from a wider spectrum.
- Results in strong surface reflections due to the full omni-directional nature of this type of transducer. These artifacts are hard to suppress by beamforming alone, which can compromise shallow water operation.

Alternative acoustic sources are available for UXO remediation.

Tonpilz

Tonpilz transducers provide a wide bandwidth at the frequencies of interest. This type of source uses double or triple resonant modes to increase bandwidth. Despite the wider bandwidth, the spectrum of these transducers is limited by material properties. Therefore, multiple complementary transducers may need to be cascaded and pulsed sequentially to completely span the acoustic spectrum needed for UXO remediation. It should be noted that cascading multiple

transducer types introduces complexity in the electronics and will probably introduce variations in their beam patterns that will affect beamforming.

Single crystal

Single crystals have a great potential to reach a wider bandwidth at lower frequencies. They also have coupling coefficients greater than 0.90 and have very high piezoelectric constants. They are viable for miniaturization / weight reduction. Unfortunately, the cost of manufacturing sonar arrays with single crystals remains prohibitive. Also, the size of the crystals is limited by compositional gradients, which causes inconsistencies between the different array elements. Some newly developed techniques help solve composition problems, but they are very expensive for sonar applications and they involve an extremely slow process, e.g. crystals grow at a rate of 2 mm/hr.

Textured ceramics

Lead Magnesium Niobate - Lead Titanate (PMN-PT) textured ceramics are theoretically comparable to single crystal transducers but are cheaper to manufacture. They were introduced after single crystals and are manufactured by adding and aligning highly anisotropic grains into ceramic green body and promoting axisymmetric grain growth. Recently, material property values of textured ceramics have approached those of single crystal sources. While not presently standard products, some boutique commercial manufacturers are offering textured ceramics. Processes for scale-up considerations are underway by various research groups and commercial manufacturers.

Similar to single crystal transducers, textured PMN-PT ceramics have specific advantages over polycrystal PZT ceramics for transducer designers. These are:

- Higher coupling coefficient and lower mechanical quality factor.
- Higher piezoelectric coefficient, d .
- Lower compliance.
- Higher maximum drive voltage than hard PZT s PZT-4 and PZT-8.

With these properties textured PMN-PT can provide wider bandwidth, higher source level, lower impedance, and miniaturization because of less weight and volume.

Recently transducer companies and universities have started to investigate use of PMN-PT textured ceramics in fundamental transducer designs, e.g. piston design, to explore those above-mentioned advantages. Massa Products Corp. has reported significant higher TVR levels up to 12 dB and wider bandwidth compared to same size of PZT transducer. Also, it was reported that textured transducers can be significantly shorter and lighter if targeting the same source levels as PZT transducers.

Based on these recent developments, we believe more complex transducer designs with textured ceramics would be the center of interest for next generation BOSS transducers. A research concept will be established to combine multi-mode transducer designs with the superior properties of textured ceramics. These designs can be tailored to make the transmit source directional enough to suppress surface reflections.

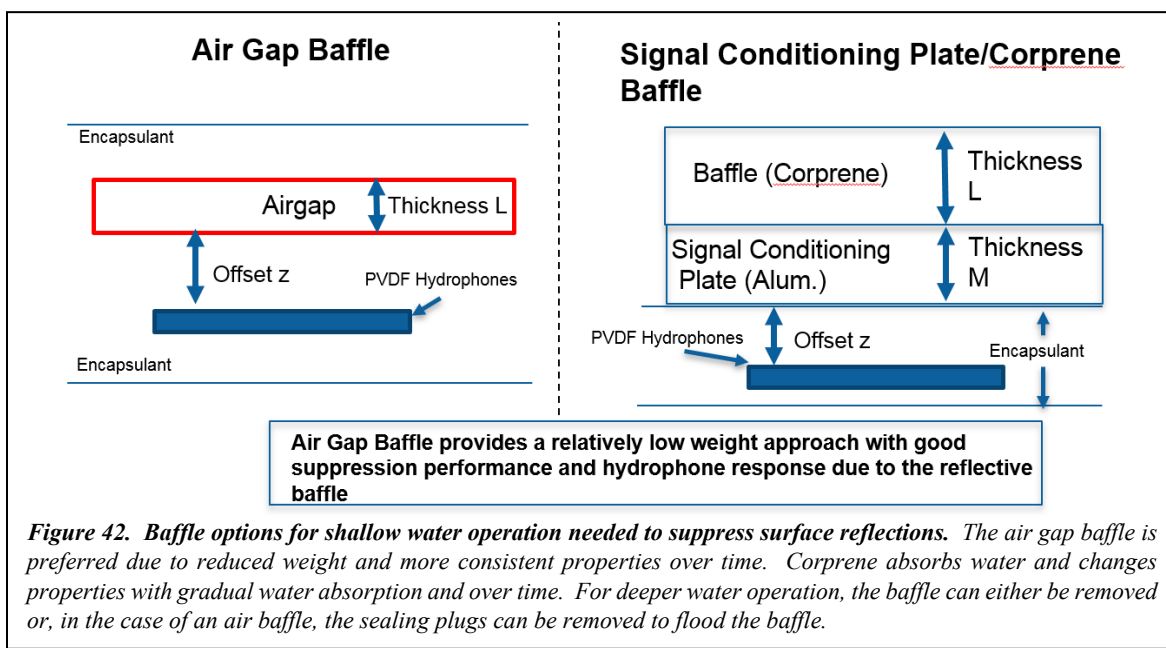
EdgeTech has a dedicated transducer design team focused on both standard and custom transducers for the broad suite of marine acoustic systems produced by the company. We remain interested in offering a next generation SERDP eBOSS source and we will propose to develop a transducer specifically for UXO remediation. We believe that both bandwidth and directivity properties can be improved using newer generation technology, but the extent of improvement is subject to modeling, research, and testing.

Shallow Water Baffle Design

There are two types of baffles have been employed: (a) an air gap baffle and (b) combination signal conditioning plate / Corprene.

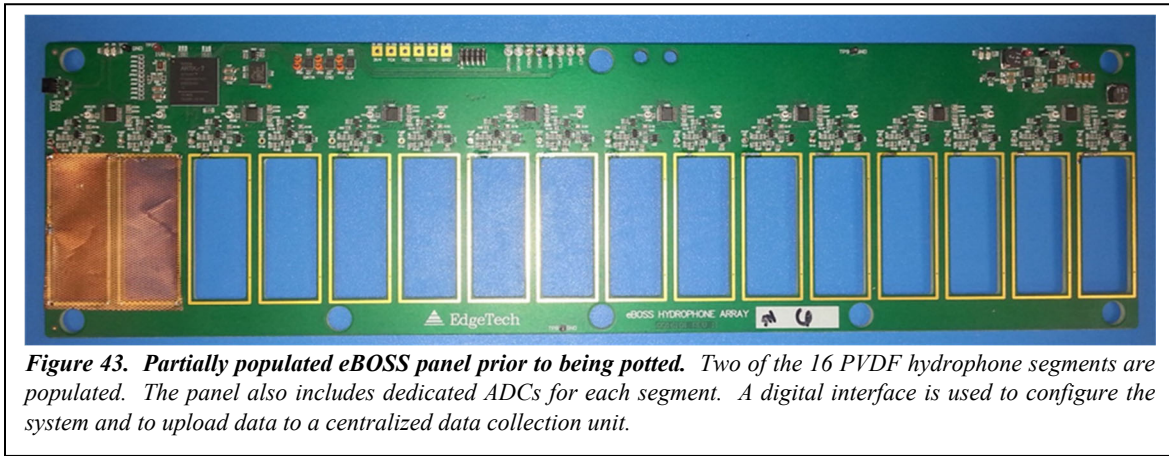
- a) Air gap baffle mounted above PVDF based hydrophone receive array
 - Transmission loss through a 5 mm air gap baffle at a mid-band frequency of 15 kHz is 23 – 65 dB.
 - Hydrophone response due to baffle at a frequency of 15 kHz is at least 5.6 dB.
- b) Signal conditioning plate / Corprene based baffle mounted above PVDF based hydrophone receive array
 - Transmission loss through a ¼” aluminum signal conditioning plate / 1.5” Corprene baffle at 15 kHz is 10.6 dB.
 - Hydrophone response due to baffle at a frequency of 15 kHz is at least 4.3 dB.

Figure 42 illustrates these two options. The properties of the Corprene baffle will change over time and exposure to water can add significant weight to the sensing platform. An air gap baffle is recommended because it is lighter and has properties that vary less over time. Steve Schock’s design notes on an air baffle design are provided in Appendix B.



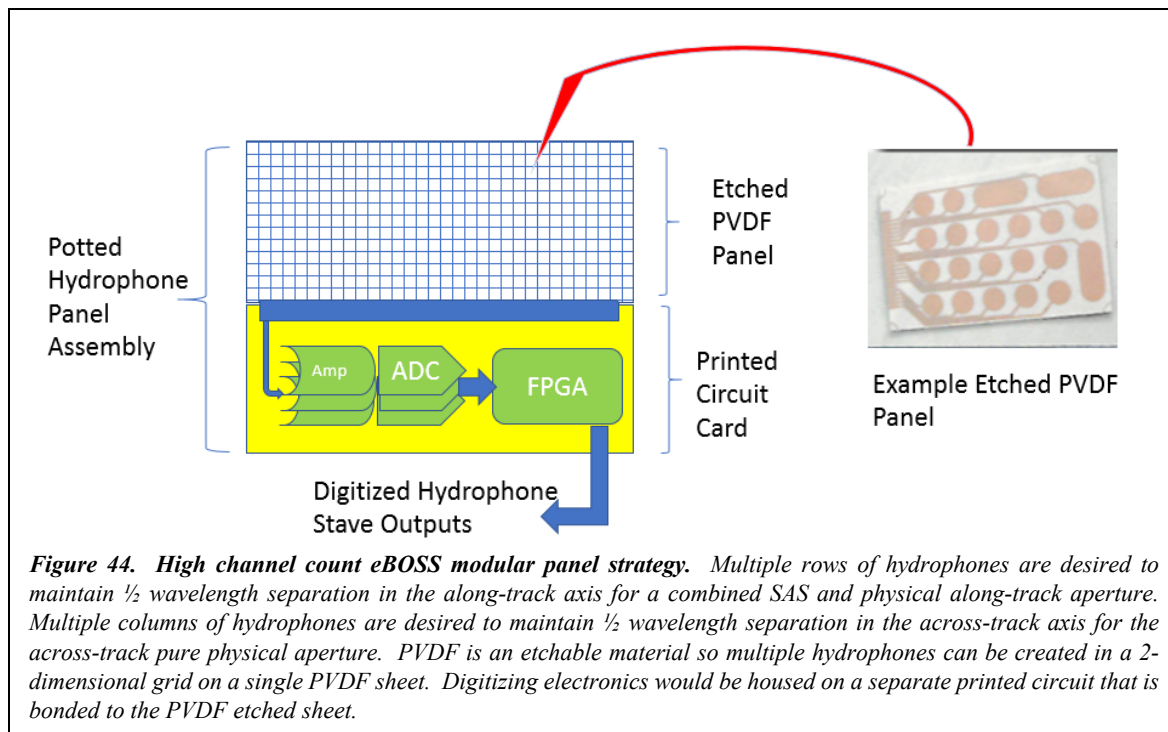
Next Generation Hydrophone Design

Recent eBOSS systems have used modular panels of hydrophones. Each panel contains 16 PVDF tiles and sigma delta audio class ADCs. A standard printed circuit board forms the structure of each panel. After automated assembly of all electronics by a printed circuit board fabrication house, PVDF tiles are cut to size and mounted inside rectangular slots in the circuit board. The board is then potted in a water tight material. Next, panels are screwed into a stiff support wing. A centralized node will collect data from each tile via a digital interface. An example hydrophone panel before potting is shown in Figure 43.



The proposed next generation eBOSS system introduces new challenges due to the increased number of hydrophones. Increasing the number of hydrophone staves from 64 per system to over 1000 requires modifying our process. Taking advantage of the properties of PVDF material, we propose etching a full sheet of the material to form individual tiles before bonding the PVDF panel to a secondary printed circuit card containing digitizing electronics. This is performed rather than cutting out individual tiles from the PVDF sheet. See Figure 44.

Airmar, a manufacturer of PVDF sheets reports their maximum sheet size as 11" X 17". For the simulations presented here, a 2 cm tile size has been assumed based on a 37.5 kHz maximum acoustic frequency. The spacing between hydrophones will depend on the band of the transmit source. For a contemporary BOSS system, the high end of the operating band is about 19 kHz (and uses approximately a 5 cm hydrophone pitch – 2-inch pitch). For a next generation eBOSS, the high end of the transmit band might be 37.8 kHz (for a 2 cm – 0.79-inch pitch). Using these values, a single PVDF sheet would then support about 5 x 8 (40) hydrophones for a low frequency system to as many as 13 x 21 (273) for a high frequency system.



The full 11 inches of PVDF may not need to be populated with hydrophone rows – the number of transmit sources, platform forward velocity, and the target operating altitude will dictate how many along-track rows are needed. In the simulations throughout this report, we use 4 rows of hydrophones whereas a single PVDF panel can support up to 13 rows at the 2 cm spacing. Each panel would span an across track aperture of about 18 inches (with about $\frac{1}{2}$ inch of dead space on each side where panels abut).

To reduce digital data rates, which can be quite high, each panel would likely contain a modern generation FPGA such as a Xilinx Artix-7. These have dedicated multipliers that can be used to match filter, baseband, and down sample to Nyquist rates. EdgeTech is presently using this class of devices for similar high-channel-count systems.

Data rates on these systems can be quite high, but unless bistatic configurations are used, only hydrophone staves near the active transmitter need to be recorded for beamform processing. For the simulated examples, the uncompressed data rate would be about 56 MB/s.

The manufacturing process for such a system would need to be tested for reliability, and complexity in terms of panel density and data rates will depend on the overall system parameters.

Acoustic Positioning and Alternative System Concept

The output for the proposed multi-source eBOSS system is a mosaic created by combining the data collected by each transmitter. The currently fielded, single-source BOSS systems might be able to create a mosaic equivalent to the proposed multi-source system if the platform's position was (a) accurately controlled and (b) precisely known over time. The tolerances for real-time

position control are less stringent than the mosaic alignment requirements, perhaps on the order of 50 cm for the 2 m altitude case for example, versus perhaps 5 cm (on the order of the systems resolution) for ideal overlays of a composite mosaic.

EdgeTech has a product line for acoustic positioning with concepts applicable to the eBOSS system. Based on this experience, we believe it is feasible to navigate a single-sourced eBOSS to within 50 cm of a desired track, which can be improved upon with postprocessing to within a 5 cm accuracy using a combination of high-end INS, high-frequency DVL, LBL, and multi-frequency GNSS with satellite-based corrections. Additional external aiding systems such as USBL, slant range, sonar based Self-Localization and Mapping (SLAM), and terrain comparison may be necessary to augment the system. LBL is the most accurate of these underwater navigation aids and would be the first area of investigation. EdgeTech personnel have first-hand experience with many of these technologies, however, the overall concept remains untested. We believe that acoustic positioning techniques used in conjunction with a simpler conventional eBOSS single source system are worth investigating as an alternative and possibly simpler solution than a large aperture multi-source system.

The following sections contain notes on each of the navigation technologies that could play a role in this concept.

INS:

A candidate inertial navigation system (INS) is the 8" diameter iXblue PHINS that provides a navigation error of 0.1% distance traveled with DVL aiding. That is, with an error of 0.1% distance traveled the platform would have roughly 2.5 cm of error after 25 m. One can further improve that error by paying the INS manufacturer to "cherry pick" a better gyro off the assembly line. Gyro's are like microprocessors in the sense that they are graded and binned into performance categories, *e.g.* you can pay to get better performance than what is specifically offered.

DVL:

Because the BOSS platform should operate at approximately 2 m above the seafloor, a high frequency DVL (on the order of 2 MHz) can be utilized to achieve accurate velocity measurements, which will in-turn improve positional accuracy. Depending on the concept of operation, a multi-frequency DVL (with an additional lower frequency) may be desirable to ensure that the DVL has bottom lock during its descent from the sea surface.

LBL:

A long base line (LBL) acoustic range, with 3 or more transponders, is the most accurate external aiding solution that we are aware of for this application. Sub-centimeter accuracies are possible with ranges up to 100 m from the transponders. LBL measurements also provide constraints to assist in "Re-nav" (post processing navigation solution after the fact). The acoustic positioning system consists of transponders that must be accurately surveyed on the order of single digit centimeters. These transponders must be rigidly mounted to the sea floor. For accurate positioning, a BOSS platform will need to continuously interrogate the transponders, including

while on the surface. As long as LBL responses are received, the navigation error is bounded and the vehicle can remain underwater indefinitely.

GNSS with satellite-based corrections:

The accuracy of an eBOSS system's initial position before diving is important because navigation error will increase in the absence of external aiding solutions. Normal GNSS solutions have accuracy on the order of single-digit meters, which is far too large for this application. One solution is to use satellite-based correction services such as Atlas or Novatel Oceanix. These systems achieve RTK like performance without having to use RTK base stations. With a supported antenna and receiver, performance is on the order of single-digit centimeters. Additional testing is required to verify these specifications on a moving platform such as an AUV.

USBL:

In place of, or in addition to LBL, USBL can provide online external aiding. Accuracy for USBL systems is on the order of .06% of slant range (6 cm at 100 m range from USBL). In a traditional USBL installation, a chase boat combines GPS, IMU, and USBL measurements to estimate a submerged vehicle's position. This position would then be sent to the vehicle via an acoustic modem. In our experience, it is easy to accumulate error from GPS, IMU, lever arm measurements, and transmission latency that degrades the accuracy of a USBL solution. Another approach is to use a "reverse USBL" with a responder accurately surveyed at a fixed known location and the interrogation acoustics and hardware installed on the vehicle. This lowers the complexity of the USBL system, however, LBL is preferred.

Re-nav:

Re-navigation (post-processing vehicle navigation) is the process of running an algorithm (such as a Kalman or least squares filter) on all the navigation related data after the mission is complete. Re-nav utilizes all measurements and is not restricted to current and past data for position estimation. This provides more accurate and smooth trajectories. Re-nav performance improves with more data.

Feature-based Navigation:

This technique reduces navigation errors by comparing data from current measurements with previously collected data. Features are extracted from the data and are processed by a recursive filter to update the vehicle's position relative to features recognized in previous data sets. This technique works well with sonar imaging systems and can improve navigation accuracy either online or offline. If no prior information is available, the feature-based navigation system can map the environmental features in-stride. EdgeTech is currently developing this capability. Online implementations using AUVs have been demonstrated by NUWC Newport division using priori bathymetry maps.

Hydrographic modeling:

The use of a high-quality hydrographic model improves the ability to control the platform online and will also improve the accuracy of re-navigation algorithms offline.

Structural Acoustics Requirements

The enhanced bandwidth of the proposed system will allow acoustic color maps to be generated in support of target classification. The ability of the proposed eBOSS system to generate acoustic color plots over sizable target aspect windows provides a complementary approach to evaluate buried objects. For small, nominally cylindrical, UXO with radii of 25-50 mm, the 7.5-37.5 kHz frequency band corresponds to a scaled frequency range, $1 < ka < 8$, where strong fundamental elastic modes can be excited. Past efforts to make use of these phenomena have shown some success for classification [1].

Relationship to Other UXO Research

The objective of this effort is to improve the traditional BOSS system with the resolution to measure the size and shape of buried objects. The proposed approach requires low-altitude operation combined with a large wing aperture. It assumes that the primary information used to measure size and shape metrics will come from specular target returns. These specular returns tend to have significantly higher SNR compared to the more omni-directional scatterers that make up a majority of buried clutter.

Ongoing SERDP project MR-2545, “Sediment Volume Search”, takes a different approach to imaging buried objects in shallow water. Like the eBOSS, MR-2545 employs multiple transmitters and operates these sources round robin to ensonify the target area. The project reports using SAS in both the along-track and across-track axes. The along-track SAS dimension is common to this project. However, MR-2545 also employs SAS across-track by coherently combining pings from distinct transmit sources. Our approach differs in that we assume the spatially separated sources potentially represent different specular views, which will reduce SNR if combined coherently. That is why the eBOSS uses a wider spacing between transmit sources than MR-2545.

MR-2545 uses a larger sensing hydrophone tile of about 9 cm which is much coarser than $\frac{1}{2}$ wavelength spacing for the operating band of that system. The larger tile size has the advantage of reducing the number of hydrophone segments to span the sensing aperture size, meaning that less ADCs and lower aggregate recording data rates are required. The larger tiles are more spatially directional which will likely suppress grating lobes.

The problem of seabed (sand wave) scattering is common to both approaches and is suppressed/removed differently. The proposed eBOSS system excludes the direct-path reflection from the seafloor using the R_{\min} criteria. In MR-2545, it appears that the beamformed data from the nadir region is reduced in amplitude to compensate for the strong scattering from the seafloor. The details for the 2D SAS algorithms used in MR-2545 do not appear to have been published yet, but if a next generation eBOSS is developed for UXO, these details should be reviewed to determine if the SERDP-sponsored concepts can be beneficially applied to a future eBOSS system.

The proposed eBOSS system provides data products that may be useful for creation of acoustic color maps and related classification research. We are not aware of how MR-2545 can support acoustic color map creation or related structural acoustics.

SERDP Project MR-2501 (the MuST [7] platform), developed by APL-UW and discussed in Appendix E, will include an eBOSS sensor suite as well as other sensor payloads. The current concept of operation is to operate the MuST platform at an altitude of 5 m. This relatively higher altitude will result lower resolution for measuring size and shape. The focus is primarily on structural acoustics which might not benefit from low-altitude data as acoustic color maps are typically made in the far field. The use of multiple sources in MuST is primarily to improve the performance of structural acoustic classifiers. Regardless, it will likely be possible to test some of the concepts discussed here by operating the MuST platform at low altitudes. We believe that a complete solution for UXO detection should combine multiple approaches and remains an active subject of research.

Conclusions and Implications for Future Research/Implementation

This study proposes enhancements to the previous generations of BOSS systems. Our objective is to improve performance for UXO detection and classification. The key improvement is the ability to capture UXO from all aspect views by employing multiple transmitters. We believe that the simulations show a compelling need for multi-source imaging for buried UXO detection. This enhancement will require a wide across-track aperture and a low operating altitude. The deployment and control of a large wing at low altitudes will introduce engineering challenges.

A next generation SERDP eBOSS system can be characterized by some of the following parameters:

- Transmit source operating band – wider is better within physical and engineering achievable limits.
- Platform forward velocity – slower is better within the platform's stability limitations.
- Altitude – lower is better provided that the platform and its wing can avoid the seafloor.
- Across-track wing aperture – longer provides better swath / coverage.
- Maximum hydrophone stave density that can be achieved for a reasonable cost.

Proposed Next Steps : Technology Risk Reduction

The most conservative path forward requires a better understanding of the above parameters. We also recommend a divide and conquer approach by defining independent subprojects in relevant areas. We recommend the following next steps:

- Design a transmit source that is half-omnidirectional and is as wideband as possible. The wide bandwidth will provide for better image resolution and enhanced support for structural acoustics. The half-omnidirectional beam pattern will improve shallow water operation. EdgeTech's transducer design team has looked at the technical issues and believes that an improved UXO detection source is possible.
- Investigate platforms that can be stable at low forward velocities and have fine altitude control. This will determine minimum altitude and minimum velocity criteria for a future system. Continued developmental work with systems such as the MacArtney FOCUS vehicle is encouraged.
- Investigate how to deploy and stabilize a large wing aperture system. A folding wing has been suggested for deployment. This will determine the maximum wing span and swath coverage that can be achieved for a future system.
- Test manufacturing process techniques for high channel-count wing tiles. The objective is to have rugged high channel count panels that are reliable over time and have uniform sensitivity among staves.
- Evaluate approaches for accurate localization and control. Recommend instrumentation to achieve a specified coverage of an area. The recommendation might be parameterized by

sea state among other physical constraints. For some conditions it might be possible to use a single source eBOSS with accurate positioning to achieve multisource behaviors. Solutions might include acoustic positioning and feature-based mapping.

- Research algorithms to estimate sediment sound speed, which will improve the detection of buried UXO. Refraction compensation using incorrect sediment sound speeds was demonstrated to degrade imagery of buried objects. If a system is built with a large sensing aperture, it may be possible to measure sediment sound speed in stride.
- As a complement to imagery, investigate ways to extract and project non-image clues from the multi-aspect BOSS data onto parameter spaces that allow robust separation of UXO from non-UXO. Projection of spectral BOSS data collected at high grazing angles onto low grazing angle "acoustic color" maps could be considered.

The above defined subprojects will reduce the risk of implementing a next generation system and refine the architecture for this next generation.

Proposed Next Steps : Concept Validation

SERDP has been funding research in UXO detection for decades. The authors of this paper have participated in several of these. Based on our experience with the difficulties in collecting field data with these systems we believe there is value in having a controlled environment test facility where consistent and repeatable results can be obtained.

- There is particular value in such a facility for concept validation of multi-source because a multi-source system does not need to be built in this case to validate the concept. As previously noted, multi-source is equivalent to multiple passes of a single source system provided that track line placement is accurate.
- We are also suggesting that low altitude operation is of value in a future system. Low altitude testing will be easier to achieve in a controlled environment.
- We have also implied that a multi-source system is particularly useful for structural acoustics, and that a full 360 degree acoustic color map can be created in a single pass with this type of system. But we have not demonstrated that color maps created in this way can be effective for classification. Data sets from a test facility can be useful in validating this concept.
- We also believe that accurate measurement of sediment sound velocity is important for buried object imaging. Development and validation of algorithms to dynamically estimate sediment sound velocity will be easier in a controlled test facility.
- We have also indicated some future research related to algorithm tuning such as dynamic aperture processing and phase coherent imaging enhancements that could be better tuned and tested with controlled environment field data.

Restating the final paragraph in the abstract: "This study is guided by the belief that superior classification can be achieved by a system that guarantees the sensing of all specular scattering

from UXO. It proposes a hardware architecture that can meet this objective. What is the combination of hardware, signal processing data products (e.g., images and acoustic color), and operational strategies needed to meet the metrics defined by the stake holders associated with SERDP/ESTCP? The final answer to this question will undoubtedly require an iterative process relying on in-the-field lessons learned as the current generation of eBOSS systems is tested.” We believe that a controlled test facility can help facilitate this.

Proposed Next Steps : System Build Out

APL-UW will install an eBOSS system on their MuST platform; delivery of their system is expected in late 2018 / early 2019. The proposed electronics architecture has already been incorporated into its plans and the system will be equipped with electronics that support multiple transmitters. APL-UW will be able to test and validate these concepts. The planned configuration is described in Appendix E.

Ultimately a future step is of course to build and deploy a system that is effective for UXO detection. We believe this report details methods that will remain valuable throughout this process.

For the eBOSS family of systems, it should be noted that eBOSS remains a set of prototypes and is not yet a standard product of EdgeTech. The eBOSS architectures have a potential commercial use for pipeline tracking but also have value for mine hunting and UXO detection. Whether any of these applications can support eBOSS in becoming a standard offering will depend on interest from various stakeholders. For a next generation eBOSS type system, an internal engineering effort will be needed to:

- Engineer the system to support higher channel counts / data rates.
- Establish and validate techniques to manufacture higher channel count panels.
- Enhance software and firmware features to support next generation concepts.
- Develop an optimal transmit source.

We believe that NSWC-PCD can play a key role in helping develop next generation eBOSS systems, mainly because they can contribute:

- High quality acoustic test facilities.
- Expertise in sonar signal processing, target scattering physics, modeling, automatic target recognition, sensor fusion, and acoustic color.
- Symbiotic relationship with other littoral acoustic programs.
- Access to representative UXO targets.

Conclusions

Simulation results illustrate the benefits of this next generation system. Since simulations have limitations and it is difficult to model real-world clutter and noise conditions, it is suggested to test a next generation system in a controlled and instrumented test field to determine its effectiveness

prior to a more extensive and expensive build phase. Independent technology risk reduction sub-projects have also been defined.

Literature Cited

- [1] S. G. Schock, "Buried object scanning sonar," IEEE J. of Ocean Eng. Special issue on autonomous ocean sampling networks, vol. 26, no. 4, pp. 677-689, 2001.
- [2] S. G. Schock, "Synthetic aperture 3D buried object imaging," Int. J. Soc. Underwater Tech., vol. 27, no. 4, pp. 185-193, 2008.
- [3] D. D. Sternlicht, J. K. Harbaugh, A. K. Shah, M. L. Webb, and R. Holtzapple, "Buried Object Classification using a Sediment Volume Imaging SAS and Electromagnetic Gradiometer," in Proceedings MTS/IEEE Oceans, Boston, MA, Sept. 2006.
- [4] D. D. Sternlicht, J. E. Fernandez, R. Holtzapple, D. P. Kucik, T. C. Montgomery and C. M. Loeffler, "Advanced Sonar Technologies for Autonomous Mine Countermeasures," in Proceedings MTS/IEEE Oceans, Kona, HI, Oct. 2011.
- [5] T. R. Clem, D. D. Sternlicht, J. E. Fernandez, J. L. Prater, R. Holtzapple, R. P. Gibson, J. P. Klose, and T. M. Marston, "Demonstration of Advanced Sensors for Underwater Unexploded Ordnance (UXO) Detection," in Proceedings MTS/IEEE Oceans, Hampton Roads, VA, Oct. 2012.
- [6] W. Jans, D. D. Sternlicht, K. L. Williams and M. D. Richardson, "Emerging Technologies in Underwater Munitions Mapping," in Proceedings of the Underwater Acoustics Conference and Exhibition (UACE), Skiathos, Greece, 2017.
- [7] K. L. Williams, "SERDP project MR-2501 final report: Limited Scope Design Study for Multi-Sensor Towbody," SERDP, Washington, DC, June 2016.
- [8] K. L. Williams, "Buried targets in layered media: A combined finite element/physical acoustics model and comparison to data on a half-buried 2:1 cylinder," J. Acoust. Soc. Am., vol. 140, pp. 504-509, 2016.
- [9] R. Lim, "SERDP project MR-2230 final report: Data and Processing Tools for Sonar Classification of Underwater UXO," SERDP, Washington, DC, Aug. 2015.
- [10] D. D. Sternlicht and C. de Moustier, "Remote sensing of sediment characteristics by optimized echo-envelope matching," J. Acoust. Soc. Am., vol. 114, no. 5, pp. 2727-2743, 2003.

- [11] S. G. Schock, "A method for estimating the physical and acoustic properties of the seabed using chirp sonar data," *IEEE J. of Ocean. Eng.*, vol. 29, no. 4, pp. 1200-1217, 2004.
- [12] K. L. Williams, "SERDP project MR-2501 final report: Limited Scope Design Study for Multi-Sensor Towbody," SERDP, Washington, DC, June 2016.
- [13] Robert J. Urick, "Principles of Underwater Sound" third edition 1983.
- [14] Jorge Camacho et al, "Phase Coherence Imaging" *IEEE Transactions on Ultrasonics, Ferroelectrics, and Frequency Control*, Vol. 56, No. 5, May 2009.
- [15] *APL/UW High frequency ocean environmental acoustic models handbook*, APL/UW Technical report 9407, Applied Physics Laboratory, University of Washington, Seattle, WA, 98105-6698.
- [16] O. George and R. Bahl, "Simulation of backscattering of high frequency sound from complex objects and sand sea-bottom," in *IEEE Journal of Oceanic Engineering*, vol. 20, no. 2, pp. 119-130, April 1995. doi: 10.1109/48.376675.
- [17] Owsley, L, Espana, A. "SERDP project MR-2324 final report: Modeling Buried Target Acoustic Response by Component," SERDP, Washington DC, November 2014.
- [18] J.A. Bucaro, A. Sarkissian, B. H. Houston, H. Simpson, Z. J. Waters, D. Amon, K. Jig, S. Liskey, T. Yoder. "SERDP project MR-2103 final report: Structural Acoustic UXO Detection and Identification in Marine Environments, " SERDP, Washington DC, April 2014.
- [19] K. L. Williams, S. G. Kargl, E. I. Thorsos. "ONR final technical report: Acoustic scattering from an aluminum cylinder in contact with a sand sediment: Measurements, modeling, and interpretation." ONR, August 2009.

Appendix A: History of BOSS Systems

In reverse chronological order some of the more significant BOSS platforms are described below. Figures for some of these systems follow.

There are presently 3 operational eBOSS systems, the 2012 Atlas Seahorse, 2015 RAZOR Highly Maneuverable Platform, and 2014 Pipeliner Demonstrator. Each consists of four 16-channel hydrophone panels and an omni-directional 7-19 kHz spherical transmit source. The RAZOR panels have a stave to stave 1" pitch and can support an optional higher frequency source. The Atlas Seahorse staves have a 2" pitch.

The 2007 SERDP-BOSS platform demonstrator was developed as an initial attempt to address shallow water UXO detection. It contained an air-baffle for surface reflection suppression, and 4 rows of hydrophones (20 per row) per wing for a total of 160 total staves.

In 2005, a Bluefin 12" AUV was equipped with a BOSS payload. Its BOSS hydrophone staves were embedded in carbon fiber wing support structure, 20 staves per wing (40 total). The staves had a 2" pitch and the platform was equipped with a 7-19 kHz spherical transmit source. Extensive data was collected with the Bluefin 12 system over test fields in Panama City, Florida.

Not shown in the figures was the 2003 BOSS-252 platform, named for its 252 channels, which had a circular hydrophone aperture fully populated with hydrophone tiles also with a 2" pitch. The BOSS-252 was the last full physical aperture BOSS system, all future systems used an across track physical aperture and along-track SAS aperture.

An older precursor is the 2001 Ceros funded BOSS demonstrator which is the last BOSS system to have a steerable transmit sources, and analog data to the centralized acquisition engine interface. All future systems included preamps and ADCs near each hydrophone and a digital interface to the centralized acquisition engine interface. The analog interface cabling was too difficult to maintain. The Ceros system demonstrated the need for an omni-directional source to ensonify from multiple look angles, all future BOSS systems used an omni-directional spherical source. References [1] , [2] , [3] , [4] , [5] , [6] discuss some of these systems.

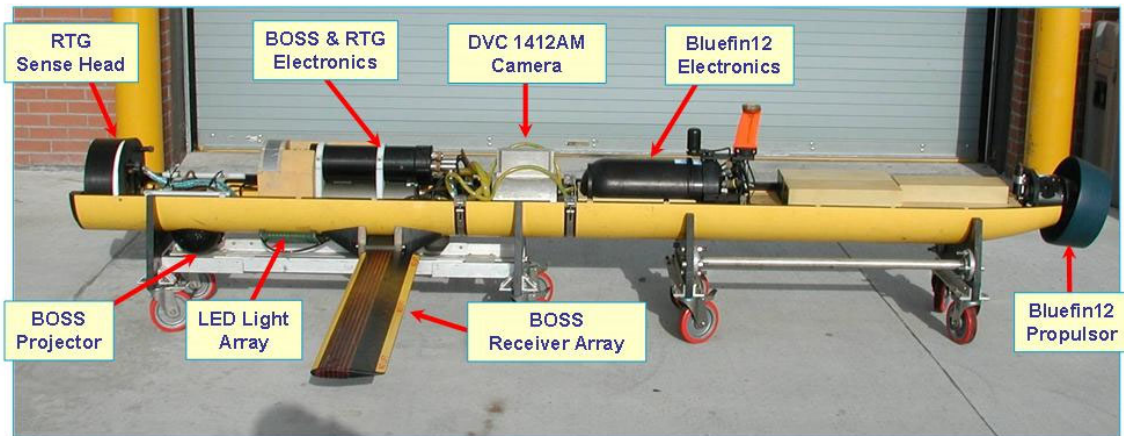


Figure 45. BlueFin 12 AUV with 40 channel BOSS hydrophone wing. Each wing has 20 hydrophones embedded in it with a 2" pitch. Other payloads also shown.



Figure 46. Razor AUV with eBOSS. Four 16-channel wing tiles are mounted below the across track wing. A Corprene signal conditioning plate / baffle (not shown) suppresses surface reflections.



Figure 47. Atlas Sea Horse with eBOSS Payload. Hydrophone wing consists of 4 panels, 64 channels total, with 2" spacing between segments. The wing rotates into the across-track position after deployment.

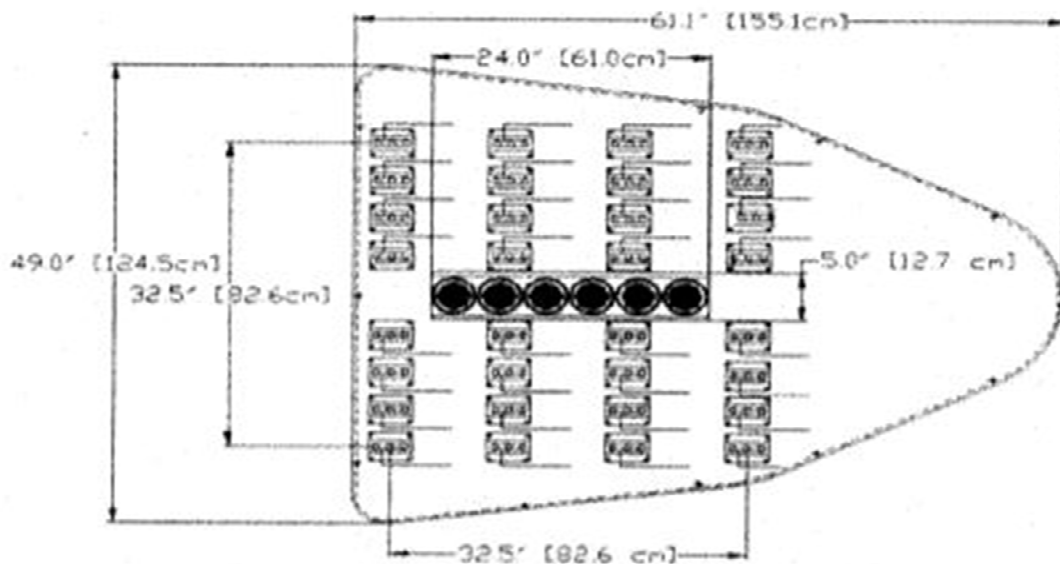


Figure 48. Ceros BOSS. This demonstrator had 32 hydrophone staves arranged in a 4 x 8 grid and a steerable 6 Tonpiz transmit array.

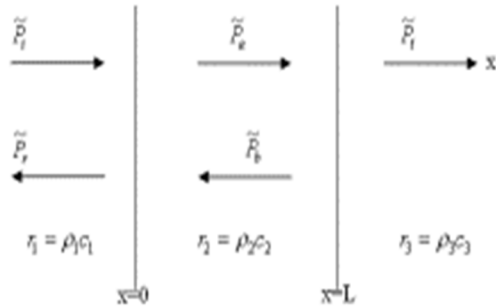


Figure 49. *SERDP BOSS-160 demonstrator being deployed in Panama City, FL. Each carbon fiber wing is embedded with 4 rows by 20 hydrophone staves with a 2" pitch. The optionally floodable air gap baffle is seen at the wing tops.*

Appendix B: Baffle Design

Below are Steve Schock's notes on the design of an air gap baffle for BOSS Systems.

Consider a fluid layer of thickness L lying between 2 fluid half spaces



Ref: Fundamentals of Acoustics

Develop an expression for the pressure reflection coefficient $\tilde{R} = \frac{\tilde{p}_r}{\tilde{p}_i}$ in terms of the specific acoustic impedances of the three fluids:

Consider the following monofrequency, steady state, harmonic waves:

$$\begin{aligned}\tilde{p}_r &= \tilde{p}_r e^{j(\omega t + k_1 x)} \\ \tilde{p}_i &= \tilde{p}_i e^{j(\omega t - k_1 x)} \\ \tilde{p}_e &= \tilde{A} e^{j(\omega t + k_2 x)} \\ \tilde{p}_b &= \tilde{B} e^{j(\omega t + k_2 x)} \\ \tilde{p}_t &= \tilde{p}_t e^{j(\omega t - k_3 x)}\end{aligned}$$

$$\text{At } x = 0 \quad \tilde{p}_i + \tilde{p}_r = \tilde{A} + \tilde{B} \quad (\text{pressure continuity}) \quad (1)$$

$$\tilde{U}_i + \tilde{U}_r = \tilde{U}_A + \tilde{U}_B \quad (\text{normal velocity continuity}) \quad (2)$$

$$\text{Substitute } \tilde{U}_+ = \frac{\tilde{p}_+}{r} \quad , \quad \tilde{U}_- = -\frac{\tilde{p}_-}{r} \quad \text{into (2)} \quad (3)$$

$$\frac{\tilde{p}_i - \tilde{p}_r}{r_1} = \frac{\tilde{A} - \tilde{B}}{r_2} \quad (4)$$

Divide (1) by (4):

$$\frac{\tilde{p}_i + \tilde{p}_r}{\tilde{p}_i - \tilde{p}_r} = \frac{r_2}{r_1} \frac{\tilde{A} + \tilde{B}}{\tilde{A} - \tilde{B}} \quad (5)$$

At $x = L$

$$\tilde{A}e^{-jk_1L} + \tilde{B}e^{jk_1L} = \tilde{P}_t e^{-jk_1L} \quad (6)$$

$$\tilde{U}_s e^{-jk_1L} + \tilde{U}_b e^{jk_1L} = \tilde{U}_t e^{-jk_1L} \quad (7)$$

Subst $\tilde{U}_s = \frac{\tilde{P}_s}{r}$, $\tilde{U}_b = \frac{-\tilde{P}_r}{r}$ into (7)

$$\frac{\tilde{A}e^{-jk_1L} - \tilde{B}e^{jk_1L}}{r_2} = \frac{\tilde{P}_t e^{-jk_1L}}{r_3} \quad (8)$$

Divide (6) by (8):

$$\frac{\tilde{A}e^{-jk_1L} + \tilde{B}e^{jk_1L}}{\tilde{A}e^{-jk_1L} - \tilde{B}e^{jk_1L}} = \frac{r_3}{r_2} \quad (9)$$

Use (9) and (5) to eliminate \tilde{A}/\tilde{B} and solve for $\frac{\tilde{P}_r}{\tilde{P}_t}$ to yield

$$\tilde{R} = \frac{\left(1 - \frac{r_1}{r_3}\right) \cos k_2 L + j \left(\frac{r_2}{r_3} - \frac{r_1}{r_2}\right) \sin k_2 L}{\left(1 + \frac{r_1}{r_3}\right) \cos k_2 L + j \left(\frac{r_2}{r_3} + \frac{r_1}{r_2}\right) \sin k_2 L} \quad (10)$$

Using the conservation of energy and $A_i = A_t$, it follows that

$$\Pi_I = \Pi_R + \Pi_T$$

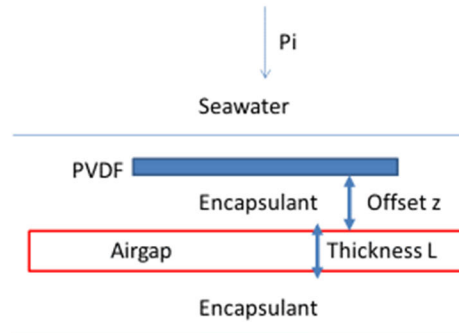
$$R_{\Pi} + T_{\Pi} = 1$$

$$R_f + T_f = 1 \quad T_f = 1 - R_f = 1 - |\tilde{R}|^2 \quad (11)$$

Subst (10) into (11) to yield

$$T_f = \frac{4}{2 + \left(\frac{r_3}{r_1} + \frac{r_1}{r_3}\right) \cos^2 k_2 L + \left(\frac{r_2^2}{r_1 r_3} + \frac{r_1 r_3}{r_2^2}\right) \sin^2 k_2 L} \quad (12)$$

Geometry



Appendix B.1: MATLAB program for airgap baffle design:

```
%
% airgapdeep.m
%
% program for determining thickness of airgap, offset between airgap and
% hydrophone, and frequency response of hydrophone / airgap
% curves are plotted for depths of 0m and 10m
clear all
%f1=input('Enter lowest frequency of analysis (kHz) ');
%f2=input('Enter highest frequency of analysis (kHz) ');
f1=1;
f2=30;
df=.1;
f=f1:df:f2; % frequency
depth=100; % meters
atmabs=(depth +10)/10; % absolute pressure atmospheres
c1=1500;
d1=1026;
r1=c1*d1; %impedance of encapsulant; same as seawater impedance
c2=343;
d2=1.2;
r2=c2*d2; %impedance of air
r2deep=r2*atmabs; % air density is proportional to absolute submergence pressure
L=0.005; %airgap thickness m
Ldeep=L/atmabs; % airgap thickness is inversely proportional to absolute submergence pressure
k2=2*pi*f*1000/c2;
% Transmission Intensity Coefficient of airgap
% for r1=r3, equation 12 becomes
TI=4./(2+2*(cos(k2*L)).^2+((r2/r1)^2+(r1/r2)^2)*(sin(k2*L)).^2);
TIdeep=4./(2+2*(cos(k2*Ldeep)).^2+((r2deep/r1)^2+(r1/r2deep)^2)*(sin(k2*Ldeep)).^2);
TL=10*log10(TI);
TLdeep=10*log10(TIdeep);
figure(1)
plot(f,-TL,f,-TLdeep,'r')
grid on
title(['Transmission Loss Through Airgap of ',num2str(L*100),' cm Thickness    blue=0m;
red=',num2str(depth),'m'])

xlabel('Frequency(kHz)')
```



```

ylabel('Transmission Loss (dB)')
%Reflection coefficient of airgap
% for r1=r3, equation 10 becomes
R=j*(r2/r1-r1/r2)*sin(k2*L)/(2*cos(k2*L)+j*(r2/r1+r1/r2)*sin(k2*L));
Rdeep=j*(r2deep/r1-r1/r2deep)*sin(k2*Ldeep)/(2*cos(k2*Ldeep)+j*(r2deep/r1+r1/r2deep)*sin(k2*Ldeep));
figure(2)
subplot(2,1,1)
plot(f,20*log10(abs(R)),f,20*log10(abs(Rdeep)), 'r')
grid on
title([' Reflection Coefficient of Airgap with ',num2str(L*100),' cm Thickness blue=0m;
red=',num2str(depth),'m'])
ylabel('Amplitude(dB)')
subplot(2,1,2)
plot(f,angle(R)/pi*180,f,angle(Rdeep)/pi*180,'r')
grid on
xlabel('Frequency(kHz)')
ylabel('Phase(degrees)')

%Determine how frequency response of perfect hydrophone is modified by
%echoe off of airgap
zmm=input('Enter thickness of encapsulant between sensor and airgap (mm)');
z=zmm/1000;
wlen=c1/(f*1000);
zwlen=z./wlen; % airgap offset in wavelengths
k1=2*pi*f*1000/c1; % wavenumber of encapsulant sound propagation
SLhyd=20*log10(abs(1+R.*exp(j*k1*2*z))); % Response of hydrophone with airgap
SLhyddeep=20*log10(abs(1+Rdeep.*exp(j*k1*2*z)));
figure(3)
subplot(2,1,1)
plot(f,SLhyd,f,SLhyddeep,'r')
grid on
title(['Response of Hydrophone with Airgap Baffle with ',num2str(z*100),' cm offset blue=0m;
red=',num2str(depth),'m'])
xlabel('Frequency(kHz)')
ylabel('dB')
subplot(2,1,2)
plot(zwlen,SLhyd,zwlen,SLhyddeep,'r')
grid on
xlabel(['Sensor-gap offset wavelengths'])

```

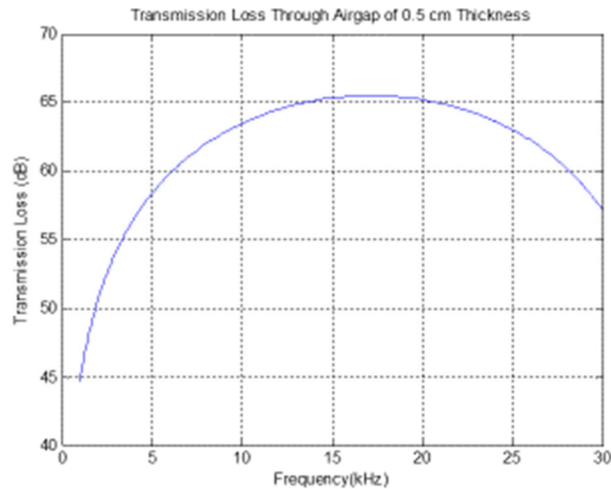
```

ylabel('dB')
%
% Set Sensor-gap offset at 0.4 wavelengths at highest operating frequency
%
fh=20000;
wavelength=c1/fh;
z=0.4*wavelength;
SLhyd=20*log10(abs(1+R.*exp(j*k1*2*z))); % Response of hydrophone with airgap
SLhyddeep=20*log10(abs(1+Rdeep.*exp(j*k1*2*z)));
figure(4)
subplot(2,1,1)
plot(f,SLhyd,f,SLhyddeep,'r')
grid on
title(['Response with ',num2str(z*100),' cm offset based on 0.4 wavelen at fh = ',num2str(fh/1000),'
kHz blue=0m; red=',num2str(depth),'m'])
xlabel('Frequency(kHz)')
ylabel('dB')
subplot(2,1,2)
plot(zwlen,SLhyd,zwlen,SLhyddeep,'r')
grid on
xlabel(['Sensor-gap offset wavelengths'])
ylabel('dB')

```

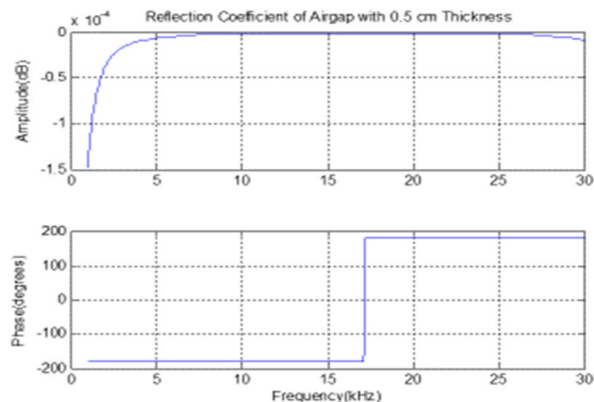
The following slides provide an example of the matlab program's output

Sound Transmission Through Air Gap Baffle



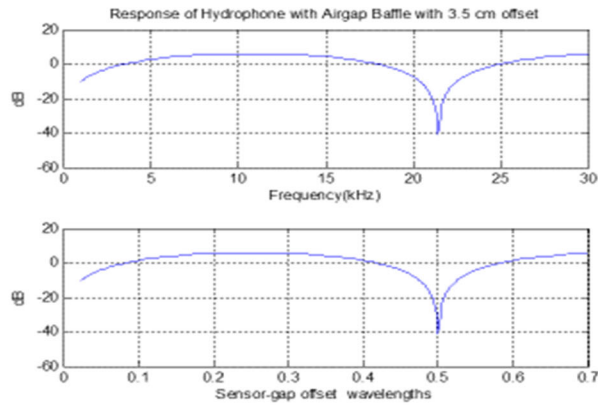
This graph shows downward traveling multipath sound from sea surface would lose at least 60 dB between 6 and 28 kHz as it passes through a 5mm airgap.

Reflection Coefficient of Airgap Baffle



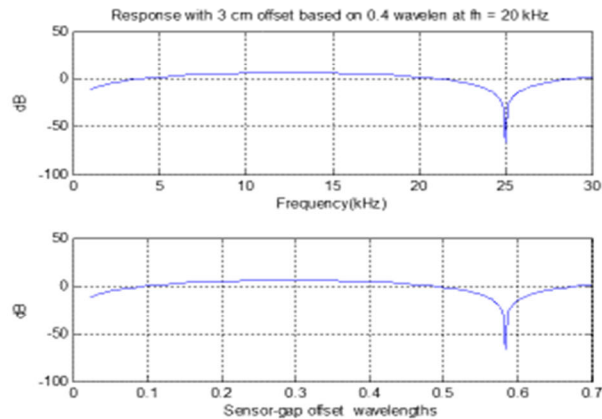
This graph shows the 5 mm airgap is practically a perfect reflector causing echo phase to invert

Modification of Hydrophone Response by Airgap Baffle



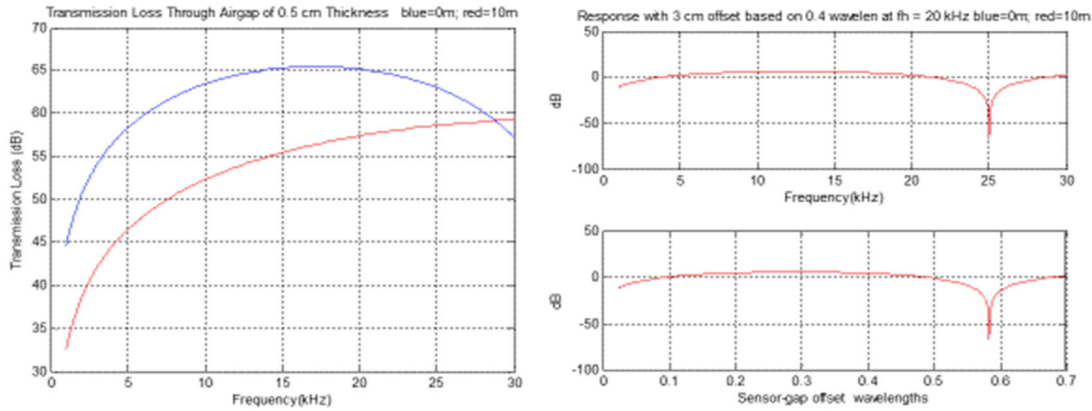
This graph shows an hydrophone – airgap offset between 0.1 and 0.4 wavelengths causes the direct path sound to constructively add to sound reflected off airgap. Therefore, the offset should be set to 0.4 wavelengths at the highest operating frequency.

Modification of Hydrophone Response by Airgap Baffle



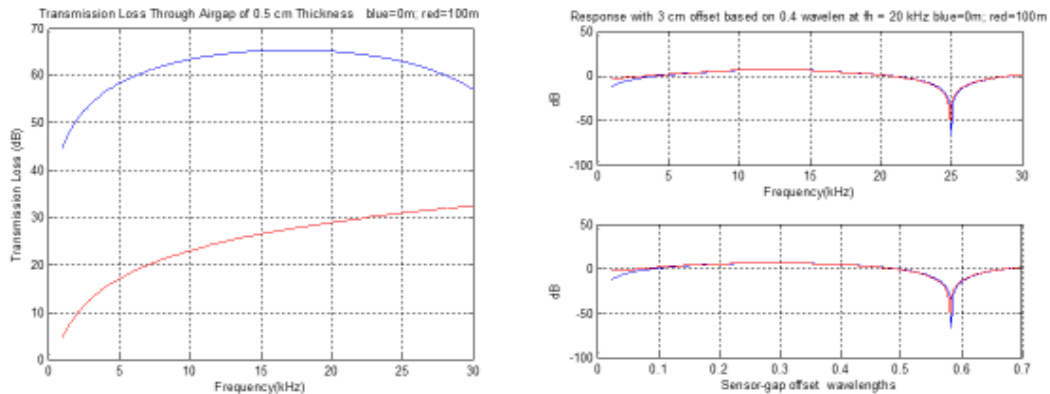
This graph shows how the hydrophone response is modified by the airgap baffle when the offset is set to 0.4 wavelengths at 20 kHz.

Effect of Submergence Pressure on Baffle Performance at Depth of 10m



At depth of 10 m, transmission loss decreased by about 10 dB and the change in hydrophone response is insignificant. The system calibration would not change.

Effect of Submergence Pressure on Baffle Performance at Depth of 100m



At depth of 100 m, transmission loss decreased by about 40 dB but surface multipath is weak at that depth, and the change in hydrophone response is less than 1 dB over the 6-20 kHz operating band. The system calibration would not change significantly.

Appendix C: PC SWAT Simulations

PC SWAT (Personal Computer Shallow Water Acoustic Tool-set) is a set of acoustic propagation and scattering computer software developed at NSWC-PCD to simulate the performance of acoustic sensors in a wide array of ocean environments. It is distributed among DoD and DoD contractors for this purpose and appears in 2 forms. The first is a GUI driven version which allows the user to set up and run PC SWAT using the familiar windows interface. The second is a DLL version which allows users to create their own interface and to call various functions within PC SWAT from within their own code. This second interface is primarily used to perform numerous case studies, since it allows the user to automate thousands of cases.

PC SWAT primarily uses the GRAB (Gaussian Ray Bundle) propagation model developed by Henry Weinberg [1] for propagation, although the Bellhop3D Gaussian beam program developed by Michael Porter [2] was recently added. PC SWAT also has wavenumber integration and normal mode algorithms [3] built into it for use when propagation in simpler plane-stratified environments is sufficient or it is desired to sacrifice speed for higher precision.

Several environmental models are available for use in PC SWAT to account for various propagation effects. The environmental models developed and documented by APL/UW [4] are used to account for reverberant noise effects. The bubble model of Prosperetti and Commander [5] is used to describe attenuation by bubble clouds and their effects on sound speed. The surf zone model developed by Svein Vagle, David M. Farmer, and Grant B. Deane [6] is used to describe the time evolution of bubble plumes in the surf zone due to breaking waves. Several options are available in PC SWAT for computing the response of targets embedded in environments of interest. Monostatic and bistatic scattering from rigid targets are computed using the Kirchhoff Approximation method along with GTD (Geometric Theory of Diffraction) [7] corrections if needed to account for diffractive effects at lower frequencies. The Kirchhoff Approximation integrates the scattering contribution from the illuminated facets of a faceted target model, where the reflected field from each “rigid” facet is determined from the plane-wave reflection coefficient corresponding to the actual target material and an angular scattering function associated with the shape of the facet. A library of 20 different rigid target shapes is included in PC SWAT for the user’s convenience. Computations with rigid shapes allow the fastest simulations and generally account for the dominant scattering contributions from real targets. When more fidelity is desired in the scattering response, the scattering by elastic targets can be included using spherical T-matrix computations [8] for elastic spheres and spherical shells or spheroidal-basis T-matrix computations [9] for large aspect ratio elastic targets. PC SWAT also allows the user to import target response data created by the Finite Element Method.

Notional sonar systems can be configured in PC SWAT with multiple sources and receiver elements. The user can specify a rectangular, or cylindrical receive array, or define an arbitrary array by specifying the position and orientation of each element in the array. By properly tracking the source and receiver element positions, sonar data propagated from a given source to each point in a specified area and then scattered/reflected back to each receiver array element can be generated and stored as the sonar is moved through an environment. The user can specify all 6 degrees of motion of the sensor, and have the sensor follow a user defined trajectory.

PC SWAT computes the SNR (Signal-to-Noise-Ratio) for active and passive sensors, shadow contrast for active sensors, the transmission loss, and monostatic and bistatic images of volume, proud, and buried targets.

In the current study, PC SWAT was used to create synthetic data for free-field and buried targets for a next generation BOSS sonar design. The sonar considered consisted of 4 transmitters arranged as shown in Figure 12 and configured according to the coordinates in Table C1, where the x -coordinate is across track, the y -coordinate is along-track, and the z -coordinate is altitude above the bottom. The origin of these coordinates is located at the center of the receiver array. The receiver consists of 4 rows of 318 elements with 2-cm spacing along-track and across track. Since PC SWAT is normally set up to simulate ahead-look or side-scan sonar, the downward-looking BOSS array is modeled as a starboard side-scan sonar with a 4 row receive array deployed on a wing-like structure operated at a depression angle of +90 degrees downward.

Table C1. Position of transmitters

	x (m)	y (m)	z (m)
A	-2.184	-.24	2
B	-.728	-.24	2
C	+.728	-.24	2
D	+2.184	-.24	2

The 4 transmitters do not emit sound simultaneously but are fired in a round robin sequence. Transmitter A emits an LFM (Linear Frequency Modulation) pulse of 2 milliseconds. The sonar travels 2 centimeters and transmitter B emits the same LFM pulse. The sonar travels 2 centimeters and transmitter C emits the LFM pulse. The sonar travels another 2 centimeters and transmitter D emits the LFM pulse. The sonar travels another 2 centimeters and transmitter A repeats the cycle. This behavior was simulated in PC SWAT and the computed raw stave data of the 4 transmitters separated into 4 datasets for image processing, one for each transmitter. A file, staveA.txt, was output containing the raw stave data for all 1272 received elements, where transmitter A emits an LFM pulse each time the sonar advances 8 centimeters between pings. The file, staveB.txt, contained the raw stave data for transmitter B, where the first ping occurs 2 centimeters ahead of the first ping for transmitter A. Similar files were generated for transmitters C and D, where the first ping of transmitters C and D were advanced 2 centimeters ahead of the previous transmitter.

The free-field synthetic data created by PC SWAT was used to check new image processing algorithms written by EdgeTech researchers for the prototype design. For these simulations, propagation and scattering in water by various rigid target shapes as listed and illustrated in Table C2 were modelled. Generic water properties were assumed: a sound speed of 1500 m/s and a density of 1000 kg/m³. Simulations for buried targets from Table C2 were performed assuming an underwater environment with a medium sand seafloor. Parameters used for the sediment are given in Table C3. For the simulations with buried targets, the sonar was assumed to be moving along straight tracks typically 2 m above the sediment past a target buried less than 1 m deep. Sound rays propagated into the seafloor to the target from sources in the water were incident at above the critical grazing angle and obeyed Snell's law upon transmission into the sediment. Rays scattered back out to the receive array also obeyed Snell's law. Propagation in the sand was subject to attenuation that was assumed constant over the frequency band simulated. Statistically-based reverberant noise consistent with the interface and volume spectral scattering strengths given in Table C3 was included in some simulations. While PC SWAT also allows the user to account for deterministic diffractive effects of ripples and roughness on the sound transmitted into the sediment, these effects were not included in the simulations of this report.

Table C2. List of targets used

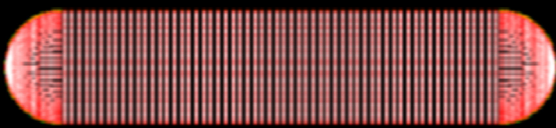
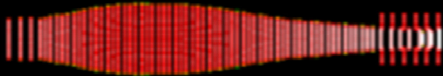
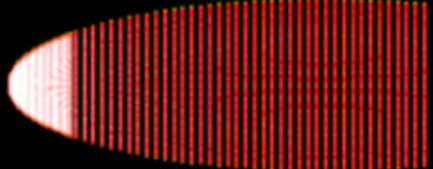
Target	Length	Width	Shape
Point target	0	0	
Cylinder with hemispherical end caps	.4	.1	
Mortar shell	1	.16	
Bullet (truncated spheroid)	.4	.2	

Table C3. Sediment properties

Density	1845 kg/m ³
Speed of Sound	1767 m/s
Attenuation @ 20 kHz	10 dB/m
Interface roughness spectral strength	0.004446e-8
Interface roughness exponent	3.25
Volume spectral strength	0.05e-8
Volume exponent	3.25

References:

- [1] Henry Weinberg, Ruth Keenan, Gaussian ray bundles for modeling high frequency propagation loss in shallow water condition, *J. Acoust. Soc. Amer.* 100(3) pp. 1421, 1996
- [2] Michael B. Porter, <http://hlsresearch.com/oalib/>
- [3] Finn B. Jensen, William A. Kuperman, Henrik Schmidt, Michael B. Porter, *Computational ocean acoustics*, Springer-Verlag, New York, 1997.
- [4] *APL/UW High frequency ocean environmental acoustic models handbook*, APL/UW Technical report 9407, Applied Physics Laboratory, University of Washington, Seattle, WA, 98105-6698, 1994.
- [5] Kerry Commander and Andrea Prosperetti, *Linear pressure waves in bubbly liquids: Comparison between theory and experiment*, *J. Acoust. Soc. Amer.* 85(2), pp 732-746, 1988.
- [6.a] David M Farmer, Sein Vagle, and Grant B. Deane, *The influence of bubble clouds on acoustic propagation in the surf zone*, *IEEE Ocean Engineering*, 26 pp. 113-124., 2001.
- [6.b] Svein Vagle, David M. Farmer, and Grant B. Deane, Bubble transport in rip currents, *J. Geophysical Res.*, 106(c6), pp. 11677-11689, 2001
- [7.a] Allan D. Pierce, *Acoustics: An introduction to its physical principles and applications*, McGraw Hill, New York, 1981.
- [7.b] E. Skudrzyk, *The foundations of acoustics: Basic mathematics and basic acoustics*, Springer-Verlag, New York, 1971.
- [8] V. K. Varadan and V. V. Varadan, eds., *Acoustic Electromagnetic and Elastic Wave Scattering – Focus on the T-Matrix Approach*, Pergamon Press, New York, 1980.
- [9] R. H. Hackman, "The transition matrix for acoustic and elastic wave scattering in prolate spheroidal coordinates," *J. Acoust. Soc. Am.*, vol. 75, no. 1, pp. 35-45, 1984.

Appendix D: MATLAB Script for Computing Trade Space Table

This is the MATLAB script for computing the BOSS Geometry discussed in the Trade Space section.

```
%
% BossGeometryDesign.m
%

clear
close all

p1 = 'Number Of Transmit Sources';
p2 = 'Transmit Band Start Frequency kHz';
p3 = 'Transmit Band End Frequency kHz';
p4 = 'Altitude in Meters';
p5 = 'Platform Velocity M/s';
p6 = 'TBD';
p7 = 'TBD';
p8 = 'TBD';
p9 = 'TBD';
p10 = 'TBD';
pTitle = 'Enter Parameters';
prompt = {p1, p2, p3, p4, p5, p6, p7, p8, p9, p10};
DefFile = 'BossGeometryDesign.dat';
Parameters = 0;
if exist(DefFile)
load(DefFile, '-mat');
end
if size(Parameters, 1) ~= 10
Parameters = {'4', '7.5', '37.5', '2.0', '1.5', '0', '0', '0', '0', '0'};
end
input0 = inputdlg(prompt, pTitle, 1, Parameters, 'on');
if size(input0, 1) ~= 10
return;
end
Parameters = input0;
save(DefFile, 'Parameters', '-mat');

%Water sound speed
```

```

c=1500;

%Number of transmit sources
Ns=sscanf(Parameters{1}, '%d');

% Transmit Frequency Range
TXFLowKHz = sscanf(Parameters{2}, '%f');
TXFHiKHz = sscanf(Parameters{3}, '%f');

% Transmit Pulse Length in ms. Typically between 2 and 5. Time bandwidth
% products above 100 not very useful, and generally want a BT product
% of at least 20. Here we use BT product of 100.
TXLengthMs = 100 / (TXFHiKHz - TXFLowKHz);

% Wavelengths in meters
bandwidthKHz = (TXFHiKHz - TXFLowKHz);
wavelengthHighFrequencyHz = c / (1000 * TXFHiKHz);
wavelengthCenterFrequencyHz = c / (1000 * (TXFHiKHz + TXFLowKHz) / 2);

% Hydrophone Spacing - 1/2 wavelength criteria
hydrophoneSpacingMeters = wavelengthHighFrequencyHz / 2;

% Altitude Above Seabed in meters
altitude = sscanf(Parameters{4}, '%f');

% Platform Velocity M/s
platformVelocity = sscanf(Parameters{5}, '%f');

% Maximum repose of sand waves in degrees
sandWaveMaxDegrees = 35;

% Maximum imaging incident angle. Must not exceed critical angle
% but need some extra margin because of the length of the receive
% aperture. Value of 55 degrees chosen to be approximately double
% the spacing between transmit sources
maxImagingDegrees = 55;

% Maximum imaging radius in meters.
RMax = altitude * tan(maxImagingDegrees * pi / 180);

```

```

% Minimum imaging radius in meters to avoid sand wave speculars.
RMin = altitude * tan(sandWaveMaxDegrees * pi / 180);

% Spacing between transmit sources - based on excluding sand waves in
% imaging bands
txSpacingMeters = tan(sandWaveMaxDegrees * pi / 180) * altitude;

% Hydrophone Across Track Aperture in Meters, based on capturing a
% 0 degree specular of a target midway between two TX sources
hydrophoneMeters = 2 * txSpacingMeters;

% SAS Aperture in meters - same as along track. We could probably cut this
% in half for comprable resolution.
hydrophoneSASMeters = altitude;

% Maximum burial depth - assumed constant
maxBurialDepthMeters = 1.0;

% Time interval required for a pings worth of data
% Based on distance from transmit source to RMax plus
% distance on RMax to furthest hydrophone.
timePerPing = ...
TXLengthMs / 1000 + ...
sqrt((altitude + maxBurialDepthMeters) ^ 2 + RMax ^ 2) / c + ...
sqrt(...
(altitude + maxBurialDepthMeters) ^ 2 + ...
(RMax * sind(45) + hydrophoneMeters) ^ 2 + ...
(RMax * cosd(45) + hydrophoneSASMeters) ^ 2) / c;

% Distance moved per ping for the same TX source - assumes sources
% fire round robin.
DistancePerPing = platformVelocity * timePerPing * Ns;

% Number of hydrophone rows. Based in maintaining 1/2 wavelength spacing
% between hydrophone elements in the along track (SAS) direction.
HydrophoneRows = ceil(DistancePerPing / hydrophoneSpacingMeters);

% Revised values
DistancePerPing = HydrophoneRows * hydrophoneSpacingMeters;
timePerPing = DistancePerPing / (platformVelocity * Ns);

```

```

% Ping rate for 1/2 wavelength spacing
pingRateHz = 1.0 / timePerPing;

% Resolutions
AlongTrackSASResolution = wavelengthCenterFrequencyHz / 2;
AcrossTrackResolution = wavelengthCenterFrequencyHz;
RangeResolution = (c / 2) / (bandwidthKHz * 1000);

% Across track swath. Distance from first transmitter to last less
% lost range due to RMin criterial at each end of across track aperture.
swath = (Ns - 1) * txSpacingMeters - 2 * RMin;

% Across track wingspan. Distance from first transmitter to last plus
% 1/2 of hydrophone across track aperture on each side.
AcrossTrackWingSpan = (Ns - 1) * txSpacingMeters;

% Add this back in to have symmetric aperture for peripheral TX sources
% AcrossTrackWingSpan = AcrossTrackWingSpan + hydrophoneMeters;

% Number of hydrophones total
AcrossTrackHydrophones = ceil(AcrossTrackWingSpan / hydrophoneSpacingMeters);
TotalHydrophones = AcrossTrackHydrophones * HydrophoneRows;

% Summarize Results
disp(sprintf('TXSources:%d FLow:%7.3f FHigh:%7.3f Speed:%7.3f Altitude:%7.3f, ...
Ns, TXFLowKHz, TXFHiKHz, platformVelocity, altitude));
disp(sprintf('TXSourceSpacing:%7.3f WingSpan:%7.3f CoverageSwath:%7.3f, ...
txSpacingMeters, AcrossTrackWingSpan, swath));
disp(sprintf('HydrophoneSpacing:%7.3f NumberPerRow:%d Rows:%d Total:%d', ...
hydrophoneSpacingMeters, AcrossTrackHydrophones, HydrophoneRows, ...
TotalHydrophones));
disp(sprintf('Ping Rate:%7.3f Resolutions(AlongTrack:%7.3f Across:%7.3f Range:%7.3f, ...
pingRateHz, AlongTrackSASResolution, AcrossTrackResolution, RangeResolution));

```

Appendix E: APL-UW MuST Multisource

The APL-UW MuST Focus ROV funded by SERDP (SERDP project MR-2501 [7]) will have a set of eBOSS sensors including some support for multi-source when delivered late in 2018. It will be wired to support 6 transmit sources total, 2 of which will be omni-directional. The other transmitters are targeted to APL's TIER (Target-In-The-Environment) concept for acoustic color.

The 2-meter width of the support frame will limit its ability to capture more extreme look angles. The omni-directional sources planned for multi-source will be placed at the extreme ends of the aperture to optimize its multisource capability. The platform plan view, looking up from the bottom is shown in Figure 50. A potential future enhancement for multi-source would be to retrofit the system with higher channel count multi-row hydrophone panels for potential improved SNR

